# Dissertation

---

# Wireless Impedance-Monitoring of Adherent Cell-Cultures

ausgeführt zum Zwecke der Erlangung des akademischen Grades eines Doktors der technischen Wissenschaften unter der Leitung von

Prof. Dr. Michael J. Vellekoop

eingereicht an der Technischen Universität Wien
Fakultät für Elektrotechnik und Informationstechnik

von

DI Jürgen Markus Wissenwasser

Brandjochstraße 4B, 6020 Innsbruck
Matr-Nr. 0026169

Innsbruck, im Juni 2012

| | |
|---|---|
| Erstbegutachter | Prof. Dr. Michael J. Vellekoop<br>Universität Bremen<br>Bremen, Deutschland |
| Zweitbegutachter | Univ. Doz. Mag. Dr. Anton Köck<br>Austrian Institute of Technology<br>Wien, Österreich |

# KURZFASSUNG

Diese Arbeit behandelt elektrische Impedanzmessung an adhärenten biologischen Zellkulturen. Der variable Bedeckungsgrad (Konfluenz) von Elektrodenflächen durch adhärente Zellen geht mit einer Änderung der elektrischen Impedanz gegenüber der Nährlösung einher. Die Konfluenz vergrößert sich beispielsweise aufgrund von Zellwachstum oder verringert sich durch Seneszenz oder äußere toxische Einflüsse. Eine weitere Quelle für Impedanzänderung sind die Veränderung der Zellen selbst, wie hier bei der induzierten Differenzierung von Stammzellen beobachtet werden konnte.

Die im Rahmen dieser Arbeit entwickelten Sensoren basieren auf Glaschips mit definierten metallischen Elektrodenstrukturen, die in direktem Kontakt mit dem Nährmedium bzw. den Zellen stehen. Ein darauf aufbauendes modulares Sensorsystem erlaubt die Reinigung und Wiederverwendung der eingesetzten Chips. Um Anwendern in der Zellkulturtechnik möglichst große Flexibilität zu geben war der Einsatz einer drahtlosen Messtechnik gefordert. Hierbei wurde großer Wert auf die Kompatibilität zu bestehenden Zellkulturwerkzeugen und –materialien gelegt, sodass konventionelle 6-well Microtiter-Platten als Basis und Kontaminationsschutz gewählt wurden.

Der drahtlose Ansatz zur Messtechnik kommt ohne Akkus bzw. Batterien aus und basiert auf einem patentierten Ablauf. Hierbei wird aus dem für die drahtlose Kommunikation erforderlichen Hochfrequenz-Feld, in Anlehnung an die Radio Frequency Identification (RFID) Technologie, Energie gewonnen.

Die Sensoren selbst arbeiten im Frequenzbereich von 5 bis 50 kHz, wobei die meisten hier präsentierten Untersuchungen bei 10 kHz durchgeführt wurden. Die Elektronik der Sensorschnittstelle wurde besonders energieeffizient dimensioniert.

Messungen an 3T3 Mausembryo-Fibroblasten, wie auch an menschlichen mesenchymalen Stammzellen, wurden in Kurzzeit- (bis zu 3 Tage) und Langzeitversuchen (bis zu 4 Wochen) ausgeführt. Bei den Fibroblasten konnte das Meßsystem zur Bewertung des Wachstumsverhaltens und der Terminierung durch hochtoxische Substanzen eingesetzt werden. Dabei wurde auch ein starker Einfluss der Inkubatoratmosphäre auf die Messergebnisse erkannt, insbesondere durch den Verlust von Nährmedium durch Verdunstung.

Die mesenchymalen Stammzellen wurden einer osteogenen und adipogenen Differenzierung unterworfen. Die dabei gewonnen Daten zeigen, dass charakteristische Impedanzänderungen bereits binnen 24 Stunden nach der induzierten Differenzierung erkennbar sind, wogegen konventionelle Färbemethoden erst nach 5 bis 7 Tagen zuverlässige Ergebnisse liefern.

# SUMMARY

This work concerns electrical impedance measurements on adherent biological cell cultures. The variable coverage (confluence) of electrode structures by adherent cells alters the electrical impedance with respect to the cell culture medium. Confluence increases e.g. by cell growth or decreases by senescence or external toxic influences. Another source for impedance variation is the change of the cells, e.g. by induced differentiation of stem cells.

The invented sensor is based on glass chips carrying electrode structures which are in direct contact with the cells and the culture medium. The introduction of a modular sensor system allows cleaning and reuse of the sensor chips. A maximum of flexibility for the operators in the cell culture laboratory is achieved by the implementation of wireless technique, where one constraint was the compatibility to established cell culture tools and materials. Thus, conventional 6-well microtiter-plates were chosen for both, as a rack and as contamination protection unit.

The wireless approach does not rely on batteries and is based on a patented energy storage procedure. There, energy is taken from the radio frequency-field which is present in wireless communication. The technique relies on Radio Frequency Identification (RFID) technology.

The sensors are operated in a frequency range between 5 and 50 kHz, most investigations were performed at 10 kHz. The presented electronic readout system was specially invented for high energy efficiency because commercially available systems exceeded power constraints.

Measurements on 3T3 embryonic mouse fibroblasts, as well as on human mesenchymal stem cells, were performed in short-term (up to 3 days) and long-term-measurements (up to 4 weeks). The monitoring of fibroblasts was used to examine cell growth behavior and the influence of highly toxic substances on the electrical impedance. There, also a strong influence of the incubator atmosphere on the measurements was found, which is caused by the loss of culture medium due to evaporation.

Osteogenic and adipogenic differentiation was induced to the mesenchymal stem cells. The results show that characteristic impedance changes were found within 24 hours, while conventional staining methods show reliable results only after 5 to 7 days of culture time.

# CONTENTS


**KURZFASSUNG** **I**

**SUMMARY** **III**

**NOMENCLATURE** **IX**

**INTRODUCTION** **1**

1.1. CURRENT MEASUREMENT METHODS ON CELL CULTURES 2
1.2. PERFORMANCE CHARACTERISTICS 6
1.3. IMPEDANCE MEASUREMENT AS A TOOL IN MICROBIOLOGY 6
1.4. THESIS OUTLINE 7
1.5. BIBLIOGRAPHY 8

**CELL BIOLOGY AND LABORATORY ENVIRONMENT** **11**

2.1. STRUCTURE OF A CELL 11
2.2. IN VITRO CELL CULTURES 13
2.3. LABORATORY EQUIPMENT 17
2.4. BIBLIOGRAPHY 20

**IMPEDANCE SENSING ON CELLS** **23**

3.1. ELECTRICAL PROPERTIES OF CELLS AND CULTURE MEDIUM 23
3.2. ELECTRODE STRUCTURES 26
3.3. INTERDIGITATED ELECTRODE STRUCTURE AS SENSOR 29
3.4. SENSOR DEVICE CONSTRUCTION 30
3.5. SENSOR CHARACTERIZATION 38
3.6. DISCUSSION 43
3.7. BIBLIOGRAPHY 44

**MEASUREMENT SETUP** **49**

4.1. RF INTERFACE 50
4.2. MEASUREMENT ELECTRONICS 58
4.3. TAG DESIGN AND PACKAGING 68
4.4. REALIZED SYSTEM 72
4.5. DISCUSSION 74
4.6. BIBLIOGRAPHY 75

**EXPERIMENTAL RESULTS** **79**

5.1. SYSTEM TESTS AND PREPARATIONS 79
5.2. 3T3 MOUSE EMBRYONIC FIBROBLASTS 83
5.3. HUMAN MESENCHYMAL STEM CELLS 92

5.4. DISCUSSION 103
5.5. BIBLIOGRAPHY 105

**OUTLOOK 109**

6.1. DESIGN PROPOSAL 109
6.2. A MONITORING TECHNIQUE FOR THE INCUBATOR 110
6.3. IMPEDANCE MEASUREMENT: A FEASIBLE STANDARD ASSESSMENT TECHNIQUE? 111
6.4. BIBLIOGRAPHY 112

**DANKSAGUNG 117**

**ACKNOWLEDGEMENTS 119**

**LIST OF PUBLICATIONS 121**

**ÜBER DEN AUTOR 123**

**ABOUT THE AUTHOR 125**

# NOMENCLATURE

## List of Abbreviations

| Abbreviation | Description |
|---|---|
| AC | Alternating Current |
| ADC | Analog-to-Digital-Converter |
| AIT | Austrian Institute of Technology |
| ASK | Amplitude Shift Keying |
| CAM | Cell Adhesion Molecule |
| CESSEC | Cell Sensor Electronics Control,<br>PC control software of the invented measurement system |
| CRC | Cycling Redundancy Chechsum |
| DAPI | 4′,6-Diamidin-2-phenylindol |
| dBc | Dezi-Bel unit in which the reference value is a carrier signal. |
| DC | Direct Current |
| DFT | Discrete Fourier Analysis |
| DMEM | Dulbecco's Modified Eagle Medium |
| DNA | Deoxyribonucleic acid |
| DUT | Device Under Test |
| E. coli | Escherichia Coli (bacteria species) |
| ECIS™ | Electric Cell Substrate Impedance Sensing,<br>a trademark of Applied Biophyics |
| ECM | Extracellular Matrix |
| EDTA | Trypsin-Ethylenediaminetetraacetic-Acid |
| EtOH | Ethanol |
| FBS | Fetal Bovine Serum, also called FCS. |
| FCS | Fetal Calf Serum, also called FBS. |
| GBW | Gain-Bandwidth (Product) |
| GCP | Good Clinical Practice |
| GFP | Green Fluorescent Protein |
| GLP | Good Laboratory Practice |
| HEPES | 4-(2-hydroxyethyl)-1-piperazineethanesulfonic acid |
| hMSC | Human Mesenchymal Stem Cells |
| IC | Integrated Circuit(s) |
| IDES | Interdigitated/Interdigital Electrode Structure(s) |
| ISO | International Organization for Standardization |
| ITU | International Telecommunication Union |

| Abbreviation | Description |
|---|---|
| I/O | Input/Output (of a digital system) |
| LOR | Lift-Off Resist |
| LTCC | Low Temperature Co-firing Ceramics |
| MEM | Minimum Essential Medium |
| MSC | Mesenchymal Stem Cell |
| NHDF | Normal Human Dermal Fibroblast (cell line) |
| NRU | Neutral Red Uptake |
| OA | Operational Amplifier |
| ÖAW | Österreichische Akademie der Wissenschaften (Austrian Academy of Sciences) |
| OECD | Organization for Economical Co-operation and Development |
| PBS | Phosphate Buffered Saline Solution |
| PC | Personal Computer |
| PCB | Printed Circuit Board |
| PDMS | Polydimethylsiloxane |
| PIC | Programmable Interrupt Controller, a microcontroller family of *Microchip* |
| PTFE | Polytetrafluorethylene |
| RF | Radio Frequency |
| RFID | Radio Frequency Identification |
| RMS | Root Mean Square |
| RNA | Ribonucleic Acid |
| UPILEX® | Trademark of a polyimide produced by *UBE* |
| UV | Ultraviolet |
| µC | Microcontroller |

# List of Constants

| Symbol | Description | Value | Unit |
|---|---|---|---|
| $\varepsilon_0$ | Absolute permittivity | $8.8541\mathbf{9} \cdot 10^{-12}$ | $\mathrm{A\,s\,(V\,m)^{-1}}$ |
| $\mu_0$ | Magnetic permeability | $1.2566\mathbf{4} \cdot 10^{-6}$ | $\mathrm{V\,s\,(A\,m)^{-1}}$ |
| $\pi$ | Ludolph's number | $3.1415\mathbf{9}$ | – |
| F | Faraday constant | $9.6485\mathbf{3} \cdot 10^{4}$ | $\mathrm{A\,s\,mol^{-1}}$ |
| R | Gas constant | $8.3144\mathbf{6}$ | $\mathrm{J\,(mol\,K)^{-1}}$ |

# List of Variables

This is not a complete list but an overview of the most important variables.

| Symbol | Description | Unit |
|---|---|---|
| $c_x$ | Concentration of a certain species $x$ of an electrolyte | $\mathrm{mol\,m^{-3}}$ |
| $C_D$ | Capacity of the diffusion layer of an electrolyte | F |
| $C_{DL}$ | Capacity of an electrochemical double layer | F |
| $C_S$ | Capacity of the idealized polarizable electrode | F |
| $D$ | Diffusion constant of a certain substance | $\mathrm{m^2\,s^{-1}}$ |
| $f_0$ | Base frequency, e.g. 13.56 MHz of the RFID-system | Hz |
| $f_C$ | Clock frequency of a microcontroller. $f_C = 1/T_C$ | Hz |
| $f_{sc}$ | Subcarrier frequency. 250 kHz for the presented RFID-system | Hz |
| $f_X$ | Frequency of a certain probe signal. $f_X = 1/T_X$. | Hz |
| $G$ | Gap distance between two adjacent fingers of an IDES | m |
| $K_W$ | Frequency-independent factor of the Warburg-impedance | $\mathrm{\Omega\,m^2\,s^{-1}}$ |
| $L_1$, $L_2$ | Coil inductance of base station and tag, respectively. | H |
| $n$ | Electrode reaction valence | - |
| $R_t$ | Charge transfer resistance | Ω |
| $T_C$ | Clock period of a microcontroller. $T_C = 1/f_C$. | s |
| $T_X$ | Period of a certain probe signal. $T_X = 1/f_X$. | s |
| $V_{pp}$ | Peak-to-peak value of a sinusoidal waveform | V |
| $W$ | Width of a finger of an IDES | m |
| $\varepsilon_r$ | Relative permittivity of a certain substance | - |
| $\Lambda$ | Limiting conductivity of a certain substance | $\mathrm{S\,m^2\,mol^{-1}}$ |
| $\lambda$ | Finger-period $G + W$ of an IDES | m |
| $\sigma$ | Electrical conductivity of a certain substance | $\mathrm{S\,m^{-1}}$ |
| $\omega$ | Circular frequency | $\mathrm{s^{-1}}$ |

# Chapter 1

# INTRODUCTION

Cells can be viewed as both, tools for processing matter and objects of research. Among the first applications of cell cultures was species *Saccharomyces Cervisiae* which conduct a transformation of sugar to alcohol and carbon dioxide. Conventionally, this species plays a major role in the production of wine and beer. The art of brewery was already known several thousands years ago in ancient Egypt. Nowadays however, yeast cells as well as bacteria, e.g. *Escherichia coli* (E. coli), found a variety of other applications. Notably, the introduction of special genes allows the modification of cell metabolism to cover a broad field of functions for the production of chemical substances. Other types of cells, fungi, are mostly unwanted guests in microbiological laboratories and can also be hazardous parasites for humans, but they may be life-savers, too. For instance, the active component of the antibiotic Penicillin is produced by a fungus of class *Penicillium* which and was discovered by *Alexander Fleming* at St. Mary's Hospital, London in 1928. This discovery initiated a major step forward in the medical system and was awarded with the Nobel Price in 1945 [Schmitz 2007, Nobel Prize].

In recent years, mesenchymal stem cells (MSC) received attention for biotechnological and biomedical applications. In the field of stem cell therapy cell cultures of high quality are needed, but up to now there are no standardized methods available to quantify MSCs. In vitro cultivation is known to diminish MSC quality which undermines novel techniques and clinical utilization [Kassem and Abdallah 2008, Roobrouck et al. 2008]. Impedance measurements may be an appropriate tool for quantification of MSCs quality.

Another use of cell cultures, whose importance is continuously rising, is the replacement of toxicity tests which conventionally rely on animal experiments. Today, established methods for the assessment of the toxicity of chemicals or pharmaceutical products correlate well with *in vitro*-methods at short-term applications. In contrast, the detection of chronic toxicology can hardly be reproduced in cell cultures with conventional techniques and is still not satisfyingly solved. For each investigation adherent cells of a certain cell type need to be detached from their surface and for a continuous measurement each evaluation requires its own cell sample. Also, the detachment process itself, as well as the employed chemicals, e.g. Trypsin, Trypsin-Ethylenediaminetetraacetic-Acid (EDTA) combination or Accutase/Accutase II, cause stress on cells and destroy the cell culture matrix.

Conventional methods for acute toxicity, like the neutral red uptake test (NRU, see Appendix A) or the release of Lactate Dehydrogenase by defect cell membranes are based on massive cell damage which is not expected in the case of chronic toxicity. In contrast, cell proliferations, morphological changes, modifications of the cytosceleton and in the cell-matrix contacts are indicators for a number of harmful influences. They do not cause an immediate cell death but will result in toxic long-term effects. Most of those toxic effects affect the cell membrane and result in changes of the electric properties of the cell cultures and can be registered by an impedance monitoring. This opens up the way to apply impedance measurements for the detection of toxic effects.

Consequently the realization and validation of an electronic impedance monitoring system for adherent cell cultures are topic of this work. A wireless approach is presented which limits cable connections and gives operators a maximized freedom of movement.

## 1.1. Current Measurement Methods on Cell Cultures

### 1. Inverted Microscope

Two properties of cells generally call for the use of a microscope: Firstly, the size of cells and their organelles are clearly too small to be investigated without magnification. Secondly and more importantly, the extremely small variations in the optical transparencies/opacities of cells, cell membranes, cytosol, organelles and the culture medium require phase contrast techniques.

The inverted configuration of the optical path is necessary because the zoom property of a microscope is among other things limited by the distance of the objective to the object. If a microtiter plate or a flask is investigated with a conventional microscope the height of those objects limits the object distance and, therefore, limits the zoom factor. Even though it would be possible to flip the flask this procedure cannot be recommended (and is impossible for microtiter plates) because the cell layer with a thickness of just 5 to 10 µm would simply dry out. Thus, the whole optical system is inverted with a light source and condenser unit above and the objective below the object. FIG 1.1 shows a microscope including a second optical path for a digital camera.


FIG 1.1: An inverted microscope for the inspection of cell cultures including a digital camera. With permission of Ehlert & Partner, 53859 Niederkassel-Rheidt, Germany.

## 2. Fluorescence Microscopy

Fluorescence microscopy is a staining method which is based on the property of certain chemical substances to change their fluorescence behavior when they bind to specific molecules [Lichtman and Conchello 2005]. The investigated objects (cells or tissue) are treated with such chemicals, i.e. fluorescence marker. Those bind to proteins which are related to processes under investigation or which are part of a structure. In the latter case those proteins, for instance, may be Actin or Tubulin respectively, which build up the cytosceleton and microtubuli. The treated cell or tissue sample is then exposed to light with a well-defined spectral distribution and the bound markers are thus stimulated to emit light with a defined, longer wavelength.

Microscopic pictures taken of such cells enable investigation on the localization of those proteins, .e.g. in the cell nucleus, cytoplasm, or bound to the cell membrane. Hence proteins or structures can be localized and visualized. Moreover, binding processes and their dynamics can be studied.

Cell may also be genetically modified to express fluorescent proteins, e.g. the Green Fluorescent Protein GFP. The necessary ribonucleic acid (RNA) synthesis is controlled by specific substances, known as promoters. This allows the detection of specific cell types which cannot be clearly identified by a classical microscopic technique. FIG 1.2a shows a picture known as the *Glowing California Sunshine*. There, Escherichia Coli (E. coli) bacteria cultures were genetically modified to express fluorescent proteins [Tsien 2009].

In FIG 1.2b *Normal Human Dermal Fibroblasts* (NHDF) are treated with 4′,6-Diamidin-2-phenylindol (DAPI). The stimulating wavelength is 358 nm, the emission at 461 nm. DAPI markers are preferred if deoxyribonucleic acid (DNA) alone is the subject of investigation while *Acridin Orange* also emits light if it binds to RNA.

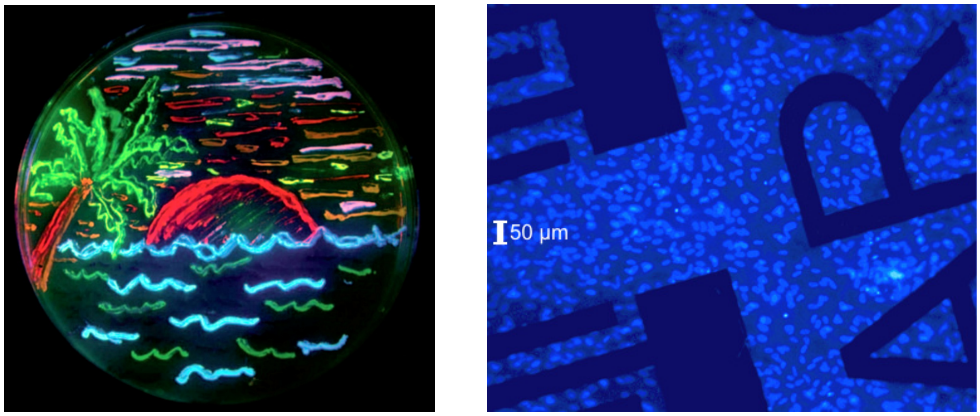


(a) (b)

FIG 1.2: Examples for Fluorescent microscopy. (a) *Glowing California Sunshine*, a number of different Escherichia coli bacteria cultures on a petri dish which were genetically modified to express different fluorescent proteins [Tsien 2009]. (b) Glass chip with Au metal structures (opaque), marker substance is DAPI which binds on DNA.

## 3. Coulter Counter

In 1956 Wallace H. Coulter introduced a novel counting principle for cells [Coulter 1956]. Here, particles or cells in a weak electrolytic solution are guided through a small hole from one basin into another. Each reservoir has an integrated electrode. A voltage between those electrodes forms a measurement zone inside the tube. When the particles or cells pass the hole they replace the solution and cause a change in the measured impedance between the electrodes. This change can be further processed. If a well defined volume of the electrolyte passes the hole the particle density can therefore be determined. The shapes of the pulses also provide information on the size of the particle which in turn depicts information on the size distribution. FIG 1.3a shows a detail from the original drawings in [Coulter 1956] while in FIG 1.3b a modern Coulter counter is shown.


(a) (b)

FIG 1.3: **(a)** Detail of the original setup introduced in [Coulter 1956]. Two electrodes *C* and *D* are positioned in a cell suspension sample *E* and a reservoir *B*. Both volumes are connected via an aperture *A*. A pumping system built up by a vacuum from outlet *P* via vent *F* starts a sample flow through *A*. The outlet on the left of vent *F* leads to a mercury-based pumping system (not shown) which does also start and stop a counting electronics being in contact with *C* and *D*. Outlet *O* and vent *G* are for fast regeneration of the system pressure for a further counting. **(b)** *Z1 series Coulter Counter Cell and Particle Counter* suitable for counting cells or particles with diameters in the range of 1 µm to 120 µm. With permission of *Beckman Coulter, Inc.*, Miami, USA.

## 4. Flow Cytometry

Flow cytometry is conventionally used for counting, sorting, and investigation of microscopic particles as well as cells suspended and flowing in a proper dilution liquid [Dittrich 1975]. It allows the determination of the properties of single cells flowing through a measurement capillary. A monochromatic light beam, e.g. a laser, is focused onto the flow in this tube. Specific detectors analyze the light scattered from the particles and cells also registering one or more fluorescence signals emitted from the cells. Each particle or cell in the liquid scatters light in a characteristic way when it passes the capillary. The scatter-signal in forward-direction is used to detect the cell volume while the signal of a detector in a 90° angle gives information about the inner complexity of a cell (shape of the nucleus, roughness of the membranes). Before the analysis takes place cells can in addition be marked by a treatment with agents containing fluorescent components (e.g. antibodies). A combination of the scattered and fluorescent light is then analyzed. Fluctuations of the detector signals allow the characterization of cells and their components and can even be used for deriving conclusions regarding the cellular metabolism.

## 1.2. Performance Characteristics

Basic properties of a cell culture can be inspected with an inverted microscope, e.g. confluence or morphology. Such work is currently done manually, even though automated systems are under investigation [Ji *et al.* 2005, Moscelli *et al.* 2011]. The only active component is a light source. Apart from that, this method is non-invasive but during visual inspection culture medium and the cells may cool down. Such temperature-shock can be minimized by heat-able cross-tables. Microscopy is the first step for almost any investigation on cell cultures. Nevertheless, the information value is limited by the optical resolution of about 1 µm. Also, details of the inner structure are hidden. For a more detailed analysis on a molecular level fluorescence microscopy is needed.

Fluorescence microscopy allows the detection of many events and dynamic processes within a cell culture and is also useful for identification of specific structures, e.g. organelles, the cytosceleton, or DNA. Depending on the used marker some methods only show viable cells while others show both viable and dead cells. Information of details on the viability can also be achieved.

If a marker is added to a cell culture, this culture will not be used for further experiments since the marker substance can be toxic or a chemical reaction with the substance during the test may occur. For instance, the use of DAPI requires the cell culture to be washed and incubated with methanol. Also, marker molecules are often larger than the substance under test (antigen-antibody reactions) and thus influence system kinetics. Many conventional markers lack of long-term stability and repeated stimulation leads to bleaching, long-term tests are therefore not applicable. Furthermore, there is only a limited number of markers available, which are useful for the detection of a certain event and the executed procedure is strongly determined by the selected marker. In many applications only endpoint detection is realized because some processes (e. g. hybridization processes) are merely possible under well defined process parameters in incubators (temperature, $CO_2$-atmosphere). Moreover, the analysis is punctual and online-monitoring of the kinetics is not possible.

Coulter Counter and Flow Cytometry basically differ in their means of detection and represent single-analysis methods where cell cultures need to be extracted from their matrix and brought into suspensions. Thus, information about the cell matrix is lost. Single cells show a different behavior compared to a cell matrix because of the absence of signal paths and cell-cell-interactions. In such a system, a long-term online-monitoring cannot be carried out without the extraction of single cells.

## 1.3. Impedance Measurement as a Tool in Microbiology

A non-invasive detection system allows a continuous monitoring of the same cell culture over a long period. In the 1920’s first impedance measurements on cell cultures were

carried out. These, and further measurements on cells in the following decades, were primarily performed on suspension cultures commonly used in an industrial scale [Fricke 1925, Colvin *et al.* 1977, Cady *et al.* 1978].

Experiments with adherent cell cultures started in the late 1970's and several experiments were published by *Ivar Giaever* and *Charles R. Keese* in the 1980's and early 1990's. Since then, investigations in impedance measurements on different types of adherent cells were continued and multiple sensor geometries presented [Giaever and Keese 1984, Ehret *et al.* 1997, Acea Biosiences 2009]. Today's applied voltages and currents do not show signs of a harmful influence on cell cultures. The absence of specific markers enables continuous measurements on cell cultures and reduces the hazardous potential for operators since DNA-markers are often mutagenic and cancerogenic substances (e.g. DAPI, Methylene blue, or Hoechst 33342).

In this work an interdigitated electrode structure as the sensing device is combined with a novel wireless impedance measurement technique to be operated within the humid atmosphere of an incubator. Initial experiments for the verification of the system functionality on *3T3 mouse embryonic fibroblasts* [1] [Todaro and Green 1963] are followed by a long-term monitoring over three weeks on *human mesenchymal stem cells* (hMSC).

## 1.4. Thesis outline

The introduction is followed by chapter 2 which describes cell biology and the required laboratory environment. Generally, biologic cells have cell-type-specific requirements for optimal growth and proliferation conditions. A widely used and standardized set of materials and methods for their handling which incorporates culture flasks, sterilization techniques and devices such as an incubator or a laminar flow cabinet, is presented.

Chapter 3 introduces the impedance sensing methodology and describes a biological cell and its environment from an electrical point of view, in detail the capacitive and conductive properties of the cytoplasm, the cell membrane, and the extracellular matrix and the culture medium. The geometric and electric properties of a cell culture allow a variety of impedance sensor structures. Some of them are presented followed by a characterization of the selected sensor geometry and the specification of the sensor device.

Chapter 4 describes the impedance measurement setup. A wireless approach for a comfortable handling of the system within the laboratory environment is presented. That requires the design of an RF-interface and a measurement technique with low power consumption. The requirements for the RF-interface are discussed and a realization is

[1] 3T3 is a labeling suggested in [Todaro and Green 1963] and represents an initial cell number of $3 \cdot 10^5$ and cell passage every 3 days when this cell line was established. *3T3 fibroblast* or *3T3 cell* (*culture*) are commonly used abbreviations.

presented. The operation within the humid environment of an incubator is ensured by a proper silicone-based encapsulation and packaging of the measurement electronics.

Experimental results are presented in chapter 5. First, the system is tested and an operation procedure established. It will be shown that the humidity level and the system temperature have a strong influence on long-term measurements. The proliferation of 3T3 fibroblasts and the proliferation and differentiation of hMSC to bone and fat cells is presented.

An outlook on the impedance monitoring technique is given in chapter 6. Side-effects such as the sensitivity of the sensor to temperature and humidity as a qualitative indicator for the incubator atmosphere are examined. Finally, advantages and disadvantages of impedance monitoring compared to conventional methods are discussed and how those different techniques of a microbiologist's toolbox may complement one another.

## 1.5. Bibliography

Acea Biosiences: *Impedance based apparatus and methods for analyzing cells and particles*. European Patent EP 1527328 B1 (2009).

Cady P., Dufour S.W., Shaw J., Kraeger S.J.: *Electrical Impedance Measurements: Rapid Method for Detecting and Monitoring Microorganisms*. J. Clinical Microbiol. 7 (3), pp. 265-272 (1978).

Colvin H.J., Sherris J.C.: *Electrical Impedance Measurements in the Reading and Monitoring of Broth Dilution Susceptibility Tests.* Antimicrobial Agents and Chemotherapy 12 (1), pp. 61-66 (1977).

Coulter W.H.: *High Speed Automatic Blood Cell Counter and Cell Size Analyzer*. Natl. Electron. Conf. 12, Chicago (USA), pp. 1034-1042 (1956).

Dittrich, W.: *Flow-Through Chamber for Photometers to Measure and Count Particles in a Dispersion Medium*. Patent DE 1815352 (1975).

Ehret R., Baumann W., Brischwein M., Schwinde A., Stegbauer K., Wolf B.: *Monitoring of cellular behaviour by impedance measurements on interdigitated electrode structures*. Biosens. Bioel. 12, pp. 29-41 (1997).

Fricke H.: *The Electric Capacity of Suspensions of Red Corpuscles of a Dog*. Phys. Rev. 26 (5), pp. 682-687 (1925).

Giaever I., Keese C.R.: *Monitoring fibroblast behavior in tissue culture with an applied electric field*. Proc. National Academy of Sciences USA 81 (12I), pp. 3761-3764 (1984).

Ji H., Abshire P.A., Urdaneta M., Smela E.: *CMOS contact imager for monitoring cultured cells*. IEEE Int. Symp. Circ. Sys. 4, ISBN 0-7803-8834-8, pp. 3491-3494 (2005).

Kassem M., Abdallah B.: *Human bone-marrow-derived mesenchymal stem cells: Biological characteristics and potential role in therapy of degenerative diseases*. Cell and Tissue Research 331 (1), pp. 157-163 (2008).

Lepperdinger G., Brunauer R., Jamnig A., Laschober G., Kassem M.,: *Controversial issue: is it safe to employ mesenchymal stem cells in cell-based therapies?* Exp. Gerontol. 43 (11), pp. 1018-1023 (2008).

Lichtman, J. W. and Conchello, J. A.: *Fluorescence Microscopy*. Nature Methods 2, pp. 910-919 (2005).

Moscelli A., van der Driesche S., Witarski W., Pastorekova S., Vellekoop M.: *An imaging system for real-time monitoring of adherently grown cells*. Sensors Actuat., A 172, pp. 175-180 (2011).

Nobel Price, official web site nobelprize.org.

Roobrouck V.D., Ulloa-Montoya F., Verfaillie C.M.: *Self-renewal and differentiation capacity of young and aged stem cells*. Exp Cell Res 314 (9), pp. 1937-1944 (2008).

Todaro G.J., Green H.: *Quantitative Studies of the Growth of Mouse Embryo Cells in Culture and their Development into established Lines.* J. Cell Biol. 17, pp. 299-313 (1963).

Tsien R.Y.: *Constructiong and Exploiting the Fluorescent Protein Paintbox (Nobel Lecture)*. Angew. Chem. Int. Ed. 48, pp. 5612-5626 (2009).

Schmitz S.: *Der Experimentator: Zellkultur*. 1. Auflage, Elsevier GmbH München, ISBN 978-3-8274-1564-6 (2007).

# Chapter 2

# CELL BIOLOGY AND LABORATORY ENVIRONMENT

Since the content of this work is the setup of an electronic measurement system for cell cultures, a brief introduction to the specific properties of cells is given here. It includes the basic inner structure of a cell, its behavior within a cell culture, its handling and the required laboratory environment. The latter is of high importance during the design phase of the electronic measurement system. General information on the following sections can be found in [Schmitz 2007, Lodish 2008, Horton *et al.* 2008].

The first microscopic studies on cells as living objects were conducted already more than 400 years ago with small optical lenses produced by *Antoni van Leeuwenhoek*. However, microbiology, as we know it today, is a relatively young science and has its roots in the beginning of the 20$^{th}$ century. In 1910 *Warren H. Lewis* carried out the first cultivation of cavy cells and was later able to cultivate cells of chicken's organs. In the 1950's the culture medium *Dulbecco's Modified Eagle Medium* (DMEM) was developed which based on *Harry Eagle*'s *Minimum Essential Medium* (MEM). Many of today's cell studies still rely on these media. They were also used in this work. In 1961 *Leonhard Hayflick* rebutted the 40 years persisting dogma of unlimited cell division. The latter being a result of systematic fallibility prevalent in the experiment of *Alexis Carrel*, the originator of cell cultures in a laboratory environment.

## 2.1. Structure of a Cell

A cell (lat. *cellula* = small chamber) is conventionally seen as the basic unit of biological life. There are unicellular organisms, such as bacteria, and multicellular organisms consisting of several different types of cells forming functional units within higher organisms, e.g. the human body. The size of cells varies typically between 1 and 50 µm depending on their type and actual metabolic state. Some cells may also achieve sizes above 100 µm, such as the human ovum or megakaryocytes.

Living cells can be categorized into domains[2], i.e. Bacteria and Archaea, summarized as Prokaryotes, and Eukaryotes. The latter diverges into numerous kingdoms

[2] The domains do not yet represent a fixed system. The separation is based on phylogenetic analysis as well as on the inner structure of the cells. For instance, Archaea have some properties in common with Eukaryotes.

one of which being the animal kingdom. FIG 2.1 illustrates the fundamental schematic of a eukaryotic cell.

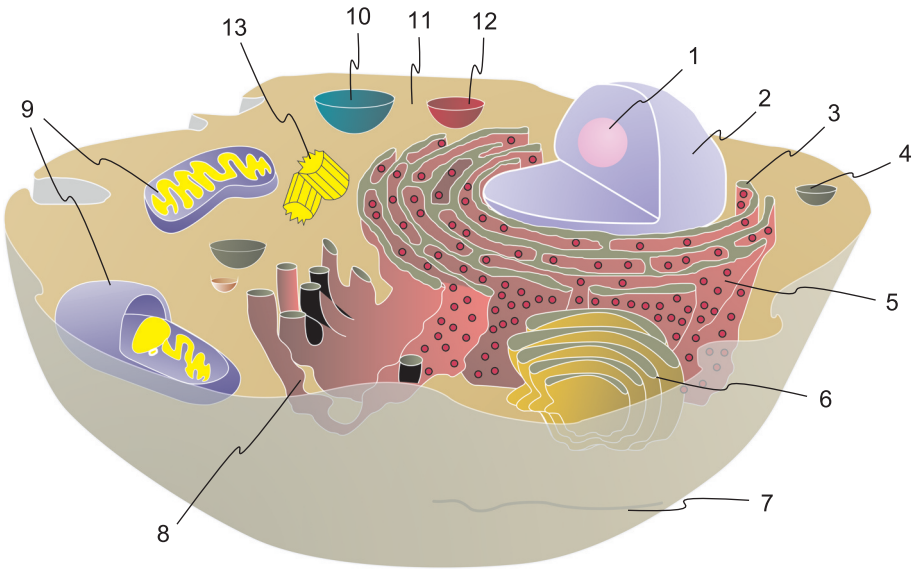


FIG 2.1: Typical structure of a eukaryotic cell with organelles. **(1)** Nucleolus, **(2)** Nucleus, **(3)** Ribosome, **(4)** Vesicle, **(5)** Rough endoplasmic reticulum, **(6)** Golgi apparatus, **(7)** Cytoskeleton, **(8)** Smooth endoplasmic reticulum, **(9)** Mitochondrion, **(10)** Vacuole, **(11)** Cytosol, **(12)** Lysosome, **(13)** Centriole.
Source: Unified resource locator http://de.wikipedia.org/wiki/Datei:Biological_cell.svg downloaded in October 2011, originally created by Wikipedia-authors *Szczepan1990* and *MesserWoland*, published under a Creative Commons BY-SA 3.0 license. The original work has been modified. The Creative Commons License is reprinted in Appendix D.

A eukaryotic cell has a cytoskeleton formed by Actin filaments and other components. The cytoskeleton gives the cell its shape and its frequent reorganization enables cell migration which is a kind of motion.

The outer hull is formed by a lipid double layer, the cell membrane, which is built up by tightly arranged phospholipids. They consist of a hydrophilic head and a tail formed by a saturated and an unsaturated carbonhydrogen-chain. This tail is lipophilic and two of the layers, oppositely arranged, form the cell membrane. Water passes directly through it but for the ion exchange with the outer environment the membrane is interstratified with proteins as ion-channels. The cytoskeleton acts as an anchor for several types of such membrane proteins. FIG 2.2 illustrates the structure of a cell membrane. More details in context with the electrical properties are provided in the following chapter which discusses the design of the sensor device.

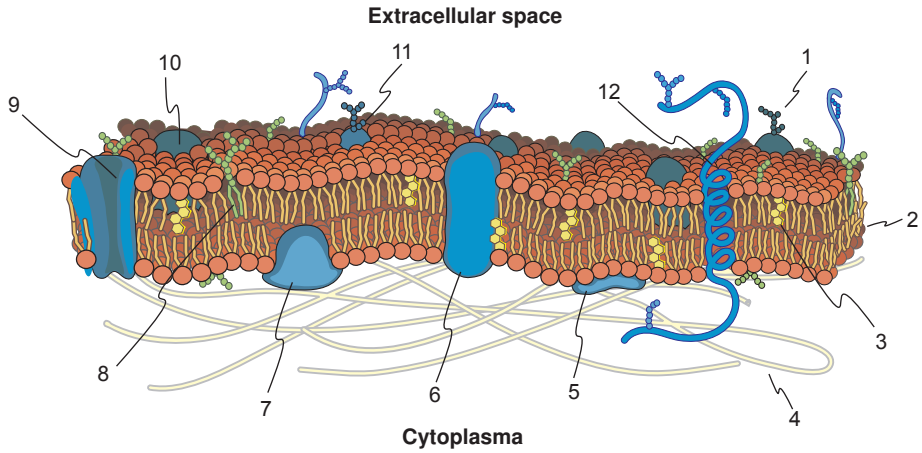


FIG 2.2: Structure of a cell membrane. **(1)** Carbonhydrate chain, **(2)** Phospholipid molecule, **(3)** Cholesterin, **(4)** Cytoskeleton filament, **(5)** Surface protein, **(6)** Integral protein, **(7)** Peripheral protein, **(8)** Glycolipid, **(9)** Channel protein, **(10)** Globular protein, **(11)** Glycoprotein, **(12)** α-helix.
Source: http://upload.wikimedia.org/wikipedia/commons/4/4b/Cell_membrane_detailed_diagram_de.svg, downloaded in October 2011, created by Wikipedia-author *LadyOfHats*, published as public domain. The original work has been modified.

The inner volume of a cell contains several organelles and a nucleus. Their boundaries are also formed by lipid double layer membranes. The residual volume is filled with cytosol which is a watery solution with a honey-like consistency. Amongst others the cytosol contains water, electrically neutral molecules, proteins and solvated ions.

Animal cells are surrounded by an extracellular matrix (ECM), a collective term for all of its components. Those are water, a network of fibers (different kinds of collagen, Fibrillin, Elastin) and a basic substance consisting of glycosaminoglycans, proteoglycans and adhesion proteins. Additionally, it contains hormones, nutrients, salts, etc. The functions of the ECM are numerous: mechanical stability, nutrient reservoir, resilience of tissue, tensile strength of bones and filaments, filter mechanisms (e.g. kidney, colon, lungs, blood-brain-barrier), etc.

## 2.2. In Vitro Cell Cultures

Generally, the source of a cell line is the corresponding tissue of a certain animal. First, the cell type of interest is extracted of the tissue and cultivated. This initial culture is known as the primary culture. The cells grow on a proper substrate (polystyrene, glass, etc) as a two-dimensional cell layer. That population growth and doubling goes on as long as cells do not inhibit each other. If inhibition due to the direct contact of cells among each other starts (known as contact inhibition), the cell layer needs to be detached, diluted with fresh culture medium and seeded again, e.g. with an initial effective occupied growth area of 10 %. This procedure is known as a cell passage.

## 1. Culture flasks and microtiter plates

The investigated adherent cell cultures are cultivated in flasks. Most of the flasks are one-way-products made of Polystyrene. This is a hydrophobic material and adherent cells cannot always grow on such surfaces. Thus, the inner lining of the flasks are often modified to become hydrophilic as a part of the production process or may even get a special coating with complex organic substances for a better cell growth performance.

A test setup requires several samples to be investigated for a significant analysis. For this purpose, microtiter plates are used which comprise of a number of wells in a common rack. The plate has a cover with condensation rings over each well avoiding well-to-well cross-contamination. Standard models have 6, 12, 24, 48, 96, 128 or 384 wells. FIG 2.3 shows a typical microtiter plate and a cell culture flask.

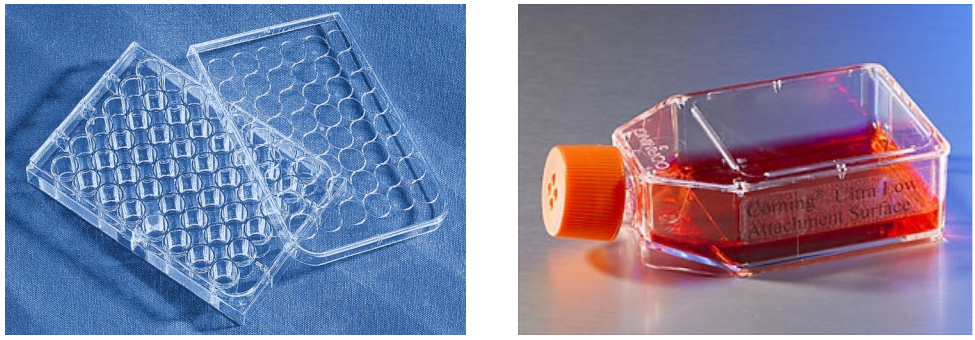


(a) (b)

FIG 2.3: **(a)** 48-well microtiter plate with cover. **(b)** Cell culture flasks with 25 $cm^2$ cell growth area filled with culture medium. The medium is supplemented with Phenol-red as pH-indicator. Both pictures with permission of *Corning Inc.* (14831 Corning, New York, USA).

## 2. Culture media

Culture media contain the inevitable nutrients to keep cells alive. Additional components such as a serum stimulate cell growth and doubling. Culture media are complex solutions with dozens of ingredients. Appendix A provides the ingredients for DMEM which is often used for fibroblasts or epithelial cells. Add-ons and variations of specific media rely on the used cell culture and the experimental setup. Culture media may be supplemented with antibiotics and antimycotics to suppress infectious contamination, e.g. Penicillin and Streptomycin. However, such substances are not always desirable as they may influence the test results, too.

Modern incubators do often have an active $CO_2$ control. Then, the gas dissolves in the medium and stabilizes the pH value. If such a system is not available the medium is supplemented with a proper buffer system, e.g. 4-(2-hydroxyethyl)-1-piperazineethane-sulfonic acid (HEPES) or Sodium Bicarbonate $NaHCO_3$.

## 3. Adherence, cell growth and population doubling

Adherent cell cultures attach to a proper surface via cell adhesion molecules. These, and several other mechanisms, also allow connections to adjacent cells. Cell adhesion molecules anchored at the cytosceleton attach on the substrate. Hence the membrane is kept within a distance of 20 to 100 nm to the surface.

Prior seeding the cells are prepared as suspension in culture medium. There, they have an almost spherical shape. During attachment and spreading cells flatten to a height of 5 to 10 µm. The adhesion process starts within a few minutes once the cells settle down. See FIG 2.4 for an illustration of that procedure.

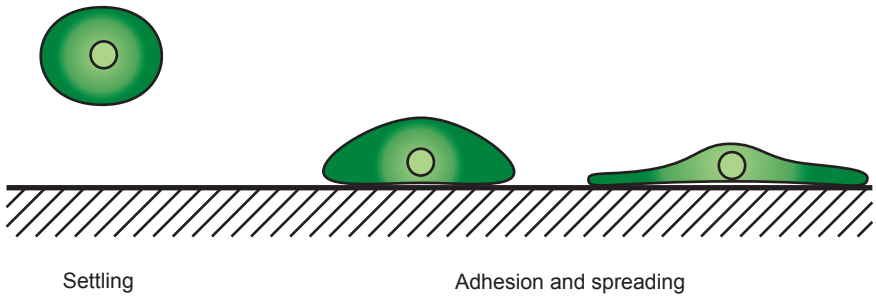


FIG 2.4: Settling, adhering and spreading of a single cell when seeded onto a substrate in a suspension. The circular inner part represents the nucleus. The height of the adhered and flattened cell is 5 to 10 µm. See also FIG 2.5 for microscopic pictures of such a process.

Generally, the ability for adherence of a cell depends on the cell type. For instance, *in vivo* lymphocytes flow in the lymphoid system while fibroblasts or endothelian cells adhere to other cells. Thus, *in vitro*, lymphocytes are cultivated in a solution whereas fibroblasts grow on a proper substrate. In that artificial environment cells are exposed to growth factors stimulating growth and population doubling (depending on the test setup). This growth factor mixture is part of a serum in the culture medium, e.g. the Fetal Calf Serum (FCS, also called Fetal Bovine Serum, FBS). Several adherent cell types grow in a 2-dimensional cell matrix until they are surrounded by other cells or another kind of border. This natural growth inhibition of adherent cell cultures (except several types of tumor cells) is known as contact inhibition. It means that cells stop doubling when they are surrounded by other cells. If a cell culture shall go on with doubling a *cell passage* needs to be conducted, this term is used to describe a small amount of the cell culture being seeded on a new substrate. The procedure is explained in detail in Appendix A.3.

If there is enough space, i.e. contact inhibition is hindered by a large growth area, cells show an exponential growth behavior which means doubling of the cell number within a defined period of time. As soon as a certain number of cell doublings took place (about $50^{\pm 10}$) cell growth is reduced and most cells die. This limitation is known as the

Hayflick-limit, named after Leonard Hayflick [3]. However, there are several cell lines which do not show such a limit or have an extended one, e.g. tumor cells, such as the HeLa cell line, or spontaneous immortalized cells such as the 3T3 fibroblasts.

Adherence is an extremely important feature for the utilized impedance measurement method. For instance, if cells die, they do often detach but remain on the surface as globular objects. Even if a full layer of such dead cells or, in the case of contamination, a confluent layer of bacteria or fungi remains on the sensor its impedance cannot be distinguished from sensors being free of cells.

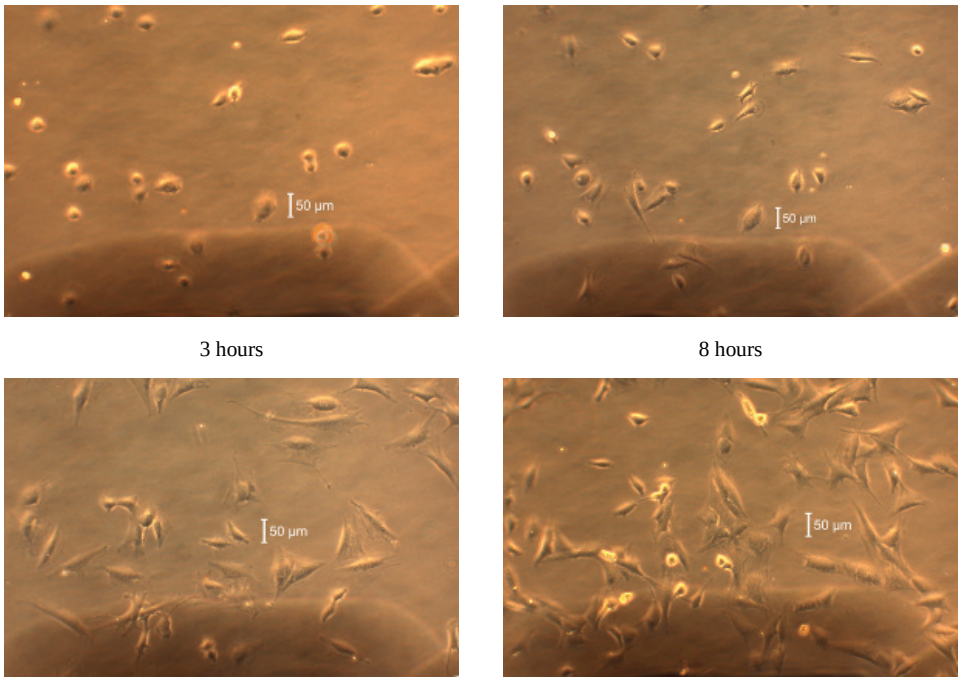


FIG 2.5: Phase contrast microscopy of the growth of 3T3 fibroblasts within a DMEM nutrient solution in a culture flask (25 $cm^2$ growth area) made of polystyrene. This cell type doubles its number in a period of about 20 h. Note, cells do not remain in the same position but migrate. The timestamps refer to the seeding time. Pictures were taken at the Austrian Institute of Technology (AIT).

FIG 2.5 shows the growth of 3T3 fibroblasts. The timestamps refer to the seeding time. Within the first hour cells settle down and adhere on the substrate. After 8 hours their

[3] Chromosomes are terminated by telomeres, i.e. repetitive DNA-sequences. Those sequences are not fully replicated in the case of a cell doubling and if they undergo a certain length apoptosis is initiated, i.e. a controlled cell-death. This limitation is an evolutionary protection mechanism against abnormal mutations as each cell doubling implies the risk of DNA replication errors.

spreading (and also movement) can be observed. A population doubling occurs within 20 hours. Hence, 24 hours after seeding the picture shows the double number of cells. Note, some cells are significantly larger than they are after seeding and require a comparably large area on the substrate.

After 48 hours the number of cells increased again and some cells accumulated enough nutrients and did the necessary preparations for another doubling within the following hours.

## 2.3. Laboratory equipment

Nowadays an operator has numerous tools for handling and investigating cells. Cell culture flasks and the culture medium were described in the previous section, the following contents show the most important inventory and devices. Standards such as EN 12469, EN 61010, EN 12741 with protocols like *Good Laboratory Practice* (GLP) or *Good Clinical Practice* (GCP) and many more define requirements for the used materials, handling and testing procedures.

### 1. Sterilization Techniques

Working with cell cultures carries the risk of biological contamination with e.g. bacteria, fungi or viruses. This risk can be minimized by wearing protective clothes and sterilization of the used tools and apparatuses.

Two different terms, namely sterilization and disinfection, are distinguished: *Disinfection* is the reduction of augmentable organisms by a factor of $10^5$. A more general meaning is the transformation of living or dead matter into a non-infective state. *Sterilization* is the reduction of augmentable organisms by a factor of $10^6$. This definition includes recognition that sterile goods are not necessarily free of augmentable organisms.

Please note, systems used in the microbiological laboratory work cannot be made 100 % free of living organisms which is reflected by both above named definitions. The following methods describe the most important techniques for microbiological laboratory work.

#### Autoclave

Microorganisms are sensitive to heat and die during exposure to high temperature. Autoclave systems consist of a heatable pressure chamber which is filled with the items to be sterilized [4].

[4] *Higher temperature* is a fuzzy terminus within this context since some hyperthermophile organisms have their optimum proliferation temperature above 100 °C. The actual record holder is an archaea *Strain 121* with a maximum growth temperature of 121 °C [Kashefi and Lovley 2003]. In contrast, several proteins of animal cells already denaturize at temperatures exceeding 40 °C.

Two methods are available, namely dry and wet sterilization. The former heats the goods to 180 °C and remains at that temperature for 45 minutes. The latter has a water reservoir in the autoclave volume and the chamber is heated to 121 °C. The water evaporates until a saturated vapor atmosphere is established at a pressure of 2000 hPa. The sterilization period is 15 to 30 minutes. The advantage of vapor is that (endo-) spores are easier affected compared to dry heat. Autoclaving may be applied to all goods which are not sensitive to heat.

**Ethanol, Isopropanol and other disinfectants**

A mixture of 70 % ethanol (EtOH) and 30 % water is widely used for disinfecting all kinds of surfaces in a laboratory, also for (latex-gloved) hands and additional instruments. During this work, ethanol is used for storage of the invented sensor devices and for the cleaning of the measurement electronics surfaces. Other disinfectants are hydrogen peroxide $H_2O_2$ (especially in surgery), ethylene oxide $C_2H_4O$ in the field of medical implants, and a number of special chemical mixtures.

**Ionizing irradiation – UV light, electron beam and γ-irradiation**

Gamma- and x-ray-irradiation as well as electron beams are used for final sterilization after e.g. cell culture plastics (disposables such as microtiter plates, pipette tips, culture flasks) are packaged for delivery. These methods ensure the sterilization of volumes of several cubic meters within seconds and avoid recontamination.

Exposure to ultraviolet (UV) light is a commonly used method in laboratories as a final sterilization step after cleaning e.g. laminar flow cabinet. For that purpose the cabinets have UV lamps installed which are illuminated for several hours. One disadvantage of UV is that it cannot be used to sterilize the interior of opaque casks and glass usually absorb at this wavelength.

During this work, UV light is utilized to sterilize the surfaces of those electronic and mechanical parts of the designed apparatus which share the incubator atmosphere with the microbiological cell cultures. Notice, γ- and electron beams cannot be used for this task since γ-sources are only available in very restricted areas of a select and moreover the high energetic irradiation causes irreversible damage in the semiconductors of the measurement electronics [Derbenwick and Gregory 1975].

## 2. Incubator

Cell cultures require specific conditions for their growth. This includes the culture medium, its pH-value and the temperature. Several shelves for stacking and storing cell culture flasks are available. Typical incubators have two doors. The outer one provides the thermal isolation while the inner glass door avoids unnecessary atmospheric exchange with the laboratory environment during a visual inspection. An incubator, as depicted in FIG 2.6, provides the necessary atmospheric conditions for the cell cultures.

FIG 2.6: Incubator with $CO_2$- and temperature-controlled atmosphere. The inner lining and racks are made of stainless steel. On the bottom a reservoir provides water for a humidified atmosphere and an external gas container is used as a $CO_2$ supply.

Mammal cells require a temperature of 37 °C for optimal growth. The temperature is controlled within ±1 K. A $CO_2$-source is needed to stabilize the pH-value of the culture medium by diffusion and a water basin at the bottom of the incubator volume ensures a sufficiently high humidity to minimize culture medium evaporation. After opening and closing the incubator the regeneration of the humidity level to values greater than 90 % may take several hours.

## 3. Laminar Flow Cabinet

A Laminar Flow Cabinet is also known as *Laminar Flow* or *Flow Box*. Its name results from the laminar air flow originating from the air ventilation system featured above the cabinets work surface. The air flow is filtered and provides protection against microbiological contamination for probes inside the box. Slits at the front of the working area are intakes for this stream. Additionally, air from the surrounding environment is ingested into these slits at the opening to the workplace. This ensures protection for the operator and likewise for the laboratory environment against pathogenous substances. Modern models have integrated UV-fluorescent tubes for disinfecting the surfaces, commonly left running overnight.

In such workbenches culture media are exchanged, cell cultures are seeded and all other work is performed which requires the protection of samples against microbiological contamination or which calls for a degree of protection for the operator.

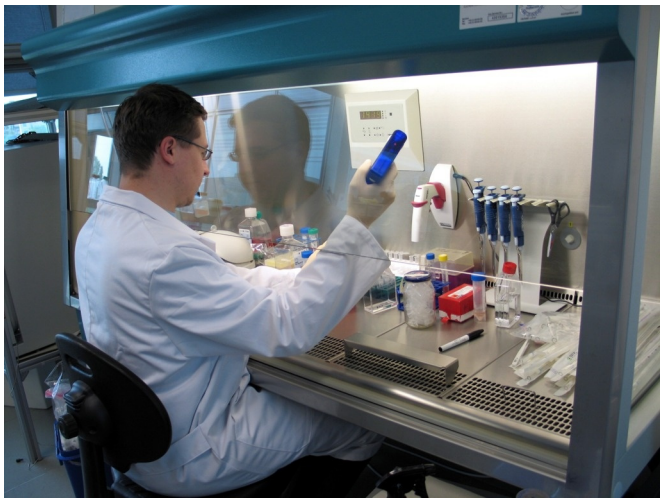

FIG 2.7: Class II laminar flow cabinet. The slits at the edge of the work bench are intakes for a laminar flow of filtered air coming from the top inside the box. Also, air from the laboratory environment is ingested. This double flow ensures contamination protection inside the work bench and a protection of the operator and the laboratory against chemicals and microorganisms which could otherwise get out of this restricted volume.

## 2.4. Bibliography

Derbenwick G.F., Gregory B.L.: *Process Optimization of Radiation-Hardened CMOS Integrated Circuits*. IEEE T. Nucl. Sci. 22, pp. 2151-2156 (1975).

Horton H.R., Moran L.A., Scrimgeour K.G., Perry M.D., Rawn J.D.: *Biochemie*. 4. Auflage, ISBN 978-3-8273-7312-0, Pearson Studium (2008).

Kashefi K., Lovley D.R.: *Extending the Upper Temperature Limit for Life*. Science 301 (5635), p. 934 (2003).

Lodish H.F.: *Molecular Cell Biology*. 6th edition, W.H. Freeman & Co, ISBN 978-0-7167-7601-7 (2008).

Schmitz S.: *Der Experimentator: Zellkultur*. 1. Auflage, Elsevier GmbH München, ISBN 978-3-8274-1564-6 (2007).

# Chapter 3

# IMPEDANCE SENSING ON CELLS

The evaluation of adherent cell lines via electrical impedance measurement is a young discipline with respect to measurements on suspension cultures [Fricke 1925, Fricke and Curtis 1934, Wheeler and Goldschmidt 1975]. Suspension cultures are often assessed in an industrial production scale while the estimation of adherent cells still has a highly experimental or laboratory character. In both cases differences in the impedance changes of cells and cell culture, respectively, and the surrounding culture medium are recorded. The growth of cells, as well as their morphological evolution alters the impedance of the system.

Monitoring suspension cultures is a rather straight forward process. E.g. two or four rod-shaped electrodes made of noble steel can be positioned in the suspension culture flask and an optional stirring system avoids that cells settle down due to gravity [Wheeler and Goldschmidt 1975]. Suitable electrodes may have a diameter of 1 mm and more and can be fabricated in workshops. In contrast, adherent cells require a proper substrate for settling down, adherence and growth, mostly as a two-dimensional cell layer. Such a layer has a thickness of less than 100 µm while the culture medium above may have a height of several millimeters. An impedance measurement utilizing two electrodes positioned in the culture medium e.g. from the top side will generally not allow the detection of cells as long as no electrode is covered with cells. Thus, at least one sensing electrode needs to be part of the growth area of the cell layer. Sensor structure suitable for monitoring adherent cells require fabrication methods based on thick-film and thin-film technology as well as photo lithography. This chapter provides information on the electrical properties of cells and their surrounding environment leading to a suitable sensing electrode geometry, the sensor's production process and electrical characteristics.

## 3.1. Electrical Properties of Cells and Culture Medium

### 1. Cytosol and Culture Medium

The composition of a culture medium is tailored to mimic the in-vivo-environment of the investigated cell type. Supplements are added depending on the application, i.e. serum, antimycotics, antibiotics, glucose, and other chemicals (see Appendix A).

TABLE 3.I shows the concentration of ions which are mainly responsible for the electrical conductivity of the cytosol and the extracellular matrix [Lodish 2008]. The

concentrations in ECM are almost the same as in the widely used culture medium DMEM. Data for the limiting conductivity are taken from [Hamann *et al.* 2007]. Please note, the constants are only valid for a single ion type in an aqueous solution but in the present case several solvated ions and supplements need to be taken into account [5]. They reduce the effective conductivity. The data agree well with the published values of 1.8 S/m and 1.5 S/m, respectively [Pethig 1984, Ehret *et al.* 1997].

TABLE 3.I: Ion Concentrations and calculated conductivities of the Cytosol and the Extracellular Matrix

| Ion | | Cytosol | | ECM | |
|---|---|---|---|---|---|
| | $\Lambda_0$ mSm²/mol | $c_{cyt}$ mol/m³ | $\sigma_{cyt}$ S/m | $c_{ecm}$ mol/m³ | $\sigma_{ecm}$ S/m |
| Na | 5.0 | 12 | 0.06 | 144 | 0.72 |
| K | 7.4 | 139 | 1.03 | 4…5 | 0.03 |
| $Ca^{2+}$ | 2·6.0 | $< 2 \cdot 10^{-4}$ | 0 | 2 | 0.02 |
| $Cl^-$ | 7.6 | 4 | 0.03 | 120 | 0.91 |
| Approx. conductivity | | – | 1.12 | – | 1.68 |

As a side note, the strongly different values of sodium and potassium in cytosol compared to ECM are caused by a mechanism known as $Na^+/K^+$-ATPase. This leads to a membrane potential which is essential for ion exchange with the environment. For instance, cells in the human body have resting membrane potentials ranging between -100 and -50 mV.

The cytosol has a number of macromolecules such as glycogen, enzymes, vesicles, etc. Those and the organelles influence the conductivity in the cytosol resulting in an increased effective resistance. The number or size of organelles depends on the cell type, the state of proliferation, the cells age, etc. FIG 3.1 shows confluent 3T3 fibroblasts and, in contrast, adipocytes.

Data on the electrical conductivity of cytosol is poor, but due to the high concentration of ions and macromolecules the diffusion constant for ions is about 4 times smaller in the cytosol than in the ECM and the difference increases to a factor of about 10 for proteins [Horton *et al.* 2008].

[5] Notice the used unit for the conductivity $\Lambda$: An aqueous solution of a specific ion shows an almost linear relation of the ion concentration $c$ to the electrical conductivity $\Lambda$ in the case of $c < (1…10)$ mol/l. The valid range for this approximation depends on the ion type. Therefore, in electrochemical topics the concentration-independent limiting conductivity $\Lambda_0 = \sigma/c = (1\ \mathrm{S/m}) / (1\ \mathrm{mol/m^3}) = 1\ \mathrm{Sm^2/mol}$ is used.

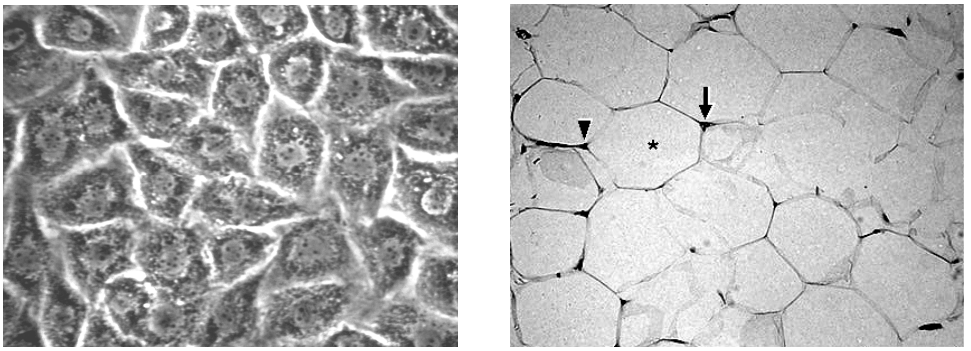

(a) (b)

FIG 3.1: **(a)** 3T3 fibroblasts. Nuclei and organelles are visible, especially a big number of mitochondria. **(b)** Adipose tissue with organelles and nuclei displaced to the periphery (see arrows) of the cells by the single big fat vacuoles . Source of Fig b: http://www.solunetti.fi/tiedostot/kuvat_histologia/sidekudos/1A_57_10x.jpg downloaded in February 2012, cutout reprinted with permission of Kari Törönnen (Coordinator of the Solunetti-project).

## 2. Biomembrane: Lipid double layer

From an electrical point of view the bare outer cell membrane can be modeled as a serial connection of three capacitors (see FIG 3.2). A layer with a thickness of 2 to 3 nm in the middle with $\varepsilon_r \approx 2{,}1$ and two hydrophilic parts with $\varepsilon_r \approx 78$ and a thickness of 1 to 2 nm. Hence the equivalent capacitors have values of 345 to 690 mF/m$^2$ for the lipophilic part and 6 to 9 mF/m$^2$ for the hydrophilic parts. The effective value of that capacitors lying in series is within a range of 5.5 to 8.8 mF/m$^2$ [Huang and Levitt 1977]. A range of 5 to 13 mF/m$^2$ at an overall thickness of 5 to 10 nm is also reported [Pething 1984].

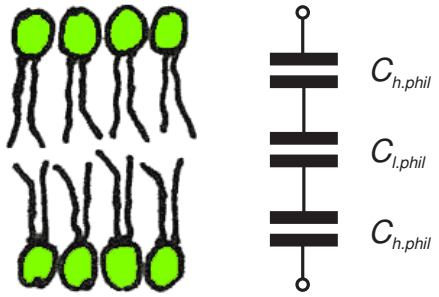


FIG 3.2: Lipid-double layer and its capacitive behavior split up into one lipophilic and two hydrophilic parts.

Small molecules like water, $CO_2$, and other gases can directly be exchanged between the cytosol and the extracellular matrix whereas ions and bigger molecules need a transport mechanism which is realized by protein channels. Those are embedded in the cell membrane as depicted in FIG 2.2.

The ion-channels bestow the membrane an additional ohmic behavior which may be described by an ohmic resistor lying in parallel to the overall membrane capacitance. The kind and number of channels depends on the cell-type. The ohmic resistance for bare cell membranes is about $10^3\,\Omega m^2$, and for membranes with protein channels the value ranges from $10^{-2}$ to $10^1\,\Omega m^2$ [Ehret *et al.* 1997, Coster *et al.* 1996].

## 3.2. Electrode Structures

As mentioned in the introduction, the measurement principle relies on an impedance change due to growth, death or changes in the shape of cells. At least two electrodes are necessary to perform such a measurement and in practice at least one of those electrodes has to be located in the growth area. The herein investigated adherent cell lines grow as single cell layers and the bulk media provide the necessary reservoir for nutrients (see chapter 2.2). Those cells need a plane area for adhesion, otherwise cell growth is hindered in most cases. Also, comparability to established methods of cell cultivation and testing procedures has to be then given. The a cell layer with a thickness of a few micrometers is formed. If cells adhere directly on the electrode(s) monitoring is possible. Consequently, several electrode structures were introduced by different research groups. An overview of the most important is given together with a short discussion.

### 1. Multiple electrodes

I. Giaver and C.R. Keese formed several small electrode spots as sensitive elements with one large reference electrode on the opposite side. This sensor connected the four sensing electrodes simultaneously.

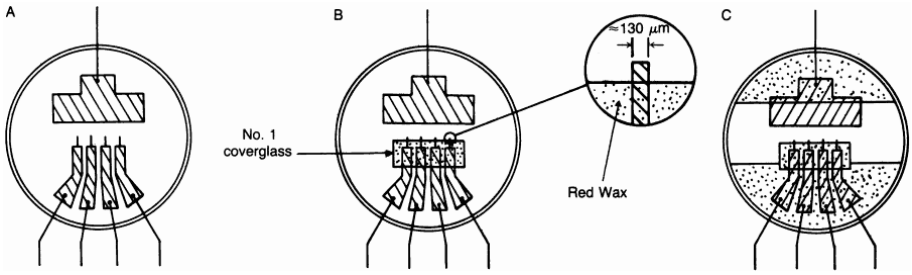


FIG 3.3: The electrode system presented in [Giaever and Keese 1984]. The sensor device was fabricated on a petri dish.

However, this array seems to be quite insensitive because of the very small effective sensing area of only $0.068\,mm^2$, i.e. clearly less than 100 cells for most adherent cell types.

In contrast, an array of individually addressable electrode dots arranged in a matrix can be used. Such an array allows a two-dimensional measurement and if the electrode

spots are realized with a narrow pitch, e.g. a mesh size of less than 20 µm, single cells can be detected, but such sensor geometry is practically not used for impedance measurements on sensors. A suitably large sensing area requires a dozen or more of such spots and the same number of electrical connections which is accompanied with fabrication issues. In practice, arrays of that kind are used for the detection of nerve action potentials in brains instead of impedance measurements.

## 2. Single circular electrodes

Another setup proposed by Keese and Giaever utilizes single sensing electrodes. Small electrodes are part of the growth area for cells while bigger electrodes are horizontally and vertically displaced.

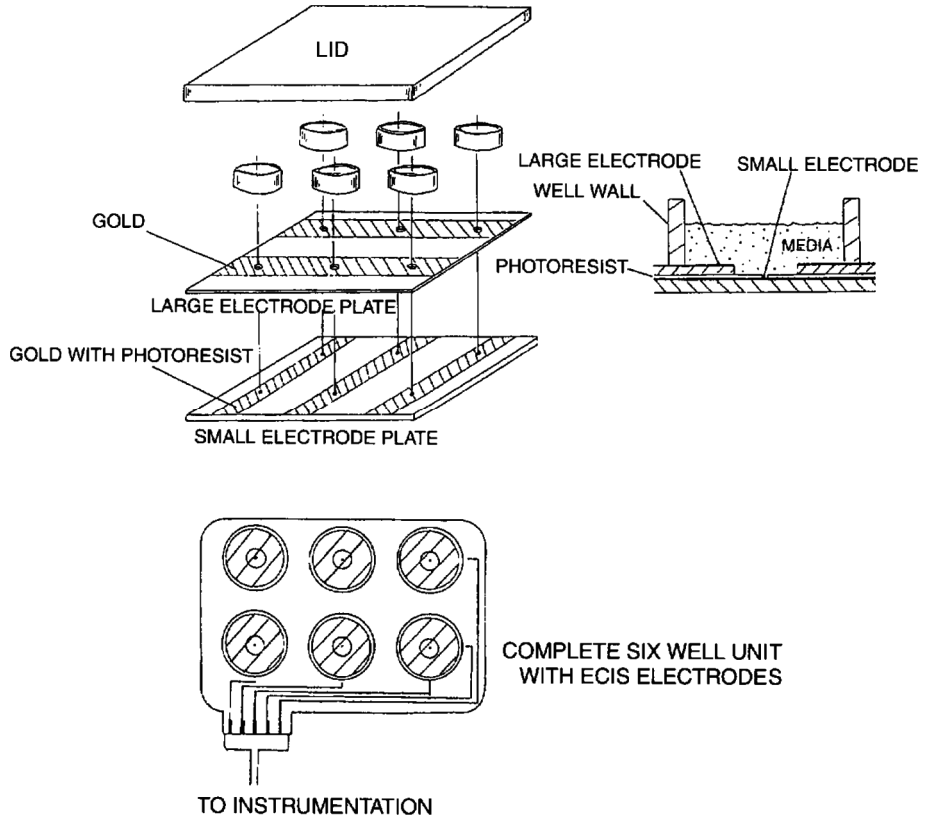


FIG 3.4: The sensor array invented in [Keese and Giaever 1994]. The small electrode has a diameter of 250 µm.

This electrode structure is used by the ECIS™ system (Electric Cell Substrate Impedance Sensing) [6]. An advantage of this technique is the quite uniform field distribution due to the dislocated outer ring electrode, but the sensing area is still very small, only 250 µm in diameter, i.e. 0.05 mm$^2$. Assuming a cell diameter of 30 to 50 µm this method would just allow the detection of 25 to 70 cells, which is an extremely small value. This structure is suitable for the reaction of a full cell layer to detergents but not for the detection of cell growth and doubling. There, an initial cell number of just 3 to 5 cells would be given which cannot be guaranteed by the seeding procedure for each well.

## 3. Interdigitated structures

Ehret *et al.* introduced a sensor design which relies on comb-like, interdigitated electrode structures (IDES). Those electrodes are almost symmetric in their shape and active electrode area. In contrast to the previously described methods, they are located on a common plane cell growth area and both electrodes are used for sensing.

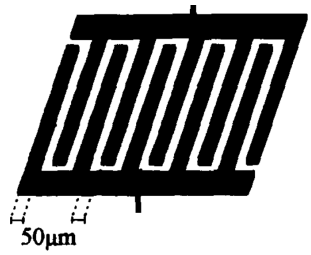


FIG 3.5: Detail of the sensor geometry introduced in [Ehret *et al.* 1997]. The active sensor area is 5x5 mm$^2$.

Fundamentally, the design is not limited to rectangular shapes [Acea Biosiences 2009, Arnold 2001]. With respect to the circular shape of most cell-growth wells proper modifications of the rectangular IDES constructions can be applied though the sensor assembly within the metallization process promotes the design of rectangular electrode structures.

A clear advantage of IDES is the quite large sensing area. However, it has to be mentioned that 50 % of the growth substrate is not covered with metal electrodes and thus is not sensitive, but allows an inspection with inverted microscopy if optically transparent substrate materials are used.

[6] Today the ECIS™ system is produced by *Applied BioPhysics*. To the author's knowledge this company was originally founded by Charles R. Keese and Ivar Giaever in 1991. Website www.http://www.biophysics.com.

## 3.3. Interdigitated Electrode Structure as Sensor

IDES have two characteristic parameters, the finger-gap $G$ and the finger-width $W$ (see FIG 3.6), which can be modified to design the sensitive region. In [Ehret *et al.* 1997] both dimensions are chosen at 50 µm. With cells growing almost equally on both electrodes it is reasonable to keep the basic structure of the IDES, namely the equal sizes of finger-gap and –width of both electrodes. A more detailed analysis of the sensor is done by filling its imaginary upper space with an electrolyte and carrying out calculations.

As a first step, a small DC-voltage is applied, which does not force an electrochemical reaction. A characteristic electric field distribution results and an electric current would follow this path with respect to $\boldsymbol{J} = \sigma \boldsymbol{E}$ , with $\boldsymbol{J}$ being the vector of the electric current density vector, $\boldsymbol{E}$ being the vector of electric field strength, and $\sigma$ being the electric conductivity. FIG 3.6 shows the field distribution for $G = W$.

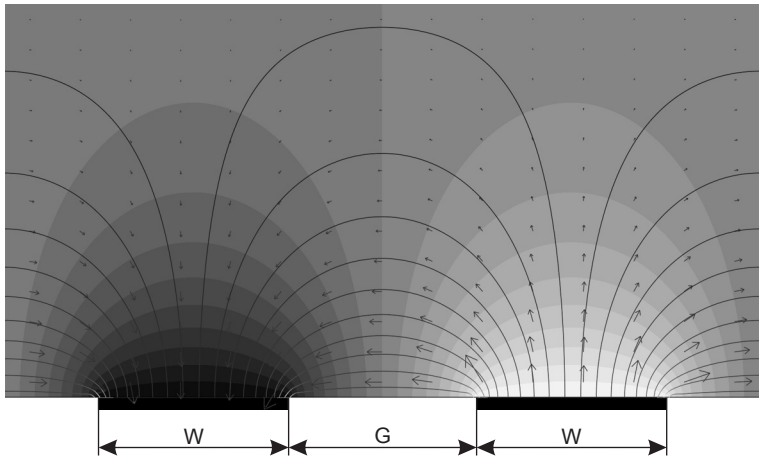


FIG 3.6: Cut-out of the cross-section of an IDES with field distribution at two electrodes (black boxes). The solid lines split the electrical flux in steps of 5 %. The arrows represent the electrical field vectors. The shaded background shows the electrical potential in steps of 5 %. 90 % of the electric flux between two adjacent electrodes (i.e. 50 % of the flux of a single electrode) appear at a height which is approximately $G+W$.

This graph is representative for sensor geometries with equal finger-widths and -gaps. About 90 % of the electric flux (or electric current) appear within a height being equal to the finger-period $\lambda = G + W$ [Igreja *et al.* 2004]. This has some substantial consequences:

- The culture medium height probed by the IDES is approximately $\lambda$.
- Residual contamination located on the glass substrate between adjacent electrodes influences the impedance. The smaller the finger-period the stronger the influence.

With respect to the height of a single adherent cell, which is usually between 5 and 10 µm, one would first assume to use a finger-period within that range. The whole cell could be detected and cells located in the finger-gap may also have a significant influence. Sensor chips with a $\lambda$ = 10 µm finger period were produced but showed strong deviations of the measured impedances. Residual contamination by photoresists or metallization artifacts from the sputtering process may be the reason for that deviations as the small finger leads to a stronger influence of the substrate surface.

Sensor configurations with finger widths and gaps of 23 µm and 80 µm, respectively, were used by other research groups [Ceriotti *et al.* 2007a, Ceriotti *et al.* 2007b]. The herein presented IDES has a finger-width and -gap of 50 µm. This is a necessary compromise with respect to the detection accuracy due to the greater structures and the request for reproducible results. Additionally the rather large gaps ease microscopic inspections.

## 3.4. Sensor Device Construction

Usually adherent cells grow on the electrodes and the substrate, thus both materials need to be selected carefully. If just one component influenced the cell growth the measured proliferation could not be compared with established test methods or experiments could fail [Appendix A, Pennisi *et al.* 2011].

### 1. Metallization

The metal layer has to fulfill three requirements:

- No toxic effect or inhibition of cell growth (oligodynamic effect).
- Compatibility to conventional clean-room techniques.
- Provide a high electrical conductivity.

The first two conditions are e.g. fulfilled by gold and platinum, but a suitable high electrical conductivity can only be found for gold, i.e. $4.5 \cdot 10^7$ S/m instead of $9.4 \cdot 10^6$ S/m for platinum. The thickness of a metal layer is limited to about 150 nm by the used Lift-Off-Resist (LOR) process presented in the following paragraphs. Also, too thick metallization may influence cell growth and migration [Pennisi *et al.* 2011, Guan and Kisaalita 2011]. High conductivity is important, since the contact lines to the sensor field represent serial ohmic resistance. For instance, the connection lines of the sensor geometry, which will be introduced later, cause a series resistance of about 27 Ω for a Pt- and 6 Ω for an Au-metallization. The lower value of the ohmic part of the sensor impedance was found to be at least 120 Ω at a measurement frequency of 10 kHz as depicted in section *3.5 Impedance model*. Even if the metal thickness was known and taken into account for the effective sensor impedance the resistance of a platinum layer would cause an unnecessary uncertainty.

The evaluation of production costs for the metallization-process in a clean-room lead to the investigation of screen-printing-based sensor production methods. Screen-printing is a more cost-effective way for the production of structures down to 50 µm but it was found that the resulting surface is quite rough and does not allow the detection of cell growth. Hence it was necessary to use conventional clean-room techniques, i.e. sputtering [Brischwein *et al.* 2007].

## 2. Substrate materials

The specification of the metallization consecutively allows the selection of a proper substrate material. The materials, like the metallization, must not cause toxic effects during cell growth and need to be compatible to semiconductor-processing steps for electrode pattern design. Investigated materials were a Low Temperature Cofiring Ceramics (LTCC), the polyimide *UPILEX*® from *UBE* and various glasses.

Polyimide layers were already previously used as substrates for electrode arrays for electroencephalography [Stieglitz *et al.* 2005]. A single foil of UPILEX is highly flexible which makes handling difficult. In this context, a laminate was better for handling, but its roughness also caused problems with the metallization with LOR-processing and significantly reduced the transmission properties for microscopic investigation. FIG 3.7 shows both, a single foil and a laminate.

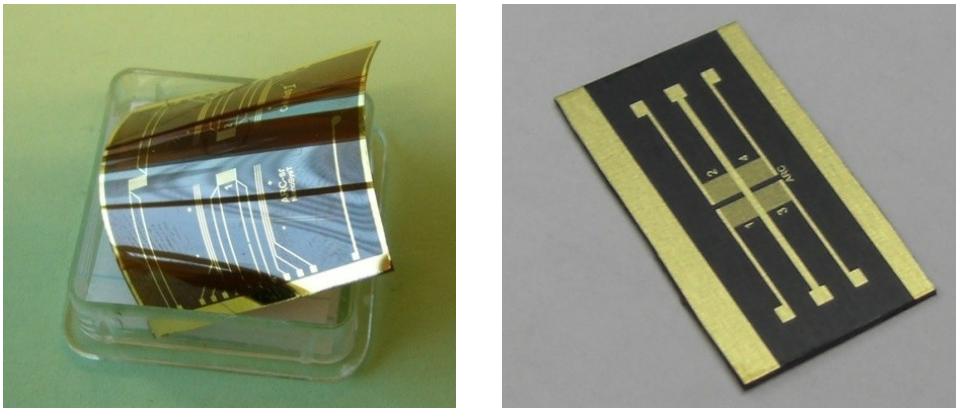

(a) (b)

FIG 3.7: UPILEX samples with 5 µm test structures for the investigation of the metallization properties. **(a)** UPILEX foil. **(b)** UPILEX laminate.

The investigated LTCC material was a *Heratape HT700* from *Heraeus* and was fired before metallization. The processed dies were very thin (a few 100 µm) and fragile. The edges did sometimes bend up making the photolithography difficult. Even though it was possible to process some sensor devices with 5 µm structures but the rough surface did

not allow a proper cleaning and microscopic inspections are not possible with the rather opaque ceramics.

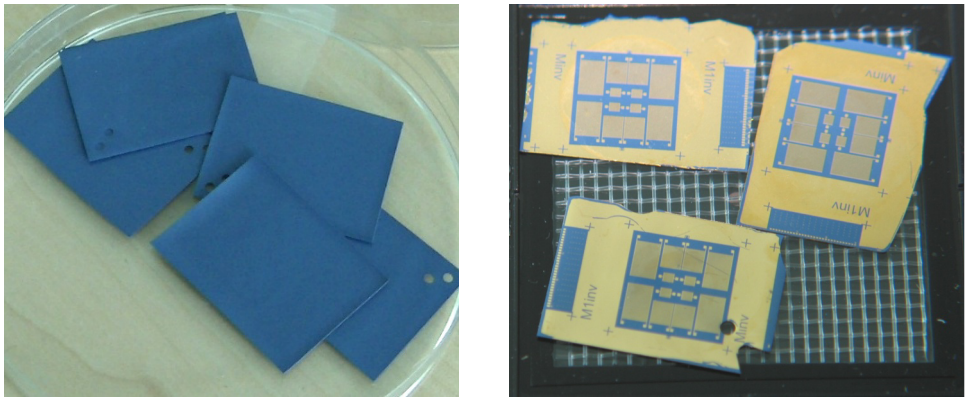

(a) (b)

FIG 3.8: **(a)** Fired LTCC tape samples with a size of about 20x30 mm² each. The bent edges are clearly visible. **(b)** 5 µm test structures for the investigation of the metallization properties.

Glass is the material of choice if compatibility to established methods, e.g. fluorescence microscopy, is to be guaranteed. Otherwise UPILEX would also be a useful substrate. The floating glasses decided on for this work were AF45 and D263T, produced by *Schott AG*. The latter type was also used in [Rümenapp *et al.* 2009].

## 3. IDES production

The sensors were designed with an electrode width of 50 µm and an electrode-electrode-gap of 50 µm. The metallization layers were fabricated using a LOR (lift-off-resist)-process shown in FIG 3.9.

The glass substrates were spin-coated with a lift-off resist *LOR 3A* and a positive-tone photoresist *AZ MiR 701*, both purchased from *MicroChemicals GmbH*. The positive resist was patterned by photolithography (FIG 3.9a) and then developed. During the process the lift-off-resist was under-etched (Fig 3.9b). Subsequently, a 10 nm thick Ti adhesion layer followed by a 150 nm thick Au-layer was deposited by a sputter-process (Fig 3.9c). The under-etched resist formed a shadow mask for the metal deposition. A lift-off of the residual resists together with the excessive metallization by an acetone-treatment was then possible (Fig 3.9d).

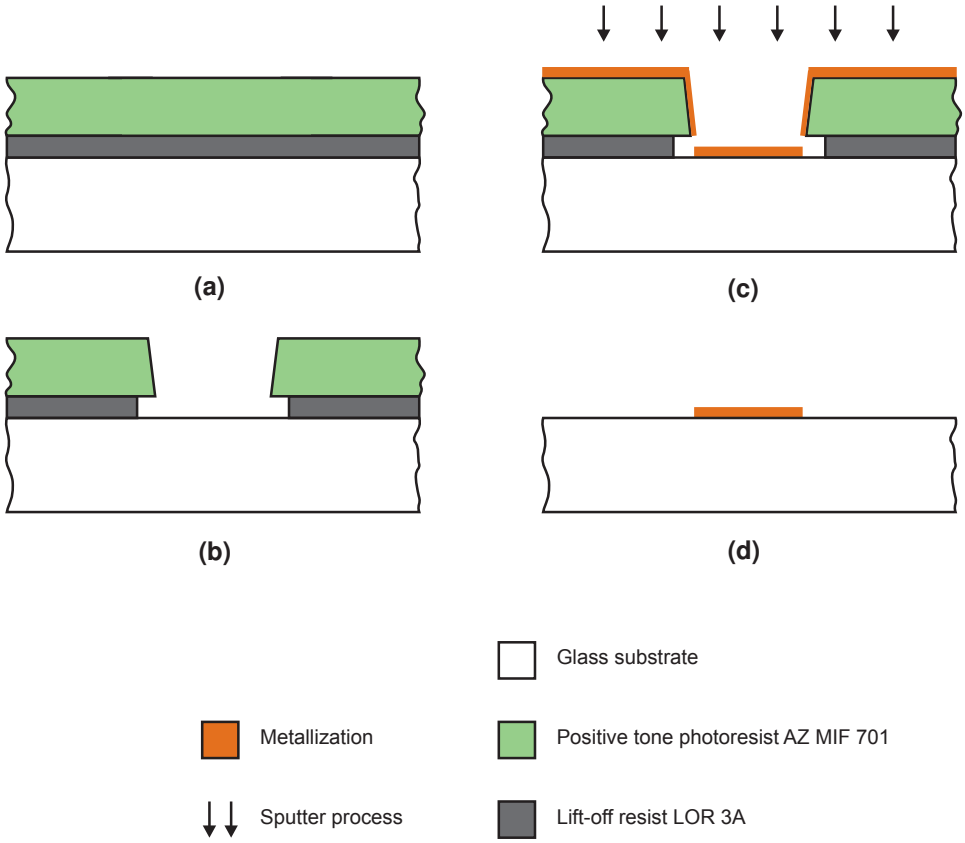


FIG 3.9: The processing steps for electrode structures utilizing a LOR process.

This production technique is quite easy and cheap compared to processing steps with a hard-mask. One disadvantage is that the layer thickness is limited by the lift-off of the photo resist. If the metallization is too thick it a bridge may be established between the metal layer on the substrate and on the resist wall remains (see FIG 3.9c). Then a lift-off would cause parts of the metallization to be ripped off and would lead to abnormal edges at the finger structures. Notably, such edges may also be caused by back-sputtering. FIG 3.10 shows a scan of the glass-metal steps made with an Atomic Force Microscope. The edges caused during the sputter and lift-off-process are clearly visible. The bumps on the metal layer may either be larger metallic clusters formed during sputtering, underlying impurities or residuals of the photo resist after the lift-off-process Thus, cleaning of the IDES is extremely important before first use. That procedure is described within this chapter, in section 3.4 *Cleaning and preparing a sensor device*.

The possibility of excessive electric fields caused by point effects at those edges was tested by impedance measurements on Phosphate Buffered Saline Solution (PBS) at several excitation voltages and frequencies. No hint on any kind of electrolysis or an abnormal frequency-dependent behavior was found.

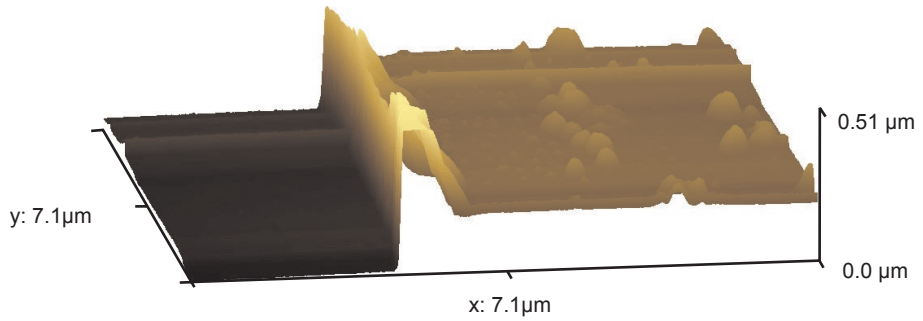


FIG 3.10: Atomic Force Microscopy of the metal-substrate-edge of a LOR process. Glass substrate is AF45 from Schott AG with a Ti-Au-metallization layer of 150 to 200 nm thickness. The bumps on the raised area are residual contamination, e.g. of the photo resist.

The produced sensor chip shown in FIG 3.11 carries four individually addressable elements with a common line in the middle. Each element measures $1.8 \times 2\,\mathrm{mm}^2$. The rather broad metal strips on the top and the bottom are introduced to facilitate the lift-off process.

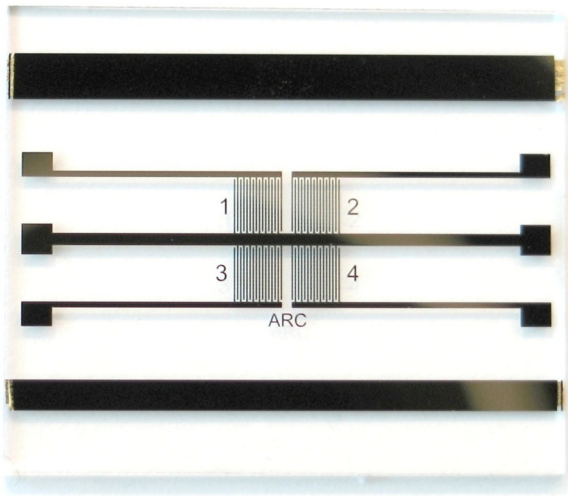


FIG 3.11: Sensor chip with an overall size of 15x18 $\mathrm{mm}^2$ carrying an array of four IDES elements à $1.8 \times 2\,\mathrm{mm}^2$. The fingers in each IDES have widths and gaps of 50 µm. This construction allows the use of a single IDES element, and two or four elements in parallel.

Cells grow on an area of 50 mm², i.e. a diameter of 8 mm, and allow the incorporation of four sensor elements on a glass chip. Hence redundancy for fabrication failures like broken connection lines, contact pads or problems at the lift-off-process is provided. The size of a single IDES element is limited because a large IDES element would lead to a very small impedance value. Then the intended 2-point-impedance measurement would

have had to be replaced by a 4-point-measurement with more complexity of the impedance measurement system.

## 4. Device assembly

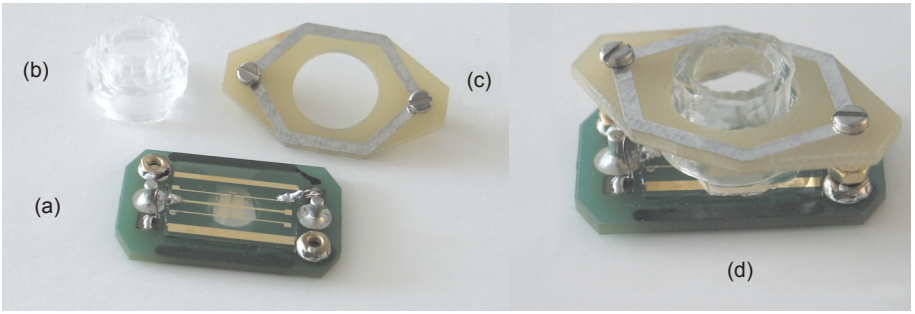


FIG 3.12: Sensor device components. **(a)** PCB with jackets and the sensor element glued on it, **(b)** PDMS-tube, **(c)** clamp plate, **(d)** assembled device. The dimensions of the bottom plate are 15 mm × 32 mm. In this picture, only one of four sensor elements was connected for measurements.

A printed circuit board (PCB, FIG 3.12a) of type FR4 (epoxy resin impregnated fiberglass) is used as carrier. The sensor is bonded onto the board with the silicone Polydimethylsiloxane (PDMS) derivative *TSE399* from *GE Bayer Silicones*. The PCB has a window underneath the IDES, thus an inverted microscope can be used for optical checks. Jackets for the mechanical and electrical connection to the tags are placed on the left and the right side of the PCB. The electrical connections to the metal pads of the IDES are established via thin Ag-coated copper wires.

The tube, which forms the well for the uptake of cells, (FIG 3.12b) is made of a PDMS (*Sylgard 184 silicone elastomer* from *Dow Corning*). PDMS is a well known material for the production of microfluidic channels and no negative effects on cell growth have been published to date [Whitesides 2006].

The clamp plate (FIG 3.12c) is screwed on the carrier and fixes the PDMS tube on the sensor. The metallic closed structure is intended to provide an additional barrier to bacteria and fungi because tin as well as copper suppress their proliferation, also known as the oligodynamic effect. The use of copper-doped noble steel for the inner linings of incubators also relies on this effect [Schmitz 2007].

## 5. Electrical connections

The electrical and mechanical connection of the sensor device with the measurement system is established by jackets with integrated contact springs. FIG 3.12a shows the bottom plate of the sensor device carrying the electrical connections. A high degree of usability is given by the fast reassembly of a sensor device if failures occur. Excessively strong mechanical cleaning procedures, which may detach the leads from the pads, or

rough handling, may cause damages. Solder-tin cannot be used for electric bonding because of the generation of intermetallic SnAu-phases which virtually dissolve the gold-pads. On an industrial scale bonding with aluminum or gold-wires is used for connecting pads in an IC package. With respect to the mechanical dimensions of the sensor device, the requirement for an inherent mechanical stability, the request of a fast and easy-to-use replacement method for the connection as well as the need of a special apparatus wire bonding was out of this work's scope.

**Indium**

Indium can be used for a soldering-like electrical connection of the leads with the pads. It has a very low melting point of about 160 °C and does not lead to an intermetallic phase with the gold-pads. FIG 3.12a shows such connections at the Au pads of the sensor substrate. The tip of the connecting wire is coated with indium by hand with a solder iron and is subsequently pressed onto the pad on the glass chip using tweezers. Mechanical and electrical connection is established via surface roughness and adhesive forces.

The contact has a reasonable electrical conductivity but poor mechanical stability. An operator needs to have experience with the soldering properties of indium which is very different from tin-solder. For long working periods in the humid incubator atmosphere it was found that indium turned into a brittle material which could not be removed by melting with a solder-iron anymore. With respect to its whitish color Indium Hydroxide $In(OH)_3$ may have been formed. Indium is not known to be toxic to organisms.

**Silver loaded epoxy adhesive**

*Silver loaded epoxy adhesive* by *RS Components Ltd.* has an electrical conductivity better than $2 \cdot 10^4$ S/m and is useable within a temperature range of -55 to 150 °C. This connection method became the new standard after Indium because it could be easily produced without the need of special equipment or experience in soldering. Mechanical resistance and electrical long-term stability of the material was not affected by the incubator's humidity within the incubator.

It is essential that the sensing area must not be contaminated by the epoxy resin. Even if the adhesive is completely cured and dried out some chemicals seem to be resolved into culture medium during operation. This was proved by a proliferation test on 3T3 fibroblasts which showed that cells died within 8 hours even though only the culture medium was in contact with the adhesive.

## 6. Cleaning and preparing a sensor device for (re-) use

The fixation of the PDMS tube on the glass chip by a clamping plate, i.e. without glued junctions, allows easy disassembly and also provides access to the sensor area. Thus, it is possible to clean the sensor device and reuse it. Especially the small number of systems

produced within this work justified at least reuse within a laboratory experiment. The cleaning procedure consists of the following steps:

(a) Disassembly of the device as shown in FIG 3.12. The top plate may be rinsed and stored in ethanol (EtOH) before reassembling.

(b) Elimination of macroscopic contamination and salts by a cleaning liquid. A perforated plate is hinged into a beaker glass and the sensor elements placed on it. The cleaning liquid is a mixture of water and crushed dish washer tabs. The ingredients of such tabs, enzymes such as proteases, amylases, and basic chemicals, are perfectly suited for the cleaning of glass and metal from organic contamination. The setup is placed onto a hot plate and a magnetic stirrer provides a turbulent flow. The PDMS-tubes can also be cleaned with this setup and subsequently rinsed with water and stored in EtOH afterwards. These cleaning step takes are performed as long as contamination is visible on the surfaces.

(c) The sensor element is rinsed with purified water. A small drop of a dish-liquid is then directly dropped onto it. Cotton sticks allow chemical-mechanical cleaning. Then the sensor is rinsed in a water-jet to completely remove the cleaning-liquid from the sensor area. This is necessary because of the high toxicity of the cleaning-liquid for cells.

(d) Drying with a clean air or nitrogen jet removes residual water drops and prepares the sensor for the next use.

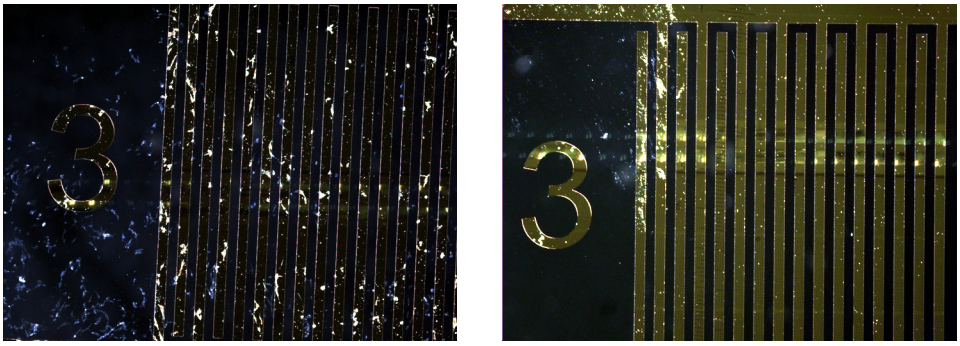


FIG 3.13: Dark field microscopy of a single sensor field before (left) and after (right) cleaning. Almost all contamination is removed. Only a few spots are left on two fingers. The horizontal stripes may be results of the mechanical cleaning step and is sometimes found on the sensor fields.

The quality of the cleaning procedure may influence the electrode-electrolyte-interface, which is reflected by the imaginary part of the sensor impedance [Ceriotti *et al.* 2007a]. This cleaning method ensures at least a five time reuse of one sensor chip. However, some experiments, e.g. an osteogenic differentiation, may hinder the reuse of sensors due

to the expressed minerals by the incorporated cells. FIG 3.13 shows a dark field microscopy of a sensor element before and after the described cleaning procedure.

The above presented sensor cleaning is neither an antiseptic procedure nor a sterilization technique. Thus, a separate sterilization is required. After reassembly the sensor devices are put onto tags and the tags are placed into the wells of a microtiter plate. The completed microtiter plate is then placed into a UV light exposure unit and left there for about 30 minutes for sterilization.

## 3.5. Sensor Characterization

### 1. AC voltage levels

The sensor impedance is measured by applying an AC-voltage and recording the generated current. In many cases this task is fulfilled by potentiostats which use a driving AC-voltage but it is also possible to drive current. The latter was done within the development of integrated systems in which electrical current sources were employed [Sacristán-Riquelme *et al.* 2009, Segura-Quijano *et al.* 2010, Xu *et al.* 2009]. The current approach eases circuitry design, but leads to considerable consequences regarding the handling of electrodes. In particular, the electrode surface area may vary due to contamination or voids in metallization, thus resulting in increased sensor impedance. As a consequence, a pre-set current amplitude leads to an increased voltage which may be limited by additional protection circuits. However, if the voltage on the electrode-electrolyte interface exceeds the electrolyte's decomposition voltage, it corrupts the chemical composition and also the electrode's integrity. These risks are circumvented by a voltage-based approach where an AC probe voltage is applied and the generated current recorded.

A literature research shows that the probe signal levels are reported in a very different manner. The values range from less than 1 to 35 mV rms for sensor elements with electrode-shapes comparable to the here presented geometry. In [Ehret *et al.* 1997] measurements were conducted with an impedance analyzer working at 3.5 mV rms. The *RT-CA-system*, developed by *ACEA Biosiences* and *Roche Applied Science*, takes measurement at several frequencies with probe voltages up to 22 mV rms, the *CellKey*-system developed by *Molecular Devices* works at a voltage of 100 mV [7]. In [Huang *et al.* 2003] 18 mV rms were used which mainly appeared at the sensing electrode due to the more than 100 times larger outer ring electrode of the smallest sensor electrode. Carter *et al.* compared measurements on PBS with results achieved with culture medium. Significant changes only appeared for low frequencies below 1 kHz and an applied voltage of 70 mV rms [Carter *et al.* 1992].

[7] This information was not available on the company website but was received by a request at Molecular Devices.

The herein designed system uses a maximum AC-component of 35 mV rms according to [Huang *et al.* 2003, ACEA Biosiences and Roche Applied Sciences, Carter *et al.* 1992]. The symmetric electrode structure leads to an applied voltage of less than 18 mV rms for each electrode with respect to the culture medium. Visual inspection of the cell growth behavior of 3T3 fibroblasts and viability tests on human mesenchymal stem cells did not show significant difference if a sensor was measured, i.e. an electrical current was flowing, or if the sensor was not measured during the proliferation over several days. The number of dead cells was below 3 % in both cases (see section *5.3 Human Mesenchymal Stem Cells*).

## 2. DC-Behavior

If the sensor electrodes are in contact with an electrolyte and a DC-voltage is applied consecutively electrochemical double layers are formed on the electrodes. Such layers consist of a (fixed) Helmholtz-double layer and a diffuse Gouy-Chapman-layer. The fixed layer has a thickness of several Ångström, whereas the dimensions of the diffuse layer rely on the ion concentration of the electrolyte and is thus rather flexible. In the case of a culture medium or PBS that concentration leads to a thickness of less than 1 nm (see FIG 3.14).

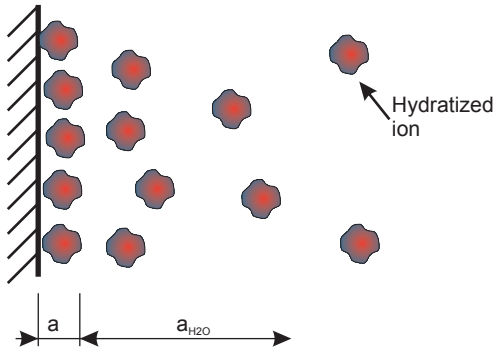


FIG 3.14: Double layer at a polarized electrode. $a$ is the diameter of a hydratized ion. A single layer of such ions is situated directly on the electrode surface. $a_{H2O}$ the effective thickness of the diffuse Gouy-Chapman-layer layer. Its thickness depends on the ion concentration and temperature.

The effective capacitance $C_{DL}$ is formed by the series connection of capacitors representing the fixed and the diffuse layer. The area-related value $C_{DL}$' is calculated using

$$\frac{1}{C_{\mathbf{DL}}'} = \frac{a_{\mathbf{H2O}}}{\varepsilon_{\mathbf{Diff}}} + \frac{a/2}{\varepsilon_{\mathbf{fixed}}} \tag{3.1}$$

The distance $a/2 \approx 0.2$ nm characterizes a hydratized ion to the electrode with $\varepsilon_{fixed} \approx 30$ and $a_{H2O} \approx 1$ nm is representing the diffuse layer with $\varepsilon_{Diff} \approx 6$. Those values lead to an

effective electrode-area-related capacitance $C_{DL}' \approx 100\,\mathrm{mF/m^2}$. A range of 50 to 500 mF/m² is reported for $C_{DL}$ [Hamann *et al.* 2007].

The applied DC-voltage virtually appears at those double layer. Thus, even small voltages of a few Millivolts lead to electric fields strengths from one to several hundred MV/m. As a consequence, there is a measurable tunneling current. Notice that the voltage is split into two equal parts for each electrode. The effective equivalent circuit of such a double layer consists of a capacity $C_{DL}$ and a charge transfer resistor $R_t$ lying in parallel. DC-measurements were performed with a potentiostat on DMEM at voltages ranging from 1 to 100 mV, the tunnel current remained below 100 nA. A voltage of 500 mV leads to a current of nearly 1 µA, i.e. an effective resistance $R_t = 500\,\mathrm{k\Omega}$. The following measurement results will show that the sensor impedance at a frequency of 1 kHz and higher is much smaller than $R_t$, i.e. a DC-offset up to 500 mV does not influence the impedance measurement with alternating probe voltages.

Long-term measurements on culture medium with and without cells regularly resulted in sensing electrodes with a matt surface which was not the case when the same measurements were conducted on PBS or similar electrolytes. Hence that matting was caused by the deposition of components of the culture medium and could be removed by the cleaning procedure described in section *0*
*Sensor* Device Construction. The intensity of that surface layer was also linked to the residual DC-component of the probe signal which was less than 2 mV. The higher that DC-component, the faster the matting proceeded. The sensor impedance or behavior of the cells was not affected. Nevertheless it is possible that the DC-offset itself or the deposited material on the electrodes influenced cell kinetics an proliferation in a way which was not yet discovered. Therefore the offset was held as low as possible by system design.

## 3. Impedance model

The following characterization of the sensor was done with a potentiostat. A sensor device was filled with DMEM and placed in a sterile box in the incubator. Connectors to the potentiostat were led through the rubber lips of the incubator door. A period of 1 h was awaited for the stabilization of the whole system at a temperature of 37 °C. The sensor impedance was measured with a 2 minutes-interval at 1, 2, 5, 10, 20, 50, and 100 kHz. The probe voltage was 35 mV rms. After 250 minutes that voltage was increased to 70 mV rms. FIG 3.15 shows the impedance spectroscopy.

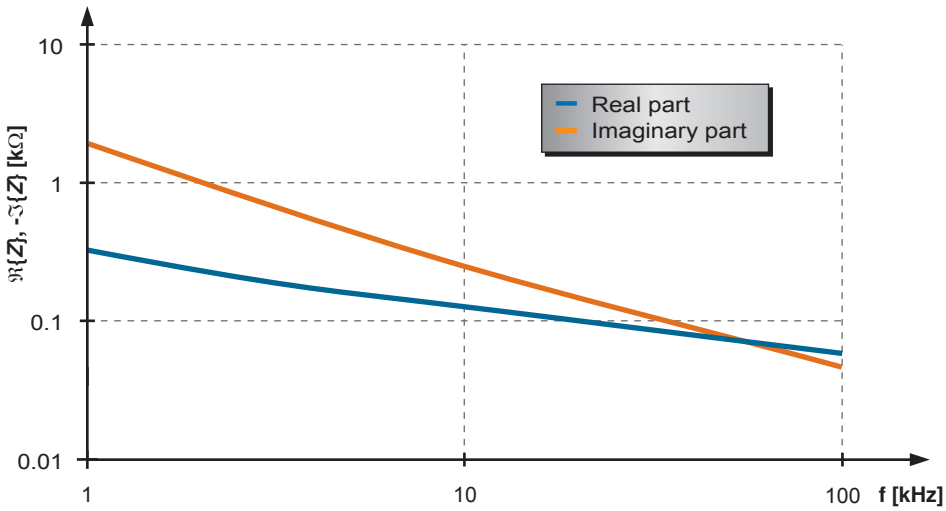


FIG 3.15: Impedance spectroscopy on DMEM for 8 hours at 37 °C in an incubator. 35 mV rms were applied for 250 minutes followed by 70 mV rms for another 250 minutes. The impedance data did not show significant changes over the full period and both voltage levels. The frequency-relation fits the data presented in [Ehret *et al.* 1997].

An ideally polarizable electrode would show a capacitor-like characteristics as there would not be a charge transfer. The equivalent circuit model would then be a capacitor which lies in series to a resistor which represents the ionic conductivity of the electrolyte. In contrast, the real and imaginary part of the upper figure can be approximated by $\Re\{Z\} \approx 3.663\,(f \cdot \mathrm{Hz}^{-1})^{-0.363}\,\mathrm{k\Omega}$ and $\Im\{Z\} \approx 46.064\,(f \cdot \mathrm{Hz}^{-1})^{-0.808}\,\mathrm{k\Omega}$. That behavior cannot be described by an RC-model with frequency-independent parameters but requires frequency-dependent components. The quite complex electrochemical behavior of an electrolyte includes a electrical representation known as the Warburg-impedance [Warburg 1899, Hamann *et al.* 2007]

$$Z_\mathrm{W} = \frac{\mathrm{R}T}{n^2\mathrm{F}^2 c_0\sqrt{2}} \cdot \left( \frac{1}{\sqrt{D_\mathrm{ox}}} + \frac{1}{\sqrt{D_\mathrm{red}}} \right) \cdot \frac{1-\mathrm{j}}{\sqrt{\omega}} = \frac{K_\mathrm{W}}{\sqrt{\omega}} \cdot (1-\mathrm{j}) \tag{3.2}$$

with gas constant R, Faraday constant F, system temperature $T$, reaction valence $n$ and the concentration $c_0$ of the reduced/oxidized species in the electrolyte with its diffusion constants $D_\mathrm{ox}$ and $D_\mathrm{red}$. Those diffusion constants may be combined to a single value $D = 10^{-9}\ \mathrm{m^2\,s^{-1}}$. All not-frequency-dependent factors are summarized to a single factor $K_\mathrm{W}$ for the following discussions.

Equation (3.2) is only valid if the diffusion layer has infinite thickness which cannot be expected for the IDES layout. Therefore, a correction factor needs to be implemented leading to the following modified equation with $l$ being the effective diffusion length [Lasia 1999].

$$Z_{\mathrm{W,lim}} = \frac{K_{\mathrm{W}}}{\sqrt{\omega}} \cdot (1 - \mathrm{j}) \cdot \tanh\left( l \sqrt{\frac{j\omega}{D}} \right) \tag{3.3}$$

The diffusion-length-dependent factor can only be neglected if $l$ is significantly larger than $(D/\omega)^{1/2}$, e.g. $l \geq 2\,\mu\mathrm{m}$ for frequencies above 1 kHz.

Since the known Randle's impedance model [Randle 1947], see FIG 3.16a, did not describe the sensor behavior properly, an alternative model was developed and is presented in FIG 3.16b .

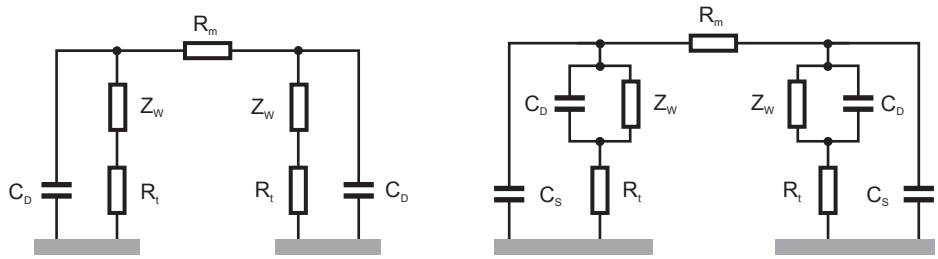


FIG 3.16: (a) Impedance model suggested in [Hamann *et al.* 2007]. (b) Modified model.

Here, the Warburg-impedance is based on Redox-reactions of the electrolyte's compounds. Those reactions occur directly at the surface in which $R_t$ represents the resistor for charge transfer. Such reactions do not appear in the measured sensor system but the high electric field strength at the electrode-electrolyte interface may cause a field-induced dissociation [8]. This means, a molecule can be split up in two parts. In parallel to that behavior a capacity $C_S$ represents the idealized polarizable electrode wherein no charge exchange occurs. A calculation using the following parameters allows a fitting with an average error of less than 3 % for the measured sensor impedance wherein a single electrode has an area of $9 \cdot 10^{-7}\,\mathrm{m}^2$.

[8] Long-term measurements such as those presented in FIG 3.15 did not lead to any visible or measureable changes of the culture media.

TABLE 3.II: Impedance Model Fitting Parameters

| Parameter | Absolute value | Electrode area-related value |
|---|---|---|
| Capacity $C_S$ | 74 nF | 82 $mFm^{-2}$ |
| Capacity $C_D$ | 75 nF | 83 $mFm^{-2}$ |
| Charge transfer resistance $R_t$ | 310 Ω | 279 $\mu\Omega m^2$ |
| Warburg-parameter $K_W$ | 407 $k\Omega s^{-1/2}$ | 0.366 $m\Omega s^{-1/2} m^2$ |
| Diffusion length $l$ | 4.5 µm | - - |
| Medium resistance $R_m$ | 47 Ω | - - |

The parameters listed in TABLE 3.II show one possible combination of values. Some of them can be varied in a wide range of more than 10 %. The impedance at low frequencies is dominated by the capacitive sensor behavior but high frequencies could not be satisfyingly investigated because of the limited frequency-range of potentiostats. Hence the parameters may not fit for frequencies above 100 kHz. However, measurements above 50 kHz were not performed.

Similar electrode area-related values could be found for the impedance curves presented in [Ehret *et al.* 1997]. The values allow a backwards-calculation for the concentration of the reduced/oxidized species. With $n = 1$, $D = 10^{-9}\,m^2\,s^{-1}$ and temperature of $37\,°C \approx 300\,K$ a concentration $c_0 \approx 34\,\mu mol/l$ could be found. For comparison, measurements conducted by Huang *et al.* delivered a value range of $K_W = (0.42 \ldots 0.62)\,\Omega s^{-1/2} m^2$, which leads to a concentration $c_0 \approx 25\,\mu mol/l$. There, the provided data relies on small circular electrodes with diameters of 140 to 900 µm and a much larger second electrode [Huang *et al.* 2004]. The comparably large diffusion length $l$ shows that the influence of the sensor geometry can be neglected for the present design.

### 4. Temperature dependence

The Warburg-impedance is the only component which shows a (proportional) dependence on temperature as shown in equation (3.2). Nevertheless, measurements showed that a higher temperature lowered the impedance which was true for the real as well as for the imaginary part. This effect is related to the viscosity of the culture medium which reduces the impedance by about 1 %/K [Hamann *et al.* 2007].

## 3.6. Discussion

Point- and circular shaped electrodes are almost only usable for the investigation of single cells or a small number of cells, but large sensing areas are required for the measurement of a whole cell layer. The developed sensor has a growth area with a diameter of 8 mm compared to a 6 mm diameter found for the wells of a 96-well

microtiter plate. 100 % confluence means about 50,000 cells wherein about 1800 are located on the metalized structures of the active sensor area. Depending on the measurement system, 2 or 4 sensor fields may be connected in parallel to enhance the sensing area. The advantage of a smaller sensing area is that edge-effects due to the tube walls (temperature or nutrition gradient) do not need to be taken into account.

The highly modular sensor device allows a multiple reuse with stable electrical properties. The presented clamping mechanism for the PDMS tubes circumvents biocompatibility problems which may arise with adhesive joints. Moreover, an additional curing period is avoided. A possible method for the electrical connection of the glass chips would be the use of spring contacts. However, those would have required a more complicated setup for the sensor devices. The changeover to a conductive epoxy adhesive circumvented the stability problems with indium and did even lead to better performance characteristics in mechanical and electrical long-term stability and reliability. In both cases, indium and adhesive, the connection pads on the glass chip need to be free of contamination. Otherwise indium rejects mechanical contact while the adhesive shows a loss of mechanical and electrical stability after a few hundred hours in the humidified incubator. The latter is a quite slow process and difficult to distinguish from other influences. The disassembly of a sensor device allows a close inspection of the active sensor field after a measurement.

The characterization of the sensor device with culture medium DMEM allowed the introduction of slightly modified version of the Randle's model. The description of the Warburg impedance fits data from other research groups and the values found for the capacities are within the range of theoretical presumptions.

## 3.7. Bibliography

Acea Biosiences: Impedance based apparatus and methods for analyzing cells and particles. European Patent EP 1527328 B1 (2009).

Acea Biosiences, Roche Applied Science: *RTCA-system*. Datasheet and characterization available online www.aceabio.com or www.roche-applied-science.com.

Arnold W.M.: *Monitoring of biological cell collection by dielectric spectroscopy*. Report on IEEE Annual Conf. on Electrical Insulation and Dielectric Phenomena, ISBN 0-7803-7053-8, pp. 40-44 (2001).

Brischwein M., Herrmann S., Vonau W., Berthold F., Grothe H., Motrescu E.R., Wolf B.: *The Use of Screen printed Electrodes for the Sensing of Cell Responses*. IEEE African Conference (AFRICON), ISBN 978-1-4244-0986-0, pp. 1-5. (2007).

Carter S.J., Linker C.J., Turkle-Husling T., Howard L.L.: *Comparison of Impedance at the Microelectrode-Saline and Microelectrode-Culture Medium Interface*. IEEE T. Biomed. Eng. 39 (11), pp. 1123-1129 (1992).

Ceriotti L., Ponti J., Colpo P., Sabbioni E., Rossi F.: *Assessment of cytotoxicity by impedance spectroscopy*. Biosens. Bioel. 22, pp. 3057-3063 (2007).

Ceriotti L., Kob A., Drechsler S., Ponti J., Thedinga E., Colpo P., Ehret R., Rossi F.: *Online monitoring of BALB/3T3 metabolism and adhesion with multiparametric chip-based system*. Analyt. Biochem. 371, pp. 92-104 (2007).

Coster H.G.L., Chilcott T.C., Coster A.C.F.: *Impedance spectroscopy of interfaces, membranes and ultrastructures*. Bioelectrochem. Bioenergetics 40, pp. 79-98 (1996).

Ehret R., Baumann W., Brischwein M., Schwinde A., Stegbauer K., Wolf B.: *Monitoring of cellular behaviour by impedance measurements on interdigitated electrode structures*. Biosens. Bioel. 12, pp. 29-41 (1997).

Fricke H.: *The Electric Capacity of Suspensions of Red Corpuscles of a Dog*. Phys. Rev. 26 (5), pp. 682-687 (1925).

Fricke H., Curtis H.J.: *Electric Impedance of Suspension of Yeast Cells*. Nature 134 (3377), pp. 102-103 (1934).

Giaever I., Keese C.R.: *Monitoring fibroblast behavior in tissue culture with an applied electric field*. Proc. National Academy of Sciences USA 81 (12I), pp. 3761-3764 (1984).

Guan Y., Kisaalita W.: *Cell adhesion and locomotion on microwell-structured glass substrates*. Colloids Surf., B 84, pp. 35-43 (2011).

Hamann C.H., Hamnett A., Vielstich W.: Electrochemistry. Wiley-VCH, 2nd, Completely Revised and Updated Edition, ISBN 978-3527310692 (2007).

Horton H.R., Moran L.A., Scrimgeour K.G., Perry M.D., Rawn J.D.: *Biochemie*. 4. Auflage, ISBN 978-3-8273-7312-0, Pearson Studium (2008).

Huang W.-T., Levitt D.G.: *Theoretical Calculation of the Dielectric Constant of a Bilayer Membrane*. Biopyhsical J. 17, pp. 111-128 (1977).

Huang X., Greve D.W., Nguyen D.D., Domach M.M.: *Impedance Based Biosensor Array for Monitoring Mammalian Cell Behavior*. Proc. IEEE Sensors 1, ISBN 0-7803-8133-5, pp. 304-309 (2003).

Huang X., Nguyen D., Greve D.W., Domach M.M.: *Simulation of Microelectrode Impedance Changes Due to Cell Growth*. IEEE Sensors J. 4 (5), pp. 576-583 (2004).

Igreja R., Dias C.J.: *Analytical evaluation of the interdigital electrodes capacitance for a multi-layered structure*. Sens. Actuators, A. 112, pp. 291-301 (2004).

Keese C.R., Giaever I.: *A Biosensor that Monitors Cell Morphology with Electrical Fields*. IEEE Eng. Med. Biol. Mag. 13 (3), pp. 402-408 (1994).

Lasia A.: *Electrochemical Impedance Spectroscopy and Its Applications, Modern Aspects of Electrochemistry*. B. E. Conway, J. Bockris, and R.E. White, Edts., Kluwer Academic/Plenum Publishers, New York, Vol. 32, pp. 143-248 (1999).

Lodish H.F.: *Molecular Cell Biology*. 6th edition, W.H. Freeman & Co, ISBN 978-0-7167-7601-7 (2008).

Molecular Devices: *CellKey-System*. Datasheet and characterization available online www.moldev.com

Pennisi C.P., Dolatshahi-Pirouz A., Foss M., Chevallier J., Fink T., Zachar V., Besenbacher F., Yoshida K.: *Nanoscale topography reduces fibroblast growth, focal adhesion size and migration-related gene-expression on platinum surfaces*. Colloids Surf., B 85, pp. 189-197 (2011).

Pethig R.: *Dielectric Properties of Biological Materials: Biophysical and Medical Applications*. IEEE T. Electrical Insulations EI-19 (5), pp. 453-474 (1984).

Randles J.E.B.: *Kinetics on rapid electrode reactions*. Discussions on the Faraday Society 1, pp. 11-19 (1947).

Rümenapp C., Remm M., Wolf B., Gleich B.: *Improved method for impedance measurements of mammalian cells*. Biosens Bioel. 24, pp. 2915-2919 (2009).

Sacristán-Riquelme J., Segura-Quijano F., Baldi A., Teresa Osés M.: *Low power impedance measurement integrated circuit for sensor applications*. Microelectronics J. 40, pp. 177-184 (2009).

Segura-Quijano F., García-Cantón J., Sacristán J., Teresa Osés M., Baldi A.: *Wireless powering of single-chip systems with integrated coil and external wire-loop resonator*. Applied Physics Letters 92, 074102 (2008).

Stieglitz T., Koch K.P., Schuettler M.: *Flexible, Polyimide-Based Modular Implantable Biomedical Microsystems for Neural Prostheses*. IEEE Eng. Med. Biol. Mag. 24 (5), pp. 58-65 (2005).

Warburg E.: *Über das Verhalten sogenannter unpolarisirbarer Elektroden gegen Wechselstrom*. Annalen der Physik und Chemie 67 (3), pp. 493-499 (1899).

Wheeler T.G., Goldschmidt M.C.: *Determination of Bacterial Cell Concentrations by Electrical Measurements*. J. Clin. Microbiol. 1 (1), pp. 25-29 (1975).

Whitesides G.M.: *The origins and the future of microfluidics*. Nature 442, pp. 368-373 (2006).

Xu J., Meynants G., Merken P.: *Low-Power Lock-In Amplifier for Complex Impedance Measurement*. 3rd Int. Workshop on Advances in Sensors and Interfaces (IWASI) 2009, ISBN 978-1-4244-4708-4, pp. 110-114 (2009).

# Chapter 4

# MEASUREMENT SETUP

Generally, investigations on cell cultures requires a large number of samples for balancing statistical uncertainties. To ease and parallelize experiments, standard microtiter plates, which have specially formed covers providing an efficient protection against contamination from the laboratory environment, are chosen. The dimensions of the sensor device allow the use of a 6-well microtiter plate as a rack and contamination protection for the developed measurement system. This means that the system can be implemented with conventional methods and operators do not need to change their procedures.

Cable connections and lead-throughs for the sensor devices are replaced by a wireless measurement and transmission technique based on RFID technology. A sensor device is plugged onto a battery-free, wireless device known as *tag* in the RFID-context. Each well of the microtiter plate is equipped with such a sensor device-tag-setup and placed onto a base station for wireless communication inside an incubator. Cells can then proliferate inside the sensor device within the humidified, temperature- and $CO_2$-controlled atmosphere of the incubator. Meanwhile, the tag electronics performs impedance measurements triggered and powered by the base station.

A variety of wireless sensors for different applications is already reported. Those may be an integrated circuit for a certain sensor or even a modulation of the RF-field itself as the sensed value [Ong *et al.* 2001, Brandl *et al.* 2009, Farinhol *et al.* 2009, Nopper *et al.* 2010, Oprea *et al.* 2008, Segura-Quijano *et al.* 2010]. FIG 4.1 shows a scheme of the invented apparatus.

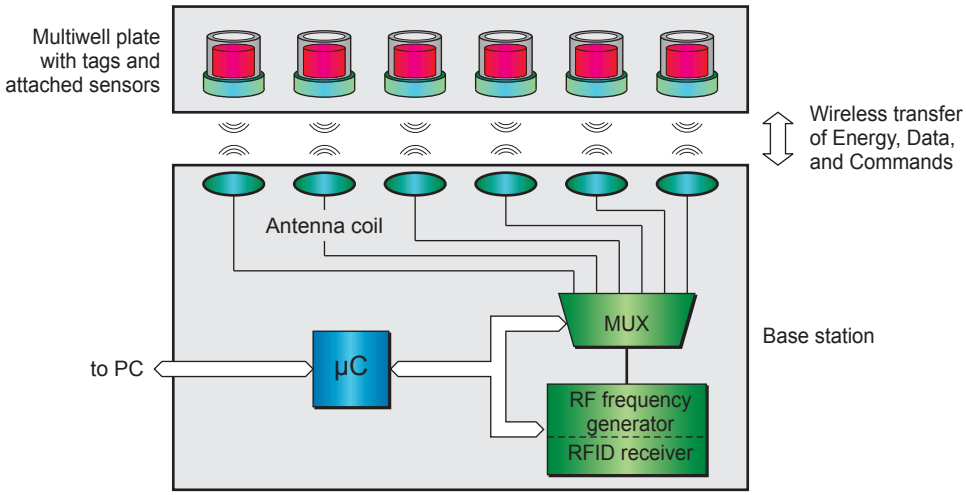


FIG 4.1: Base station schematic. A microtiter plate with sensor-equipped tags is placed onto a base station. It has an array of corresponding coils for a magnetically coupled data- and energy-transfer to the tags.

A four-wire-flatband cable is led through the rubber lips of the incubator door for power supply and communication of the base station with a computer. A hardware-addressing of the station allows the use of more than one by connecting that cable through. Outside the incubator only a small box for the power supply is required and a low-end-computer to control the system. The base station has to fulfill several requirements, i.e. power supply of the tags via an RF-field, communication with the tags via this RF-link, buffering measurement data, and communication with the computer.

## 4.1. RF Interface

A battery-free tag, also known as passive tag, is powered by the energy of the RF-field emitted by the base station. In the present case this is the alternating magnetic field of a spiral coil. Weakly coupled magnetic systems take advantage of resonant adjusted LC-circuits with the basic formula $(2\pi f_0)^2 L C = 1$. The inductance $L$ is realized by a spiral coil which is limited by size of the tag to values of less than 4 µH. The capacity $C$ will be held greater than 100 pF to limit influences of parasitic capacities. Commercially available RFID technique with a frequency $f_0 = 13.56$ MHz was found to provide a suitable basis for the wireless interface. Also, the necessary ICs and transceiver systems are available [Finkenzeller 2010].

### 1. Theory on magnetic coupling

The magnetic coupling of the base station to the tags is established via spiral coils on both sides. With respect to future miniaturization of the system and because of space

restrictions the tag coil has an outer diameter of 15 mm could be used in 24-well-systems. The base station coils have outer diameters of 18 mm. This bigger diameter provides robustness of the RF-link against lateral positioning mismatches. Even without the option for miniaturization the small coil diameters avoid eddy currents in the metallic environment of an incubator. Also, parasitic voltages at the circuitry of the base station are avoided. The PCB carrying that circuitry is situated about 20 mm below the coil array (see also Appendix B).

The inductances and ohmic resistances are $L_1 = 450\,\text{nH}$, $R_1 = 500\,\text{m}\Omega$ for a base station coil and $L_2 = 370\,\text{nH}$, $R_2 = 800\,\text{m}\Omega$ for a tag coil. The vertical distance $z$ is about 3.5 to 4 mm. An approximation of the magnetic coupling factor $k$ in the case of coaxially oriented coils is

$$k \approx \left( \frac{r_1 \cdot r_2}{z^2 + r_x^{\,2}} \right)^{3/2} \tag{4.1}$$

where $r_1$ and $r_2$ are the coil radii and $r_x$ is the larger one of those radii [Finkenzeller 2010]. The previously given geometric dimensions result in a coupling factor of $k \approx 60\,\%$. This formula is a guideline as it does not incorporate the spiral shape of the coils and lateral positioning mismatches.

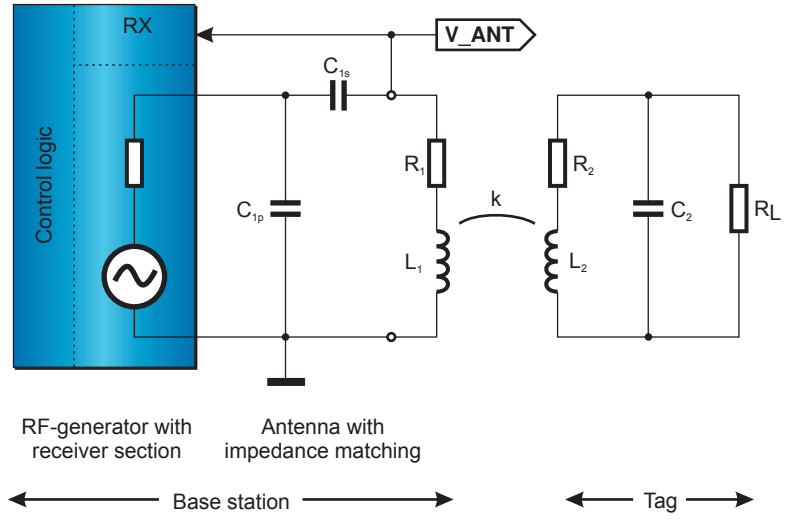


FIG 4.2: Fundamental tag schematic and coupling to the primary coil of a base station by a coupling factor $k$. The tag is formed by a coil $L_2$ with its resistance $R_2$, capacitor $C_2$ and a load resistor $R_L$. The primary coil $L_1$ has a resistance $R_1$. The tag impedance $Z_T$ can be transformed to an impedance $Z_T'$ lying in series to $L_1$. The load resistance can be set to $R_L = 8\,\text{k}\Omega$ with respect to the realized tags. An RF-generator for such an application has an output impedance of $50\,\Omega$ and is designed for a $50\,\Omega$ antenna.

In practice, $k$ is within a range 55 to 65 %. Therefore, the RF-link needs a robust design which takes that variation into account. In a first approximation, a tag can be represented by a LC-oscillator with a load resistance $R_L$ as shown in FIG 4.2.

The tag, i.e. the secondary side, with its impedance $Z_T = [R_2 + j\omega_0 L_2 + R_L (1 + j\omega_0 L_2)^{-1}]$ can be transformed to the primary side and handled as an impedance lying in series to $L_1$. This impedance is known as the *Transformed Tag Impedance* $Z_T'$ and is calculated according to formula (4.2).

$$Z_{\mathbf{T}}' = \frac{k^2 \omega_0^{\,2} L_1 L_2}{R_2 + \mathbf{j}\omega L_2 + R_{\mathbf{L}} \cdot (1 + \mathbf{j}\omega R_{\mathbf{L}} C_2)^{-1}} \tag{4.2}$$

The overall antenna impedance $Z_{Ant}$ is

$$Z_{\mathrm{Ant}} = R_1 + j\omega_0 L_1 + Z_T' \tag{4.3}$$

RF-generators are mostly designed to deal with an effective ohmic antenna impedance of $Z_0 = 50\,\Omega$. A properly defined capacitor network formed by $C_{1s}$ and $C_{1p}$ allows such an impedance matching if the real part of the antenna impedance is equal to or less than $Z_0$.

$$C_{1\mathbf{p}} = \frac{[Z_0 / \Re\{Z_{\mathbf{Ant}}\} - 1]^{1/2}}{\omega_0 Z_0}$$

$$C_{1s} = \frac{1}{\omega_0}\left[\Im\{Z_{\mathrm{Ant}}\} - \Re\{Z_{\mathrm{Ant}}\} Z_0 \omega_0 C_{1p}\right]^{-1} \tag{4.4a,b}$$

The antenna impedance is not constant due to previously mentioned changes of the coupling factor $k$. However, the capacities can be adjusted for a nominal coupling situation as the RF-generator provides enough power reserve in the case of mismatches. It should be mentioned that in some cases conductor loops of the tag circuitry influence the Transformed Impedance. Hence calculations for $C_{1p}$ and $C_{1s}$ can only be used as guidance values which are $C_{1s} = 144$ pF and $C_{1p} = 776$ pF in the present arrangement.

## 2. Data communication

Data and command transmission is only directed from tag to base station. This master-slave-principle simplifies the communication protocol and avoids the implementation of detection circuitry and program code at the tag side. The communication is established via load modulation. A modulation resistor is connected in parallel to the tag load $R_L$. This leads to a modulation of $Z_T'$ which in turn modulates the voltage $V_{Ant}$ at the antenna (see also FIG 4.2). Some RFID-systems use Amplitude Shift Keying (ASK) with a sub-carrier-frequency $f_0/2^6 = 212$ kHz. In the present case the tag works with its own microcontroller clock with an instruction cycle of 500 ns. The subcarrier frequency is set to $f_{sc} = 250$ kHz, i.e. the modulation resistor is continuously connected through and disconnected.

The channel encoding is a bitwise encoding (…1X01Y01Z0…) where X to Z represent bits of the datagram. HIGH (logic 1) is transmitted with a frequency $f_{sc}$ for a period of 68 µs while the modulation is turned off for a LOW (logic 0) for the same period. The receiver section of the base station utilizes an envelope detector, which is an incoherent transformation of the signal to the base band. The bitwise encoding of the data including sufficient timing tolerances circumvents problems due to microcontroller clock mismatches as those clock generators do not use quartz oscillators but integrated RC-circuits with a timing accuracy of about ±2 %. FIG 4.3 shows an example for the transmission of a HIGH bit.

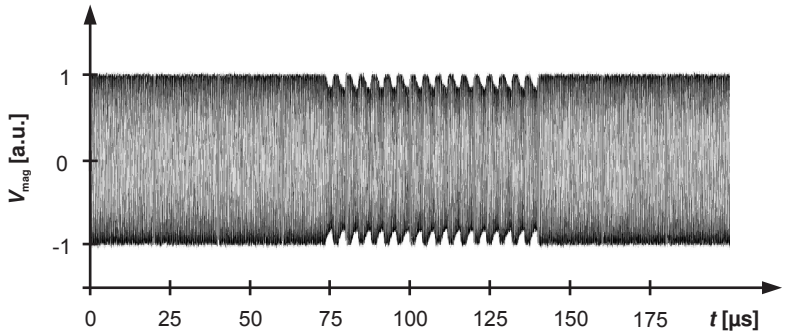


FIG 4.3: The load modulation causes a modulation of the magnetic field which can be made visible by the voltage $V_{mag}$ induced into a wire loop. The tag load is $R_L$ = 8 kΩ with a modulation resistor $R_{mod}$ = 3.3 kΩ in parallel which is turned on and off with the subcarrier-frequency $f_{sc}$ = 250 kHz. This modulation lasting for 68 µs represents a logic High.

A 24 bit-datagram is implemented for an efficient data transmission from tag to base station. It contains 4 bit control information, 16 bit data and a 4 bit Cycling Redundancy (CRC) checksum. The latter is built up using the generator polynomial CRC-4 recommended by the International Telecommunication Union (ITU) ($x^4 + x + 1$), the binary representation is 10011. Even though the 4 bits checksum can only validate a 15 bit data it was found to be a sufficient mechanism for erroneous detections within the base station's RF-receiver section [ITU-T 1998]. The effective transmission rate of (16+4) bits of data and commands is 20/(24·3·68) bits/µs = 4084 bits/s.

In the present case the $L_2C_2$-oscillator is not tuned for resonance. Hence a modulation of the tag load does only lead to a significant change of the antenna impedance $Z_{ant}$ if the modulation resistor is significantly smaller than the usual load. In the present system this resistor is $R_{mod}$ = 3.3 kΩ.

## 3. Low-noise Tag power supply

The power consumption of a conventional RFID-tag is in the sub-Milliwatt-regime. In opposite, the impedance measurement technique will require a low-noise stabilized power supply of several Milliwatts for a period of about 100 ms. As a consequence of the

system design the RF-field of the base station penetrates the tag's PCB carrying electronic components for the impedance measurements. The PCB layout causes several inevitable conductor loops which promote induced parasitic voltages. Moreover, the activation of some induction paths depends on the presence of parasitic diodes inside integrated circuits. During the design phase of the tags mistuning of the tag's microcontroller oscillator was found which caused failures in the timing of measurements if the RF field was present. In several cases the whole tag omitted operation.

The use of battery-buffered tags is hindered because a sufficient supply voltage level can only be achieved by space-consuming stacked cells. Furthermore, toxic components may influence the measurement and the highly humid incubator environment promotes self-discharge and regular maintenance would be required for replacing empty cells.

A sophisticated energy harvesting mechanism was developed which allows the use of passive tags without the problems that arise by an active RF field. While the field is active, the measurement circuitry is turned off, thus allowing a fast and efficient energy transfer. Afterwards, when the tag sends a specific command to the base station, the RF-field is blanked and the tag measurement circuitry is activated. The measurement can then be performed without any influence of the RF-field. FIG 4.4 shows the schematic of this patented principle [Austrian Research Centers GmbH 2009]. The LC-oscillator is followed by a bridge-rectifier. The switched resistor $R_{mod}$ is used for communication via load modulation and controlled via the microcontroller. Diode $D_1$ decouples that load modulator from the buffer capacitor $C_b$. The intermediate voltage circuit is followed by a fixed voltage regulator setting the supply voltage to $V_{DD} = 3.3\,V$.

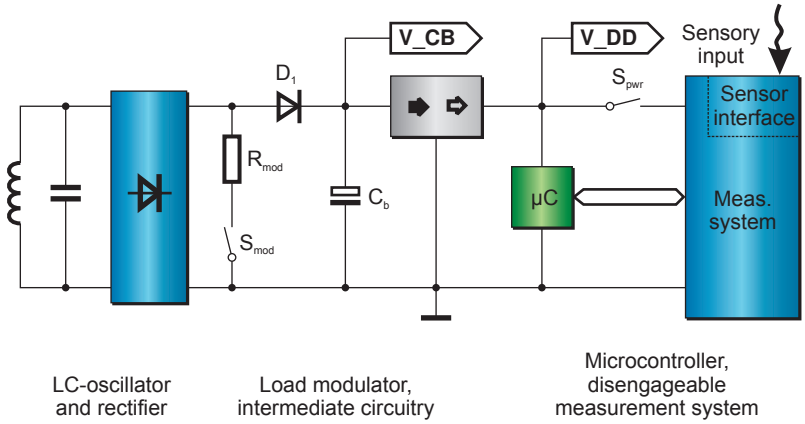


FIG 4.4: General tag schematic for the invented battery-free low noise power supply. $S_{mod}$ and $R_{mod}$ are used for load modulation, $D_1$ decouples the buffer capacitor $C_b$ from that circuitry. A certain measurement system can be disengaged via $S_{pwr}$ to optimize power consumption. Both switches are controlled by the microcontroller.

$V_{DD}$ is the power supply for both the tag-microcontroller (µC) and the measurement circuitry. The measurement system can be disengaged via $S_{pwr}$ which minimizes power needs as previously described. This leads to a maximized final voltage on $C_b$. The

impedance matching network of the base station (see Appendix B) is fine-tuned for this charging sequence. FIG 4.5 illustrates the charging-discharging sequences by the capacitor voltage $V_{Cb}$ and the antenna signal $V_{Ant}$. The latter does also show the influences caused by the load modulation which includes the command for blanking the RF-field.

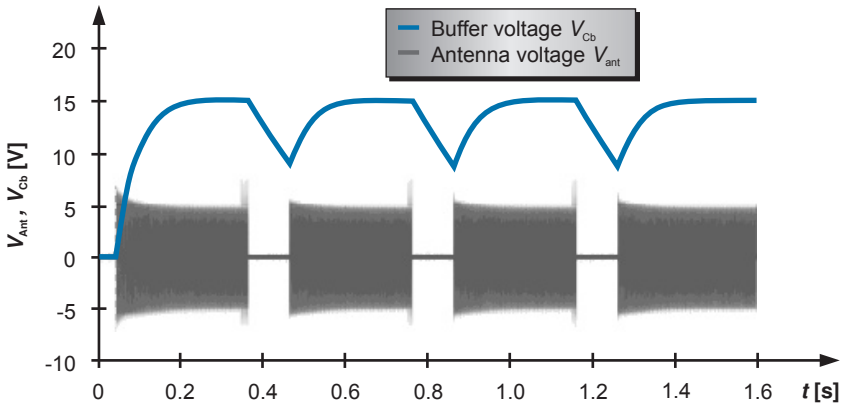


FIG 4.5: Buffer capacitor and antenna voltage during a measurement sequence. A load of 8 mA is applied for a period of 100 ms. The buffer is realized with a 100 µF tantalum capacitor.

When the RF-field is switched on a few milliseconds pass until the supply voltage level is high enough to power the tag-µC. After its startup the measurement circuitry is disengaged. The buffer capacitor is charged and the intermediate voltage rises to 15 V (or higher). After the specified charging time of 300 ms, the tag-µC sends a command to the base station to switch off the RF carrier for 100 ms, as presented in the graph. During this time span the buffer capacitor sustains the power of the whole circuitry, thus its voltage decreases. The period is long enough to conduct a measurement without disturbing effects of the RF-field. Subsequently, the measurement circuitry is blanked, the RF-field reactivated and the buffer capacitor is recharged. At this stage commands and data can be sent again. A new measurement cycle can also be initiated. This technique allows a decoupling of the tag components and thus an independent design of the measurement electronics. Whenever the buffer capacitor is charged the receiver section of the base station is set inactive for the first 200 ms. This avoids a misinterpreting of switching actions as load modulation.

## 4. An efficient power transfer

The tag microcontroller works with its full clock frequency which causes a permanent current consumption of at least 900 µA at 3.3 V. Conventional voltage regulators were not always able to deal with the ripple voltages induced by the RF-field. Hence the fixed voltage regulator was built up utilizing a micropower shunt as voltage reference and a

bipolar transistor as emitter follower [9]. This 4.1 V-shunt was connected to $V_{Cb}$ via a 10 kΩ-resistor leading to a cross-current of $I_0 = (V_{Cb} - 4.1\,V)/10\,k\Omega$, that is 1.2 mA at $V_{Cb} = 16$ V. The overall power consumption was about $16 \cdot (1.2 + 0.9)$ mW ≈ 34 mW. The power loss at the bridge rectifier increased that value to 40 mW including reserve.

The RF-generator has an output power of 200 to 250 mW at a 50 Ω-antenna. Thus, about 20 % of this power need to be transferred to the tag. The following calculations are based on the simplified schematic in FIG 4.2. A transfer efficiency $\eta_1$ is introduced and defines the fraction of the generator output power being transmitted to the tag. A second value, the tag's efficiency $\eta_2$, describes the fraction of this power which is available at the load resistor $R_L$.

$$\eta_1 = \frac{\Re\{Z_T'\}}{\Re\{Z_T'\} + R_1} \tag{4.5}$$

$$\eta_2 = \left[1 + R_2 R_L \left(R_L^{-2} + \omega_0^{\,2} C_2^{\,2}\right)\right]^{-1} \tag{4.6}$$

FIG 4.6 shows the efficiencies including the overall efficiency $\eta_{oa} = \eta_1\,\eta_2$ as a function of the tag capacity $C_2$.

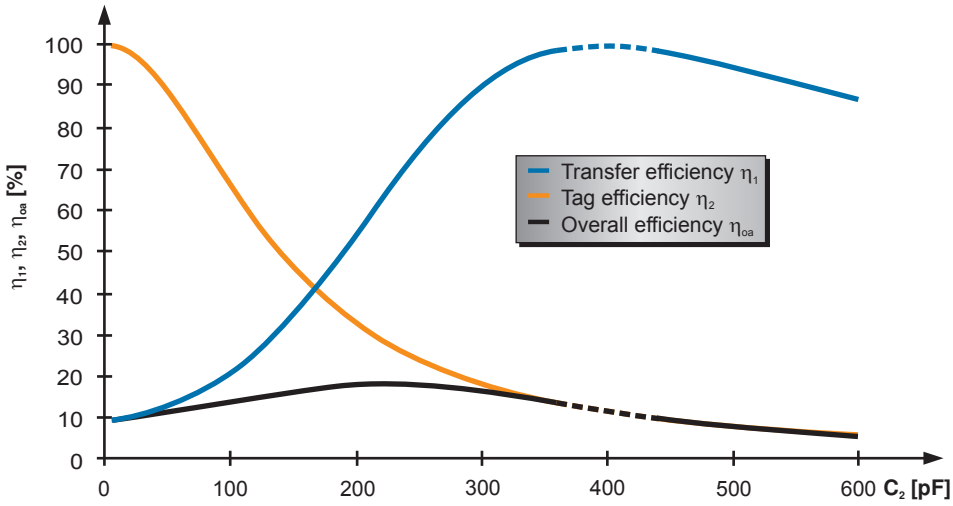


FIG 4.6: Simulation of the efficiencies as a function of the tag capacity $C_2$ for the nominal coupling factor $k = 60$ %. The dashed range around 350 to 450 pF indicates a real part $\Re\{Z_{ant}\} > 50\,\Omega$, i.e. the antenna impedance cannot be matched properly.

Higher values of $C_2$ increase the oscillating current. Hence the increasing power loss at the tag coil resistance $R_2$ decreases efficiency $\eta_2$. The peak at $\eta_1$ is given at resonance when the real part of the Transformed Impedance $Z_T'$ reaches its maximum. RFID-tags

[9] A micropower shunt is an almost ideal Zener-diode realized as an Integrated Circuit. In the present case this is a LM4040BIM7-4.1 with $V_Z = 4.1$ V.

are usually adjusted for resonance, i.e. $L_2C_2\omega_0^2 = 1$. Due to the high coupling of 60 % this real part reaches several 100 Ω [10]. That simulation does not incorporate parasitic loops, the highest power transfer was found for Capacitor $C_2$ = 300 pF.

The impedance matching for an effective antenna impedance of 50 Ω was done for the nominal coil distance $z$ = 4 mm. A simulation incorporating the $V_{Cb}$-dependent load-behavior of the tag led to a power transmission as shown in FIG 4.7. The RF-generator is simulated with a sinusoidal voltage source of 3.53 V rms and a 50 Ω output impedance for a nominal output power of 250 mW.

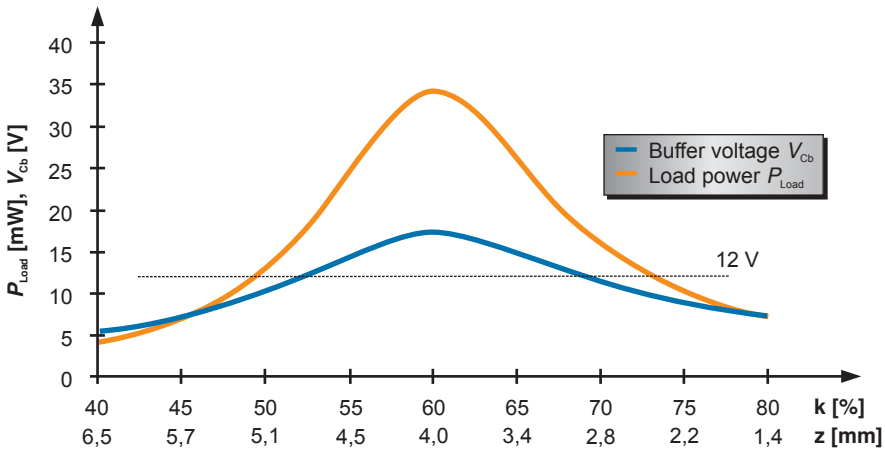


FIG 4.7: Simulation of the load behavior and buffer voltage depending on the coupling. The RF-generator is assumed to provide as sinusoidal signal of 3.53 V rms with a generator-resistance of 50 Ω lying in series. Impedance matching values are $C_{1s}$ = 153 pF and $C_{1p}$ = 548 pF. The second line of values at the x-axis is the vertical distance $z$ corresponding to $k$. 12 V mark the minimum voltage for proper tag functionality for a 100 ms RF blank period.

The minimum input voltage for the voltage regulator is 5.5 V and the measurement sequence may take up to 80 ms. With respect to lateral mismatching and the possibility of shortcuts in the DUT without causing malfunction a current consumption of 8 mA is assumed. Then a buffer capacitor of 100 µF needs to be charged to a voltage of at least (5.5 V + 8 mA·80 ms/100 µF) ≈ 12 V.

Even though the simulation data presented in FIG 4.7 shows a suitable high buffer voltage and a sufficient power transmission it does not incorporate parasitic effects. A tag has several inevitable loops by its PCB and circuit design. Those can become active if the RF-field of the base station induces sufficient high voltages making substrate and suppressor diodes of integrated circuits conductive. A practical consequence of such loops was found during the development of the first tag version as follows: The measurement circuitry has several Operational Amplifiers (OA) and the microcontroller.

[10] In several RFID-applications the coupling is smaller than 10 %. Then, RFID-antennas are fine-tuned without a tag presence. In the present case the real part would be $\Re\{Z_T'(k=0{,}1)\} \approx 20\,\Omega$.

Those require blocking capacitors at their voltage supply to suppress noise in order to achieve a suitable measurement signal quality. The blocking capacitors were continuously integrated and the whole tag tested on the base station. At a certain voltage level $V_{Cb}$ of the buffer capacitor the antenna voltage $V_{Ant}$ showed overlaid oscillations. Those were within the frequency range of the load modulation frequency, hence data communication was corrupted. However, the signal quality within the tag circuitry required the set capacitor values. That maloperation is fixed by a modification of the standby-configuration of the measurement circuits during buffer capacitor charging. The effect of such a modification is illustrated by FIG 4.8. Initially, the measurement circuit power supply is left floating as shown in FIG 4.4. A final buffer voltage of about 16 V would be achieved that way. The measurement circuit power supply is then connected through to ground after 100 ms. Hence several loops within the measurement circuit become active which in turn alters the antenna impedance. At 150 ms those loops are disconnected by opening several analog switches of the measurement circuitry. The antenna impedance again changes and a final buffer voltage of about 13 V is reached.

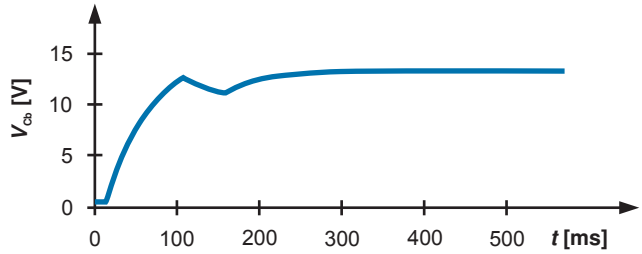


FIG 4.8: Charging behavior of the buffer capacitor $C_b$. The discontinuous voltage evolution is due to switching actions within the measurement circuitry.

The rectifying effect of substrate diodes can be found by measuring capacitor values when the RF-field is turned off. Especially RC-networks which are connected to the inputs of OAs show voltages of about 700 mV even though the power supply is shortened.

An advanced tag version circumvented such problems by a manual routing of the wires on the PCB almost eliminating conductive loops. Buffer voltages of 18 V and more were measured which were independent on analog switches' states. Residual voltages on RC-networks could still be found but no more oscillations which caused malfunction.

## 4.2. Measurement Electronics

Commercially available integrated impedance measurement circuits are AD5933 and AD5934 impedance converters from *Analog Devices*. Their high power consumption hinders the use for a battery-free low-noise implementation. Hence a discrete measurement technique needed to be designed. Within this work, two measurement techniques were developed. The second one, as an improvement of the first one, is more

power-efficient and flexible and both techniques have the almost same signal processing. Only the final data acquisition differs by a peak-detection and a sampling-method, respectively. The earlier technique is briefly discussed at the end of this section while the latest design is described in detail. FIG 4.9 shows the tag block schematic with the signal paths.

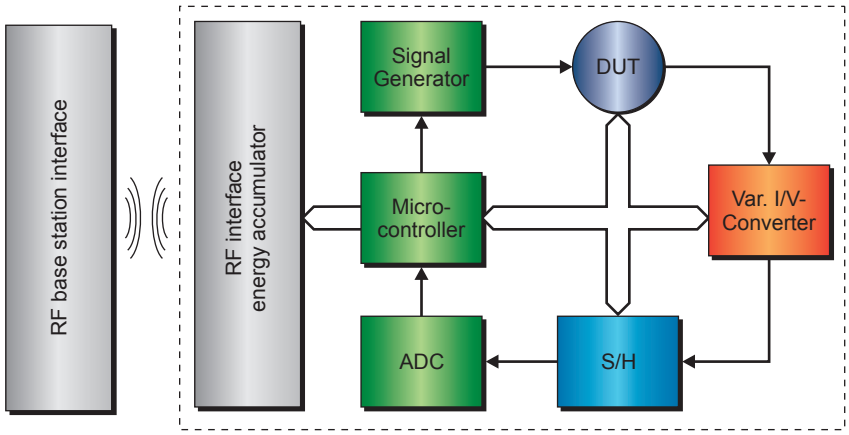


FIG 4.9: Schematic of the measurement system implemented in the tag (dashed box). The Device Under Test (DUT) can either be a reference element or a sensor selected by the microcontroller. The RF-interface and energy buffer system was previously described.

The microcontroller PIC16F688 from *Microchip Inc.* is the core of the measurement system. The PIC-family is frequently used for wireless and measurement applications [Beach *et al.* 2005, Martinez-Caltalá *et al.* 2009].

The µC generates a pulse pattern conditioned by the signal generator. The output is fed into a device-under-test (DUT), for instance, a sensor or a reference system. In addition to that a selectable reference element was incorporated, which allowed compensation of electronic drifts and component tolerances. The DUT current is then transformed into a proportional voltage. A sample-hold element buffers the output voltage for analog-to-digital conversion (ADC). The converted data are stored in the microcontroller registers and are transmitted to the reader by load modulation only when all samples were taken and the derived analog data converted to digital values. The reader is connected to a data acquisition system, in our case, a computer for further processing. FIG 4.10 shows the schematic of the invented circuitry. This chain can be split up into three parts. First, the probe signal generation, second, the current-to-voltage-conversion with variable amplification and, third, the sample-hold-element.

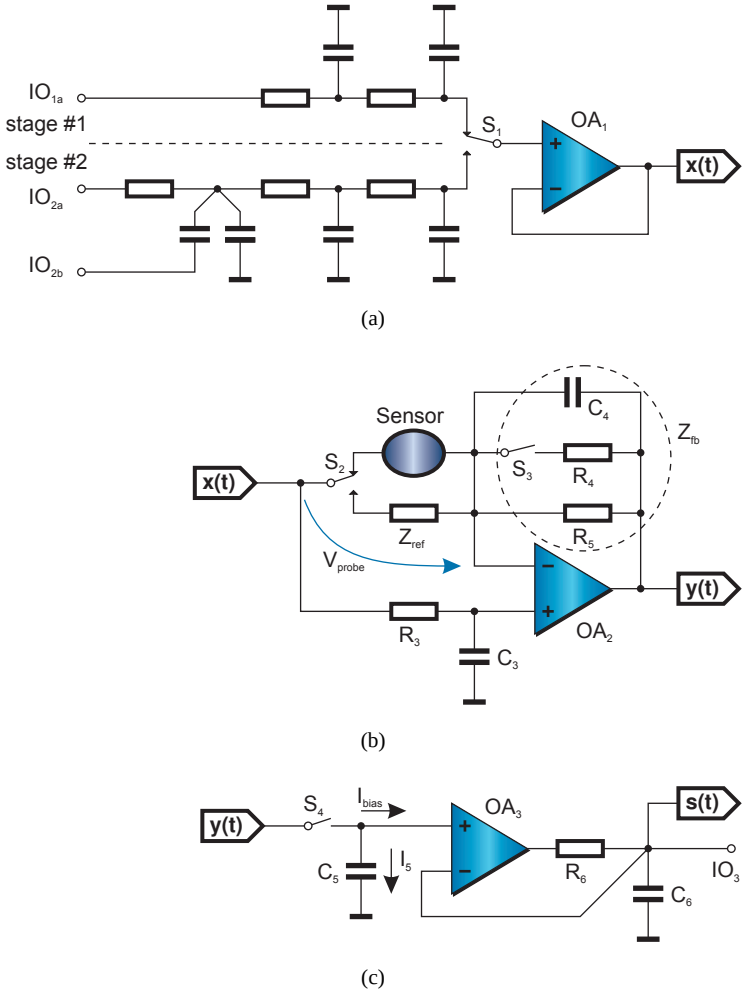


FIG 4.10: Schematic of the measurement circuitry consisting of the **(a)** signal generator, **(b)** reference element/sensor selector and current-to-voltage converter, and **(c)** sample-hold-element. The microcontroller and ADC are not shown.

## 1. Signal generator

The signal generator provides four frequencies of 5, 10, 20.8, and 50 kHz at probe voltage levels smaller than 35 mV rms. Actual methods for sinusoidal signal generation within the targeted frequency range often rely on direct digital synthesis ICs, but the required clock rates, power, and space constrictions do not allow their implementation in this system. The herein invented signal generation method builds on pre-calculated bit patterns as a hard-coded part of the microcontroller program code that is continuously fed into a low-pass filter. This pattern does already show a well-adapted frequency spectrum

with higher harmonics being formed at amplitudes below 40 dBc. This particular pattern is fed into filter stage #1 which further suppresses these respective harmonics and also adjusts the fundamental wave's peak voltage. The 5 kHz and 10 kHz signals can be generated with a total harmonic distortion of less than 0.3 %. Details on the bit pattern generation can be found in appendix C.2.

FIG 4.11 shows the FFT-analyzed probe voltage for a 10 kHz-signal. The noise shows 1/f-behavior until 20 kHz. The background-noise at higher frequencies is given by the 16 bit-resolution of the FFT-analyzer, i.e. $20 \cdot \log(2^{-16}) = 96$ dB.

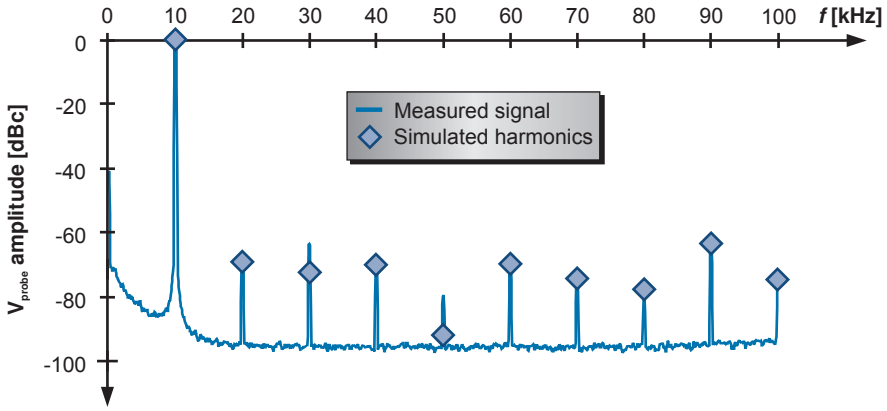


FIG 4.11: FFT-analysis of the probe signal in comparison with the simulated, filtered Fourier-coefficients of the bit pattern. The FFT was obtained with a rectangular window function of the analyzer *35670A FFT Dynamic Signal Analyzer* from *Agilent Technologies*. Differences at the 3rd and 5th harmonics may be due to nonlinearities of the OAs.

Yet due to the limited instruction cycle period of the microcontroller, higher frequencies cannot be provided in this way. To overcome this limitation the filtering of a rectangular signal by a second, carefully designed low-pass filter stage #2 is employed. A 3rd order filter with a cutoff-frequency being clearly smaller than the fundamental wave's frequency $f_X$ attenuates an $n^{th}$ harmonic by a factor approximately proportional to $n^3$. The rectangular input signal's Fourier-coefficient $n^{-1}$ effectively enhances the attenuation to $n^4$. The total harmonic distortion of a square wave filtered in this way is about 1.3%. This procedure is used for the 20.8 kHz- and 50 kHz-signal. Switch $S_1$ is incorporated to select the designated filter stage and to feed the voltage to buffer $OA_1$. The working point for the second filter is selected via $IO_{2b}$, which connects an additional capacitor through to ground for 20.8 kHz, or leaves it floating for 50 kHz.

## 2. I/V-converter and reference element

The low-pass filter $G_3 = (1 + j\omega T_3)^{-1}$ formed by $R_3$ and $C_3$ is integrated to eliminate the DC-component of $x(t)$ which results in a probe signal $V_{probe}(j\omega) = X(j\omega) \cdot [1 - G_3(j\omega)]$. Switch $S_2$ is incorporated to either select the reference, or the sensor element, but also

disconnects the sensor from the probe signal during circuitry start-up. Thus, transient voltages are avoided, which may otherwise affect the sensor surface. The measurement range can be adapted by switch $S_3$, and capacitor $C_4$ suppresses spurious peak voltages and oscillations at the output $y(t)$.

## 3. Sample-Hold and AD-conversion

Commercially available sample-hold IC's are almost only designed for high sampling rates, such as several thousand to million samples per second. In particular, their high speed is accompanied by a current consumption of several mA and supply voltages clearly above 3.3 V. Due to these boundary conditions a discrete sample-hold circuitry was designed for an adequate sampling speed and low power consumption. Fundamentally, it is built up by the analog switch $S_4$ and the sampling capacitor $C_5$. Depending on the leakage current of the analog input $IO_3$, the sampling capacitor may need to be large, which in consequence causes a significant current load when measuring with high frequencies. This problem is circumvented by the operation amplifier $OA_3$ with a low bias current, which actually allows the use of a small capacity. Resistor $R_6$ is used as a shortcut-protection (tri-state and analog input of the microcontroller) and together with $C_6$, it forms a low-pass filter against noise from stray fields.

## 4. Calculation of the Sensor impedance

The I/V-converter is an inverting voltage amplifier for $x(t)$. Hence taking into consideration the gain-bandwidth (GBW), the gain will vary by the selected measurement range and the sensor/reference impedance. In the present case the rather small probe signal amplitude of less than 40 mV is amplified up to $V_{DD}/2 = 1650$ mV (a factor $\leq 41$), and for a phase shift of less than 1° a GBW greater than 41.50 kHz/tan(1°) = 117 MHz is required. Notably, most available OAs of convenient speed have too high current consumptions, or the offset voltage as well as bias currents lead to a significant DC-offset within the probe signal. The selected OA AD8606 has a much lower GBW product of 9 MHz and its bias currents and offset voltage ensure an effective offset below 1 mV. Given the known circuit and device parameters it became possible to cancel phase shifts, which cannot be neglected at high signal frequencies, as well as amplitude attenuation. In the frequency domain the output $Y(j\omega) = \mathcal{F}\{y(t)\}$,

$$\frac{Y(j\omega)}{X(j\omega)} = \frac{G_3 - Z_{fb}\left(Z_{fb} + Z_{DUT}\right)^{-1}}{{G_{oa}}^{-1} + Z_{DUT}\left(Z_{fb} + Z_{DUT}\right)^{-1}} \tag{4.7}$$

for a DUT impedance, representing the sensor impedance $Z_{sens}$ or reference impedance $Z_{ref}$, respectively. $Z_{fb}$ is the effective feedback impedance formed by $R_4$ (lying in parallel to $R_5$ when switch $S_3$ is closed) and $C_4$ $G_{oa} = [v_{inf,oa}\,(1+ j\,f/f_{g,oa}) - 1]$ is the transfer function of the OA. After a measurement sequence, the acquired sampling values were transmitted to and processed in a proper computing environment. There, they were subjected to discrete Fourier transformation (DFT) for $Y_{ref}(j\omega)$ and $Y_{sens}(j\omega)$. The upper

equation is formed for both impedance measurements and ratio calculated according to formula (4.8).

$$\frac{Y_{\text{sens}}(j\omega)}{Y_{\text{ref}}(j\omega)} = \frac{G_3 - \dfrac{Z_{\text{fb,sens}}}{Z_{\text{sens}} + Z_{\text{fb,sens}}}}{\dfrac{1}{G_{\text{oa}}} + \dfrac{Z_{\text{sens}}}{Z_{\text{sens}} + Z_{\text{fb,sens}}}} \cdot \frac{\dfrac{1}{G_{\text{oa}}} + \dfrac{Z_{\text{ref}}}{Z_{\text{ref}} + Z_{\text{fb,ref}}}}{G_3 - \dfrac{Z_{\text{fb,ref}}}{Z_{\text{ref}} + Z_{\text{fb,ref}}}} \tag{4.8}$$

$Z_{\text{fb,sens}}$ and $Z_{\text{fb,ref}}$, respectively, represents the impedance $Z_{\text{fb}}$ for sensor and reference measurement, which may be different due to an open or closed switch $S_3$. This equation allows an explicit formula for $Z_{\text{sens}}$ and, thus, the compensation of bandwidth-limitations of OAs. Also, different measurement ranges are taken into account.

# 5. Microcontroller Firmware concepts

A well-defined system start-up state needs to be ensured. Therefore, the circuitry has to be fully initialized in a short time slot just before each measurement cycle, thereby avoiding parasitic conductive loops. The latter are inevitable in the PCB layout, induce unwanted voltages and may additionally charge the employed capacitors. During start-up the algorithm utilizes the direct control of the probe signal generation by the microcontroller.

**Circuit Initialization**

When initially powering the OAs, the voltage of capacitor $C_3$ at the non-inverting input of $OA_2$ is $V_{C3} = 0$. This demanded an accurate method for a DC-free probe voltage. The production-related tolerances of $R_3$ and $C_3$ do not allow using time-related charging sequences. Moreover, it was found that conductor loops caused by the PCB-layout in combination with protection diodes on the Integrated Circuits' inputs act as a charging system, while the RF-field is active. Thus, the initial voltage of the capacitor can go up to 700 mV making it impossible to achieve a defined charging state for $C_3$ without any feedback.

Hence a separate algorithm was implemented that directly addressed the measurement system for feedback control. Fast alternating outputs on either $IO_{1a}$ or $IO_{2a}$ led to almost ripple-free $V_{DD}/2$-outputs for $x(t)$. With $x(t) \approx V_{DD}/2$ and

$$Y(\mathrm{j}\omega) = V_{C3}(\mathrm{j}\omega) - [V_{C3}(\mathrm{j}\omega) - X(\mathrm{j}\omega)] \cdot \frac{Z_{\text{fb}}}{Z_{\text{ref}}} \tag{4.9}$$

for $\omega = 0$ the output $y(t)$ is below $V_{DD}/2$ while $V_{C3}$ was smaller than $V_{DD}/2$. This system characteristic allows the following algorithm for charging $C_3$ in a controlled manner.

(a) Set $S_2$ to reference impedance
(b) Set $Z_{\text{fb}} = R_4 \parallel C_4$ (highest impedance, minimize initial current through $Z_{\text{ref}}$)
(c) Set $S_2$ to filter stage #2 (higher dynamic behavior)
(d) Set $IO_{2a}$ to $V_{DD}$ for 500 µs (initial boost)

(e) Set $Z_{fb}$ to smallest value (for a minimized ripple on the output $y$)
(f) Rectangular output on $IO_{2a}$ with maximum possible frequency for 100 µs.
(g) Do AD-conversion (100 µs).
(h) If $y(t)$ is bigger than ($V_{DD}/2 - 13\,mV$) finish algorithm (13 mV is the ADC resolution in an easier to handle and adequate 8 bit mode).
(i) Set $IO_{2a}$ to $V_{DD}$ for 50 µs, then go to step (f).

During this process, $IO_{1a}$ is continuously fed with a 200 kHz rectangular signal to allow fast switching to the sensor after the initialization sequence if filter stage #1 is needed afterwards for a subsequent probe signal generation.

This sequence initially charges for 500 µs and the following short charging steps allow a gradual (steps of about 80 mV) convergence to $V_{C3} = V_{DD}/2$. Switching to min($Z_{fb}$) in step (e) minimizes the ripple on $y(t)$ caused by the residual ac-components of $x(t)$. FIG 4.12 shows a representative example.

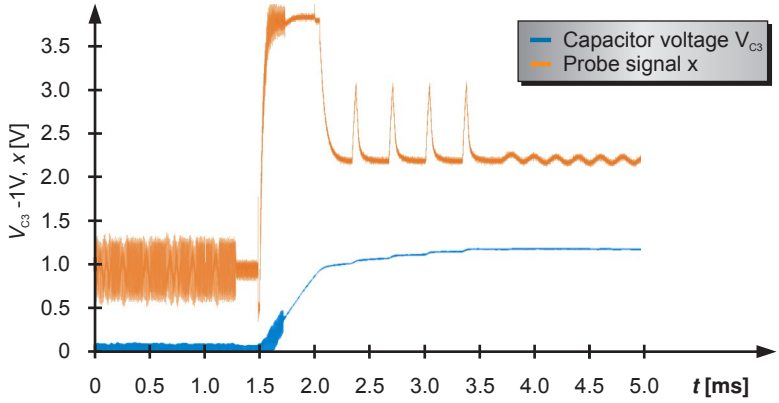


FIG 4.12: Voltages $x$ and $V_{C3}$ at $C_3$ during ramp-up with $V_{C3}$ shifted by 1 V for a better illustration. The noise within the first 1700 µs is due to the active RF-field of the reader including influences due to the load-modulation-based communication. The dip at 2000 µs is due to the changed feedback-impedance at step 5 of initialization.

Noise on $x(t)$ and $V_{C3}(t)$ is likely due to the RF-field of the base station. The blanking command sent by the tag ends at 1250 µs (visible by the modulations on the noise of $x$) and the base station takes another 500 µs to turn the RF-generator off. Moreover, $V_{C3}$ and also $x(t)$ do not start at 0 V but show offsets of a few 100 mV as explained earlier in this section.

This algorithm additionally allows the implementation of health state self monitoring. If the AD-conversion shows a too high value for $y(t)$ after the boost sequence (step c), or if too much iterations of steps (f) to (i) occur, electronic defects are easily being recognized.

**Sensor probe signal**

After the setup-boost sequence, the program switched to the actually selected measurement frequency. Meanwhile the output $IO_{1a}$ and $IO_{2a}$ consecutively alternate outputs with about 200 kHz to remain on an average $V_{DD}/2$-level.

The setup-boost set $V_{C3}$ to about $(V_{DD}/2)^{\pm 20\,mV}$. When $x(t)$ delivers the probe signal, it operated for a period of about 1 ms before the switch $S_2$ connects $x(t)$ with the sensor. With $T_3 = 1.2$ ms the residual DC-component decays to a value of less than 10 mV. Within that millisecond and after $5T_3$ it becomes indistinguishable from bias-current- or offset-voltage-related effects. FIG 4.13 shows the probe voltage $V_{probe}$ on the sensor when it is connected through to the sensor.

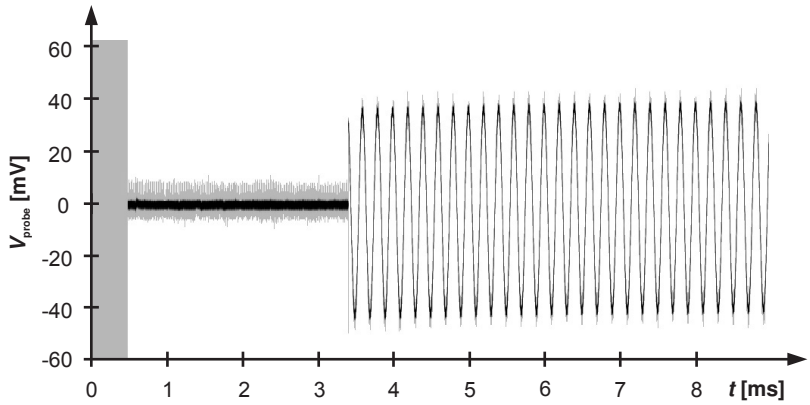


FIG 4.13: Probe signal at the sensor if it is selected for measurement. The noise within the first 500 µs is due to the RF-field inducing parasitic voltages to the probe tips. Timestamp 0 is about timestamp 1.3 ms in FIG 4.12.

**Taking samples**

Sampling starts about 50 ms after the probe signal is applied to the sensor in order to await a steady-state situation. The sampling process for five samples is depicted in FIG 4.14 including a close-up view for the 2nd sample. When switch $S_4$ is opened, conversion is triggered only after a settling time of 100 µs is reached. The overall sampling and conversion time takes about 300 µs. After the conversion process, the microcontroller shifts the digital data to a reserved place in the General Purpose Registers, and set a data pointer to a new free place on that register for the following data. All those steps, i.e. sampling, converting, and data shifting, are interlocked with the generation of the probe signal. For a better visibility the period between adjacent samples is stretched to 5 ms, the smallest period being either twice the signal periodicity, or

depending on the implemented signal generation program code and the availability of *No Operation* commands within the bit pattern generation [11].

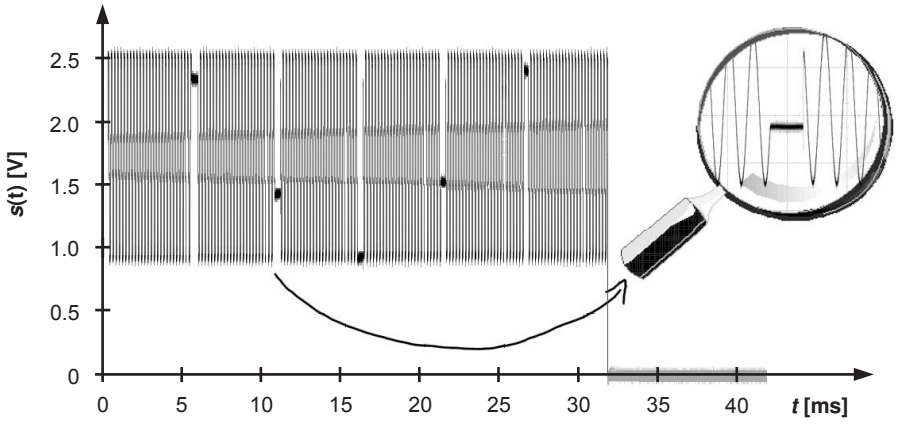


FIG 4.14: ADC input signal $s(t)$. Five samples taken in a series for a signal frequency of 5 kHz. The inset shows a close up of the 2nd sample with a time-resolution of 500 µs/div.

**Automatic measurement range selection**

The used capacitive sensors are prone to vary their impedance by a factor of 10 within the realized different measurement frequencies. Thus, the feedback-impedance of the current-to-voltage-converter has to be adapted by $S_3$ to provide an appropriate data range. During adaption phase, a first low sensitivity measurement is performed. Then the highest and lowest sampled values are accounted by the firmware to gain highest sensitivity. Next, the sensitivity range is changed accordingly. $S_2$ may be closed, and the measurement repeated. This pre-analysis also allows the detection of sensor defects and short cuts.

**System accuracy**

A test on a lumped RC-circuit with $R = 100\,\Omega$ and $C = 168$ nF lying in series showed that the absolute value of that impedance could be measured with an accuracy better than 1 % and the phase error was less than 1° for all four probe signal frequencies. A variation of the nominal values of $f_{g,oa} = 90$ Hz and also of $T_3 = 1.2$ ms of ±10 % did not show significant changes in the computed results. Thus, it can be stated that the compensation mechanism is robust enough to deal with typical device tolerances. TABLE 4.I shows the results of a DFT transformation of the reference and sensor sampling. That is followed by the calculation of the sensor impedance split into two parts. First, $OA_2$ is handled as an ideal OA, i.e. $G_{oa}(j\omega) \rightarrow \infty$. In a second approach, the cutoff-frequency and the gain are

[11] The previously shown bit patterns for the probe signal generation have unchanged states marked with „c“ whereas exactly those actions can be executed.

taken into account. The compensation calculation is a necessary step to avoid a loss on accuracy, particularly with regard to the phase at high frequencies.

TABLE 4.I: Calculated results for a test impedance (100 Ω + 168 nF)

| | **5 kHz** | **10 kHz** | **20.83 kHz** | **50 kHz** |
|---|---|---|---|---|
| $\lvert Y_{ref}(j\omega)\rvert$ [a.u.] | 819 | 723 | 656 | 806 |
| $\arg\{Y_{ref}(j\omega)\}$ [deg] | 32.4 | 44.7 | 115.7 | 90.8 |
| $\lvert Y_{sens}(j\omega)\rvert$ [a.u.] | 851 | 1175 | 1339 | 1739 |
| $\arg\{Y_{sens}(j\omega)\}$ [deg] | 94.3 | 87.2 | 137.2 | 93.6 |
| Set-values of the measured impedance | | | | |
| $\lvert Z_{sens}(j\omega)\rvert$ [Ω] | 214.2 | 137.7 | 109.9 | 101.8 |
| $\arg\{Z_{sens}(j\omega)\}$ [deg] | -62.2 | -43.5 | -24.5 | -10.7 |
| Results without compensation calculation ($G_{oa}(j\omega)\rightarrow\infty$) | | | | |
| $\lvert Z_{sens}(j\omega)\rvert$ [Ω] | 213.2 | 135.0 | 106.5 | 100.4 |
| $\arg\{Z_{sens}(j\omega)\}$ [deg] | -62.5 | -43.3 | -22.1 | -2.9 |
| Results with compensation calculation | | | | |
| $\lvert Z_{sens}(j\omega)\rvert$ [Ω] | 215.7 | 138.5 | 110.4 | 102.3 |
| $\arg\{Z_{sens}(j\omega)\}$ [deg] | -62.4 | -43.6 | -24.4 | -10.2 |

## 6. An early measurement electronics approach

The invented measurement technique was a modification of an early tag version. Even though its current consumption was much higher (up to 8 mA) and the upper frequency limit was given at about 10 kHz, essential know-how was accumulated with that approach, e.g.

- the energy transfer and -storage for a low-noise tag power supply (see chapter *4.1.3 Low-noise Tag power supply*),
- a flexible communication protocol,
- the malfunctions caused by PCB loops, so the latest design was exclusively manually routed, or
- the influence of the packaging (see following chapter *4.3 Tag Design and Packaging*).

Instead of a PIC16F688 the low-end model PIC16F676 was used. That model had a lower power consumption but did also run on the half clock frequency. Hence the bit pattern for the probe signal was not that fine with a THD of about 0.5 %. The signal

processing was different as $V_{DD}/2$ was subtracted from output $y(t)$ by an additional OA. That signal $y_{mod}$ did only carry the positive half wave and via switch $S_4$ it was fed into a peak-detector instead of the sample-hold-element. Two measurement sequences were performed at a frequency of 10 kHz. During the first sequence switch $S_4$ was kept closed and the voltage-converted and DC-shifted current-peak was detected. At the second sequence $S_4$ was opened at the probe voltage zero-crossing and the peak detector input forced to ground. Thus, the detected voltage was proportional to the peak-value multiplied with the sine of the current-phase.

The firmware-coding was much less challenging compared to a sampling-based method and even though a post-processing was required for the elimination of offset-values the raw data could directly be interpreted (e.g. the peak-values) instead of a subsequent DFT-processing. The amplitude $y_{mod}$ measured by the peak detector can be described by formula (4.10).

$$y_{mod} = (\hat{x} + O_1)\frac{Z_{fb}}{Z_{DUT}} + O_2 \tag{4.10}$$

$Z_{DUT}$ may be the reference resistor or the absolute value of the sensor impedance, respectively. Offset $O_1$ is caused by the bias-currents and the offset-voltage of $OA_2$. $O_2$ is caused by the subtractor and the peak-detector. The critical aspect on $O_1$ is that it does only take effect when measuring an ohmic load, i.e. the reference resistor. This DC-part is blocked by the sensor device and needs therefore to be taken into account.

The calculation of both offsets required the reference resistor to be measured with the original probe signal and also with another (higher) amplitude of 100 mV. Additionally, a third measurement with a different feedback-impedance is also necessary.

A disadvantage of that method was the necessity of quite fast OAs for the voltage subtractor and the peak detector. The current consumption was more than 6 mA. Also, the peak detector did not lead to satisfying results for frequencies above 10 kHz. However, that system was used for most measurements and had an endurance for several 1000 hours. The accuracy was better than 3 % for the absolute impedance value. The phase detection had an effective accuracy of about 3°. As the relative change of the real part of a sensor was more important than the absolute value, the phase offset was not critical.

## 4.3. Tag Design and Packaging

The devices listed in *Appendix B* led to a current consumption of 2.5 mA at a $V_{DD}$=3.3 V supply voltage. The resistors had tolerance values of 1 % or less and the capacitors had dielectrics of type C0G for the RF-interface, others had X5R, X7R or higher quality. The system then worked properly in a temperature range from 0 to 40 °C. An extended temperature range could be utilized if X8R or C0G dielectrics were used to avoid problems with temperature-related variations of the capacities.

## 1. PCB layout

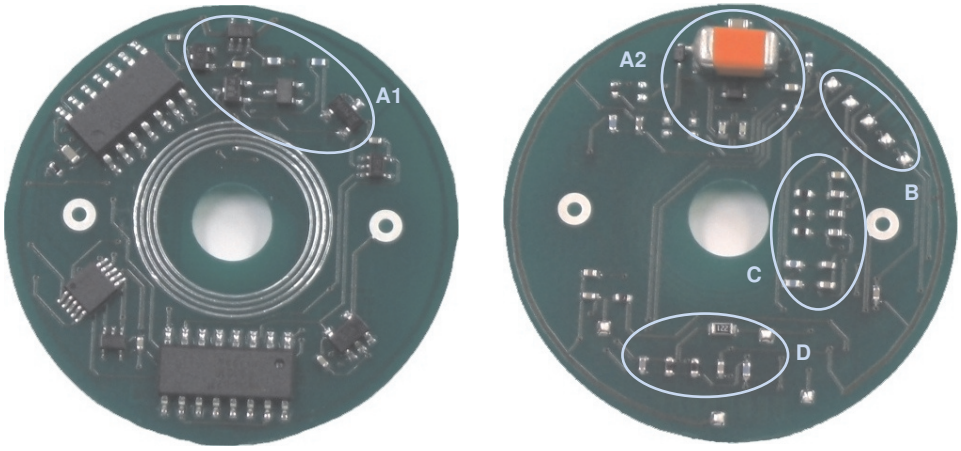


(a) (b)

FIG 4.15: The realized RFID-based impedance measurement tag. **(a)** Bottom side. Notice the 4-turn RF-coil as an integral part of the PCB. **(b)** top side. Connectors will be soldered on the pads on the left and the right side. The PCB has an outer diameter of 34 mm and a hole with 6 mm diameter for microscopic inspections of an attached sensor.

Areas A1 and A2 mark the RF interface, the 100 µF tantalum buffer capacitor $C_b$, bridge rectifier, and the necessary components for RF communication. The bottom copper layer includes the printed 4-turn coil of the LC-oscillator. Its metal layers are exposed to tin-solder to minimize the power loss of the AC current. Area B shows five pads which can be contacted via spring contacts and allow the on-board-programming of the microcontroller by Microchip's *In-Circuit Serial Programming* interface. Area C comprises both filter stages and area D holds the reference resistor and the resistors and capacitors for the I/V-converter. The other ICs comprise analog switches, OAs and blocking capacitors.

## 2. Packaging

Both, the cell culture and the tag are exposed to the same environmental conditions, namely in a standard incubator at a humidity of about 90 to 100 %. This level is necessary to minimize evaporation of culture media. Within every measurement sequence of a tag the reference element is also measured at each frequency. This allows an examination of the system reaction regarding to ageing or temperature-related drift or other influences.

Functionality tests carried out under normal ambient atmospheric conditions showed satisfactory tag behavior. The same tests carried out in the humidified incubator atmosphere indicated a drift of the measurement circuitry of bad or not encapsulated tags. In a first approach various coatings like urethane- or acrylic sprays and even paraffin

were tested as finishing varnishes but the electronic signals of some tags still showed drift of more than 10 %.

The top of each tag was packaged with the silicone PDMS. PDMS is an already biologically accepted material for medical implants, also used for microfluidic channels and therefore a promising candidate [Whitesides 2006]. The PDMS of choice was TSE399 from *GE Bayer Silicones* which cures with air humidity. During curing only small amounts of methanol are emitted, there is no further gas emission expected. The delivered tubes contained the TSE399 free of bubbles and made it easy to handle. Its transparency helped to detect and eliminate air bubbles during the encapsulation. The thickness of a single layer is limited to about 2 mm, otherwise the produced methanol leads to bubbles.

The bottom was encapsulated with an epoxy resin *Hysol* from *Loctite*. The primary reason for the encapsulation with that resin was that PDMS is quite sticky and could cause problems getting the tag out of the microtiter-plate. Also, the used ICs did not have the same height and their positioning was done for an optimized routing of the electrical connections on the PCB. So, the tags would not rest in a horizontal position. If cells were seeded onto a sensor which was attached on a non-horizontal sensor they could accumulate at the lowest point on the growth area. This would clearly influence the measurement result. The first step avoiding that was to use sensor devices attached on tags that had a well-defined horizontal alignment. After the curing process the surface was beveled and gave the whole tag a good base.

A fully encapsulated tag was sealed in a cast resin and cut along a few of the critical resistors. The cutting area was polished. TSE399 is a flexible material. Hence the polishing process was not that perfect and caused nicks in the material.

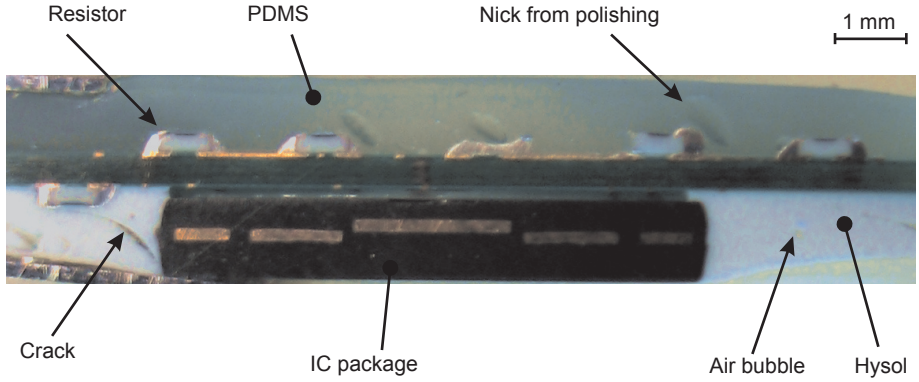


FIG 4.16: Polished cut image of an encapsulated tag.

FIG 4.16 shows the polished cut image. The bottom has the epoxy sealing and PDMS is on the top. Both materials fit the topology of the encapsulated components quite well and the epoxy resin also shows air bubbles. Those bubbles appear because the epoxy is a two-component resin which needs to be mixed. That mixing is the reason for the bubbles

which have diameters of 100 µm and more. However, those were not found to cause problems.

FIG 4.17 depicts the influence of humidity as a result of an imperfect encapsulation and contamination of the circuit elements. A tag was placed into a microtiter plate without a sensor and several measurement sequences were conducted within the humidified atmosphere of an incubator. Reference resistor data was then evaluated. Data fluctuations should remain within a small range of less than 0.5 % with respect to the ADC resolution.

Residual solder spikes of the signal generator resistors were peeking through the tag's PDMS sealing and showed a strong influence on the measurement (sequence #1). The tag was then dried in a heat chamber at 65 °C for 2 hours. In sequence #2 the well of the microtiter plate was sealed against humidity and the measurement repeated. There was no fluctuation found which encouraged the assumption of the influence of humidity. The solder spikes at the resistors were coated with Vaseline for sequence #3. There the data degradation was significantly reduced.

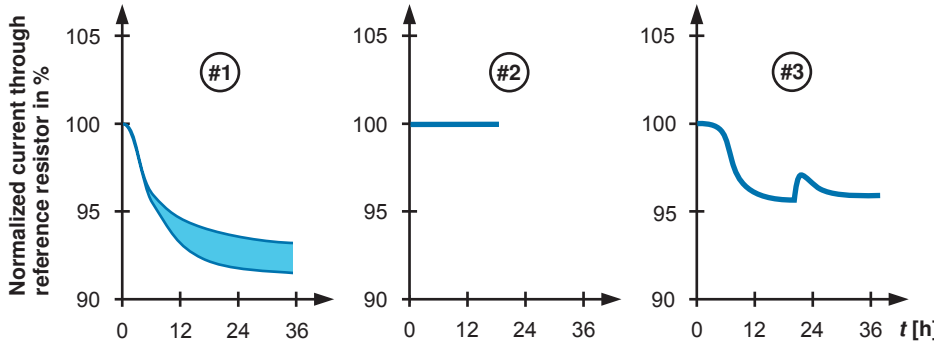


FIG 4.17: A microtiter plate with a tag was put into the incubator and the reference resistor measurements were evaluated. Sequence #1: Due to humidity parasitic resistances became active. The bright blue area indicates the range of the data. Sequence #2: After 2 h curing at 65 °C in the heat chamber the tag was again used in a hermetically sealed well of the microtiter plate. No fluctuations could be found. Sequence #3: Solder spikes of the signal generator resistors peeking through the PDMS sealing were coated with Vaseline. The reference data fluctuations were significantly reduced. The peak at 24 h occurred due to temperature fluctuations and condense water when the tag was taken out of the incubator for a visual inspection.

It was found that the residual signal reduction at measurement #3 was due to contamination of the soldered electronic parts by a zinc-chloride based flux agent which is an electrochemically active substance. Hence each tag was subject to a cleaning procedure with a sequence of chloroform, acetone, isopropanol and deionized water in an ultrasonic bath before the PDMS and epoxy resin packaging was done. Tags did then not show a degradation of the measured signals and the grip of the PDMS coating on the PCB was significantly improved.

## 4.4. Realized System

FIG 4.18 pictures a prototype for biological cell culture measurements for standard 6-well-microtiter plates. The tags are equipped with detachable sensor devices and put into the wells of a microtiter plate (transparent box). The base station (black box) with a plate of six multiplexed antenna coils is placed into an incubator and connected via a 4-wire ribbon cable to a computer. The microtiter plate is put onto the reader unit but can be displaced on the fly by an operator for microscopic inspections, culture medium replacement, etc. Appendix B contains illustrations of the interior of the base station and details on the RF-generator and receiver section

FIG 4.18: Realized system. The black box is the base station. The upper transparent part is a microtiter plate with the RFID-based tags with sensor devices attached on it. The dimensions of the base station are 145x90x30 $mm^3$.

The automated and time-resolved control of the base station and data transfer are done via a specially written software tool running on a Personal Computer (PC). This PC is connected via a RS232 interface to the base station and acts in a master-slave-principle, i.e. the PC as master sends commands and the base stations reacts to that commands. Thus, it is possible to use the RS232-interface in a bus-structure and connect several base

stations through. Each station has a unique 8 bit-hardware-address and up to 254 stations can be run in parallel.

The command set for the base stations allows to select a specific tag, i.e. the multiplexer is set, and to start a measurement sequence. Once the measurement is completed all data from the tag's ADC is available in the memory of the base station. The PC software is then able to read that data and initiate a new measurement.

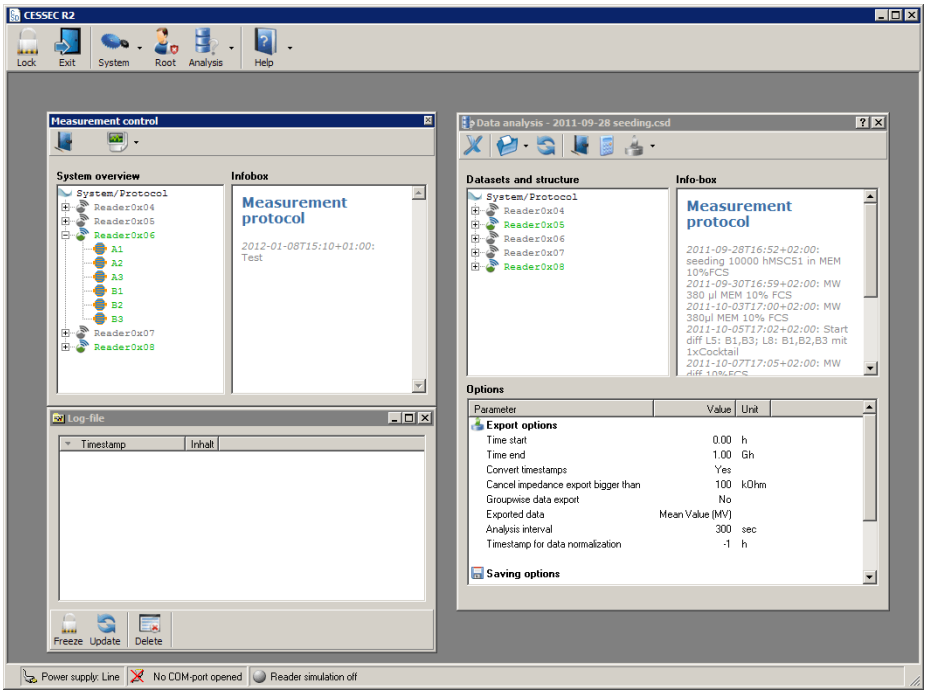


FIG 4.19: Windows-based control software *CESSEC release 2*. CESSEC as the software name is an acronym for ***C**ell **S**ensor **E**lectronics **C**ontrol*. The measurement control window shows five readers configured for measurement. Each of them has a number of tags which can be activated or disabled any time. This option allowed investigating the influence of the electrical current on the cells. In the data analysis window the raw binary data is converted to impedance data. When a measurement is running this program can be locked to circumvent accidental measurement breaks or other misuse.

An online-protocol functionality enables an operator to journalize his work and include that protocol into the same data file as the measurement data which circumvents separate paperwork. This functionality was found to be very useful at investigations on stem cells. Some of those experiments took more than three weeks and a big number of processing steps needed to be recorded in order to understand measurement results and distinguish them from artifacts.

## 4.5. Discussion

The RF-interface with its capability to blank the RF-field allows the generation of a regulated supply voltage within the tag. Noise on this supply is then caused by the circuitry itself and in the present system it could be held below 5 mV rms. An optimization of the RF-interface would be possible as the voltage at the buffer capacitor could be generated by a Delon-voltage doubler. This method requires only two instead of four diodes for a rectifier but needs additional capacitors. The overall power transfer efficiency would then be increased to 40 %. Also, the RF-interface would not need to be that accurately adjusted and the system could also work at greater distances or at lower RF-fields. The latter would be of importance in the case of parasitic loops in the circuit layout.

The blanking of the RF-field during measurement sequence and the power supply via a buffer capacitor ensured a very low noise level. Values clearly smaller than 5 mV rms could be achieved while the measurement system was fully operating. The presented technique had a power consumption of about 8.3 mW. A reduction of the supply voltage to $V_{DD}$ = 2.7 V or 1.8 V could reduce that requirements to less than 5 mW.

Even though impedance monitoring is a common practice in the field of electrochemistry there are no suitable low-power-instruments available off the shelf. Several concepts for integrated impedance measurement systems or parts of it with low power consumption were reported and realized as prototypes [Beach *et al.* 2005, Moe *et al.* 2004, Sacristán Riquelme *et al.* 2009, Xu *et al.* 2009, Yúfera *et al.* 2002, Zhang *et al.* 2009]. Integrated circuits utilizing that concepts may have a size of only a few $mm^2$, and a power consumption of less than 1 mW. The whole tag could be significantly miniaturized if such an IC could be integrated – the tag coil dimension promotes a design for a 24-well-microtiter plate. Regrettably up to now a killer application seems to be missing which could initiate a production of low-power impedance converters in an industrial scale.

Packaging and proper sealing of the tags is an inevitable step to provide a reliable functionality. There are numerous sources of contamination such as the sweat from bare hands or drops of ionic conductive fluids during operations, such as PBS or a culture medium.

The most malicious contaminations are those which are almost not conductive in the normal ambient. In the humidified incubator atmosphere they become conductive and create parasitic current paths. Tags may work without any hint of problems for a day or more and malfunction then appear within an hour – the following chapter will show that the humidity level of the incubator atmosphere is correlated to the frequency of its usage. The measurement of a (low-ohmic) resistor is thus not only necessary to get a reference for the sensor measurement. It is also a control mechanism for the tag with the encapsulation being an essential part for functionality.

Long-term measurements were performed in-house as well as at labs of the Austrian Academy of Sciences (Österreichische Akademie der Wissenschaften, ÖAW), the induced differentiation of stem cells required measurement periods for several weeks. The tags as well as the base station and the control software operated satisfactorily.

## 4.6. Bibliography

Austrian Research Centers GmbH: *Verfahren zur Datenübertragung*. Austrian Patent AT 505632 B1 (2009).

Beach R.D., Conlan R.W., Godwin M.C., Moussy F.: *Towards a Miniature Implantable In Vivo Telemetry Monitoring System Dynamically Configurable as a Potentiostat or Galvanostat for Two- and Three-Electrode Biosensors*. IEEE T. Instrum. Meas. 54 (1), pp. 61-72 (2005).

Brandl M., Grabner J., Kellner K., Seifert F., Nicolics J., Grabner S., Grabner G.: *A Low-Cost Wireless Sensor System and Its Application in Dental Retainers*. IEEE Sensors J. 9 (3), pp. 255-262 (2009).

Farinholt K.M., Park G., Farrar C.R.: *RF Energy Transmission for a Low-Power Wireless Impedance Sensor Node*. IEEE Sensors J. 9 (7), pp. 793-800 (2009).

Finkenzeller K.: *RFID-Handbook*. 3nd edition, Wiley and Sons Ltd., New York, ISBN 978-0470695067 (2010).

ITU-T: *Series G: Transmission Systems and Media. Digital Systems and Networks*. ITU-T Recommendation G.704 (10/98).

Martinez-Catalá R.V., Barrett J.: *A Modular Wireless Sensor Platform With Fully Integrated Battery*. IEEE T. Comp. Pack. T. 32 (3), pp. 617-626 (2009).

Moe A.E., Marx S.R., Bhinderwala I., Wilson D.M.: *A Miniaturized Lock-in Amplifier Design Suitable for Impedance Measurement in Cells*. Proc. IEEE Sensors 1, ISBN 0-7803-8692-2, pp. 215-218 (2004).

Nopper R., Niekrawietz R., Reindl L.: *Wireless Readout of Passive LC Sensors*. IEEE T. Instrum. Meas. 59 (9), pp. 2450-2457 (2010).

Ong K.G., Wang J., Singh R.S., Bachas L.G., Grimes C.A.: *Monitoring of bacteria growth using a wireless, remote query resonant-circuit sensor: Application to environmental sensing*. Biosens. Bioel. 16, pp. 305-312 (2001).

Oprea A., Bârsan N., Weimar U., Bauersfeld M.-L., Ebling D., Wöllenstein J.: *Capacitive humidity sensors on flexible RFID labels*. Sens. Actuat., B 132, pp. 404-410 (2008).

Sacristán-Riquelme J., Segura-Quijano F., Baldi A., Osés M.T.: *Low power impedance measurement integrated circuit for sensor applications*. Microelectronics J. 40, pp. 177-184 (2009).

Segura-Quijano F., Sacristán-Riquelme J., García-Cantón J., Osés M.T., Baldi A.: *Towards Fully Integrated Wireless Impedimetric Sensors*. Sensors J. 10, pp. 4071-4082 (2010).

Xu J., Meynants G., Merken P.: *Low-Power Lock-In Amplifier for Complex Impedance Measurement*. 3rd Int. Workshop on Advances in Sensors and Interfaces (IWASI) 2009, ISBN 978-1-4244-4708-4, pp. 110-114 (2009).

Yúfera A., Leger G., Rodríguez-Villegas E.O., Muñoz J.M., Rueda A., Ivorra A., Gomez R., Noguera N., Aguiló J.: *An Integrated Circuit for Tissue Imepdance Measure*. 2nd Annual Int. IEEE-EMBS Special Topic Conf. Microtechn. Med. Biol., ISBN 0-7803-7480-0 , pp. 88-93 (2002).

Zhang L., Yu Z., He X.: *Design and Implementation of Ultralow Current-Mode Amplifier for Biosensor Applications*. IEEE T. Circ. Sys.-II: Express Briefs 56 (7), pp. 540-544 (2009).

# Chapter 5

# EXPERIMENTAL RESULTS

The functionality of the presented measurement system is demonstrated by investigations on adherent cell cultures in a standard incubator. During the experimental phase it was found that alterations of the environmental conditions within the incubator strongly affect the electronic system. Frequent operation of the incubator door changes temperature, humidity and $CO_2$-level what is reflected by variations of the measured sensor impedance. The presented measurement data are therefore discussed for both, the cell culture-related and the environmental related trends. Most measurements were performed with a single frequency probe signal, but the long-term monitoring of the osteogenic differentiation of human mesenchymal stem cells was performed at four frequencies simultaneously.

## 5.1. System Tests and Preparations

### 1. The incubator volume

Generally an incubator provides appropriate environmental conditions for cell growth. In most laboratory incubators the temperature and $CO_2$-level are actively controlled but the humidity level is somehow passively regulated. Usually a basin, filled with water which evaporates into the unsaturated atmosphere is placed within the chamber. Whenever the incubator door is opened the atmosphere is influenced by the laboratory surrounding air. The saturation level at 20 °C is significantly smaller than that in an incubator at 37 °C (about 17 g/m$^3$ vs. 44 g/m$^3$). When the incubator door is closed again and the temperature regulated, then the humidity level significantly drops. The following example depicts that influence: The laboratory has a relative humidity level of 50 % at 20 °C while the incubator has a saturated atmosphere. When the door is opened and shut again an exchange of 20 % of the incubator atmosphere may occur. Then, the relative humidity will go down to $(44 \cdot 0.8 + 0.5 \cdot 17 \cdot 0.2)/44 = 84$ %. It should be noted that the incubator door needs to be opened four times, even if a single cell passage is carried out.

The regeneration mechanism via evaporation from the water basin is very slow. The incubators used for the experiments on cell cultures had a daily average value as low as 40 %. More than 10 h passed for a rise from 40 % to more than 90 %.

Each well needs to allow a gas exchange with the incubator atmosphere. This is achieved via specially formed slits between the microtiter plate and its cover. Those

allow gas exchange but prohibit contamination from the outside. When measurements were performed it was frequently found that a sensor lost about 60 µl of culture medium volume within one day which is a comparably big amount with respect to the filling volume of 300 µl. Subsequently, the ion concentration changed leading to changes of the osmotic pressure and also the ohmic resistance of the culture medium significantly dropped.

Several setups were tested to get that problem under control. The necessary gas exchange with the environment, especially for a constant $CO_2$ (and pH) level did not allow a sealing of the wells. Furthermore, this procedure would have complicated handling. Cover glasses were placed on the PDMS tubes onto the sensor devices to reduce evaporation, also water-soaked tissues were put in the cavities between the wells to provide an additional water reservoir for a micro-climate inside the microtiter plate.

Finally, those setups did not lead to satisfying results. Instead, a method needed to be found which would provide a fast regeneration of the humidity level of the incubator, i.e. an acceleration of the evaporation from the water basin. The evaporation rate could be increased by a resistor with a heating power of 1.5 W placed in the water basin. Also, the basin was placed on PTFE-blocks for thermal decoupling from the metal lining of the incubator.

This modification led to a significantly reduced loss of culture medium from the sensor devices. The method was verified with a separate experiment. Each well of a 6-well-microtiter-plate was filled with 4 ml of deionized water. It was then put into the incubator and its weight was regularly measured over a period of several weeks. The used *Kern 770-15* balance had an accuracy better than 10 µg. This experiment was done twice without and with the active heater. FIG 5.1 illustrates the effect of this heating mechanism.

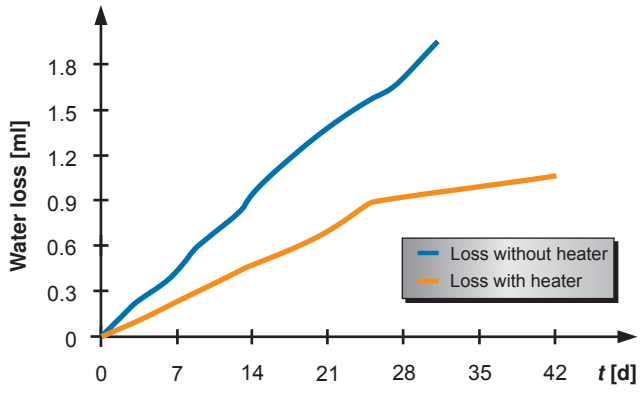


FIG 5.1: Average loss of water in a well of a 6-well microtiter-plate. The green line shows a significant reduction of water loss. After 26 days less people were working with the cell lines stored in the incubator. Therefore, its door was not that often opened. Without the heater the water loss per well is about 60 µl/d and with the heater it is 35 µl/d before, and 10 µl/d, respectively.

Without a heater the loss for each well was about the same as it was found in our sensor devices. Even though the sensors had a much smaller active evaporation area than the water-samples (50 mm² vs. 962 $mm^2$) the values were within the same range. Thus, it can be stated that the diffusion is limited by the available diffusion area through the slits between the plate and its cover. This assumption was also encouraged as the outer four wells lost about two times more water than the inner two.

The second test with a heater was separated into two lines as there was a period when the incubator was rarely used after 26 days of test. It can be clearly seen that the daily loss was reduced to the half and even less after the $25^{th}$ day when the incubator was not opened regularly. This effect showed how dramatic the changes in the incubator humidity level were and the great influence of frequent opening and closing the door.

A further influence on the sensor impedance is due to the changing $CO_2$-levels. The gas dissociates into the culture medium and is used for the adjustment of the pH-value. Subsequently, the $CO_2$-level influences the impedance of the culture medium via that pH-value. This effect is strongly related to the sensing method for the $CO_2$-concentration. Old incubators use a method which relies on the thermal conductivity of the incubator atmosphere. One may assume that the humidity will also influence that conductivity which makes it even harder to adjust the $CO_2$-level by this sensing method. Modern incubators, as that used within the presented experiments, use the infrared absorption of $CO_2$ for sensing. This method is fast and allows a regulation within minutes and no effect on the culture medium and its pH-level needs to be taken into account [Keese 1994, Schmitz 2007].

Fresh medium is, however, generally stored in a fridge without $CO_2$-control. The medium's pH-level was found to be about 8.4 instead of 7.5 to 7.6. Very sensitive measurements may show an influence due to the adaption of the pH-value but were not found within the conducted experiments.

## 2. Preparation of the sensor devices and tags

Whenever a measurement is conducted a number of preparations need to be done in advance. First, the sensor chips are cleaned according to section *0*
*Sensor Device* Construction. This step needs to be done even if the glass chips come directly out of fabrication or if they are reused. Then, the sensor devices are assembled whereas the PCB parts and the PDMS tubes were stored in EtOH. Tags are also cleaned with EtOH before they are equipped with sensor devices and placed into the wells of a microtiter plate. Then the plate is exposed to UV-light for about 30 minutes which has two effects. First, it is a final sterilization of the PCBs, tags and sensor chips. Second, due to the heat of the UV lamps residual EtOH evaporates. FIG 5.2 pictures a ready-to-use microtiter plate.

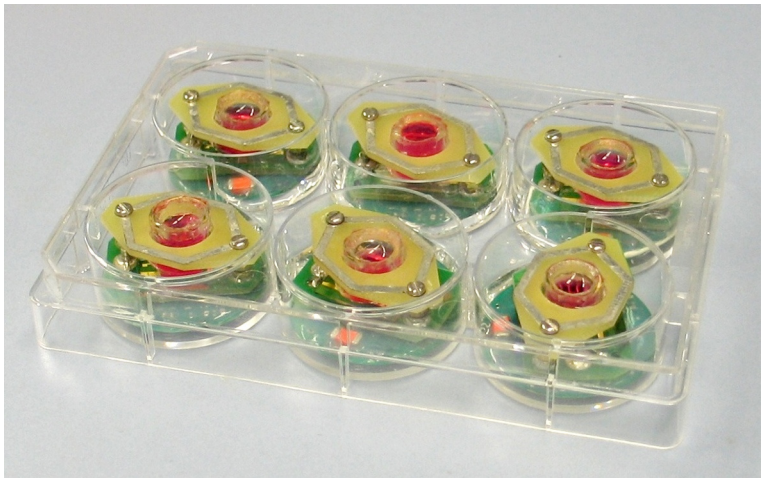

FIG 5.2: Microtiter plate (without cover) equipped with tags and sensor devices filled with culture medium DMEM.

## 3. Temperature characteristics in a well

The impedance of a sensor is related to the medium's temperature. The thermal contact of the culture medium via the sensor and metal lines to the tag leads to a significant delay for temperature relaxation of the sensor system because of the thermal capacity of a tag. The temperature behavior was tested by a Silicon Temperature Sensor *KTY81* from *NXP Semiconductors*. This sensor in a TO-92 packaging was soldered instead of the sensor chip and brought in contact with the culture medium. The system had room temperature, i.e. 20 to 22 °C, when it was brought into the incubator and the measurement initiated.

The calculation of the temperature from the sensor's resistance showed an exponential behavior with a time constant of about 15 minutes. More than one hour would have passed until the impedance measurement on cell cultures showed useful data if no further actions were conducted to set the initial temperature to a level close to the set-temperature. This is of great importance as the handling of the microtiter plate mostly occured within the laminar flowbox. There, the metal lining and environmental air had room temperature and the whole plate cooled down.

Two precautions avoided that problem. First, a thermally isolating plastic plate was placed on the workbench inside the laminar flow. This plate was then used as a working area and reduced the thermal conduction to the metal lining. Second, an aluminum plate was placed into the incubator. Its size allowed placing the microtiter plate on it. Thus, the bottom of each well was in thermal contact with that plate. The metallic inner lining of the incubator had a temperature of 37 °C and pre-warmed the tags. That procedure took about 5 minutes. Impedance drifts correlated with the temperature relaxation were reduced to an effective period of less than 15 minutes.

### 4. Impedance measurement test with PBS

Two microtiter plates were prepared and sensor devices filled with PBS. Measurements were carried out in an incubator. FIG 5.3 depicts the calculated sensor impedances for 10 samples. The deviations of the measured values are assumed to be caused by residual contaminations of the electrode surfaces. The quality of the cleaning procedure generally has an influence on the electrode-electrolyte-interface, which is mainly represented by the imaginary part of the sensor impedance [Ceriotti *et al.* 2007].

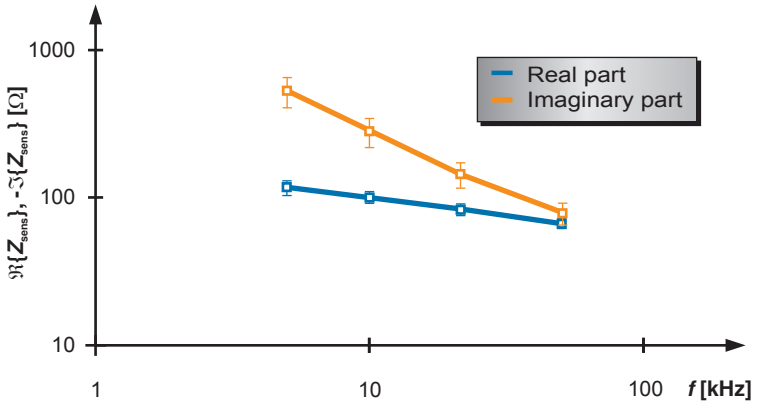


FIG 5.3: Averaged data of 10 IDES-samples with PBS. Notice the different frequency-behavior of the real and imaginary part. The real part is dominated by the Warburg-impedance with its $\sqrt{f}$-behavior while the imaginary part is dominated by the electrochemical double layer capacity.

The measurement data fit well to measurements performed with a potentiostat. Especially the NaCl concentration of PBS resulted in an impedance which was about 20 % smaller than that of DMEM (compare FIG 3.15).

Whenever a measurement on cell cultures is conducted, the sensor devices are loaded with DMEM. A measurement is done for at least 30 minutes prior to cell seeding. That allows a functionality check for all system parts and provides reference values.

## 5.2. 3T3 Mouse Embryonic Fibroblasts

The cells used for this experiment were mouse embryonic fibroblast cells, 163-CCL Balb/3T3 clone A31, obtained from the American Type Culture Collection cultivated in DMEM with 10 % FCS and antibiotics. Those have a population doubling period of 20 to 24 hours. Those fibroblasts are often used for the assessment of toxicological properties of certain substances [ICCVAM 2006].

## 1. Cell cultures on the sensor

FIG 5.4 gives an impression on the appearance of mouse fibroblast cells when they spread and proliferate on the glass chip. Pictures were taken at different levels of confluence utilizing a phase contrast microscopy. The surface area of the culture medium in a sensor device is slightly bent and causes a lens-effect. Hence the sharpness of such pictures is limited.

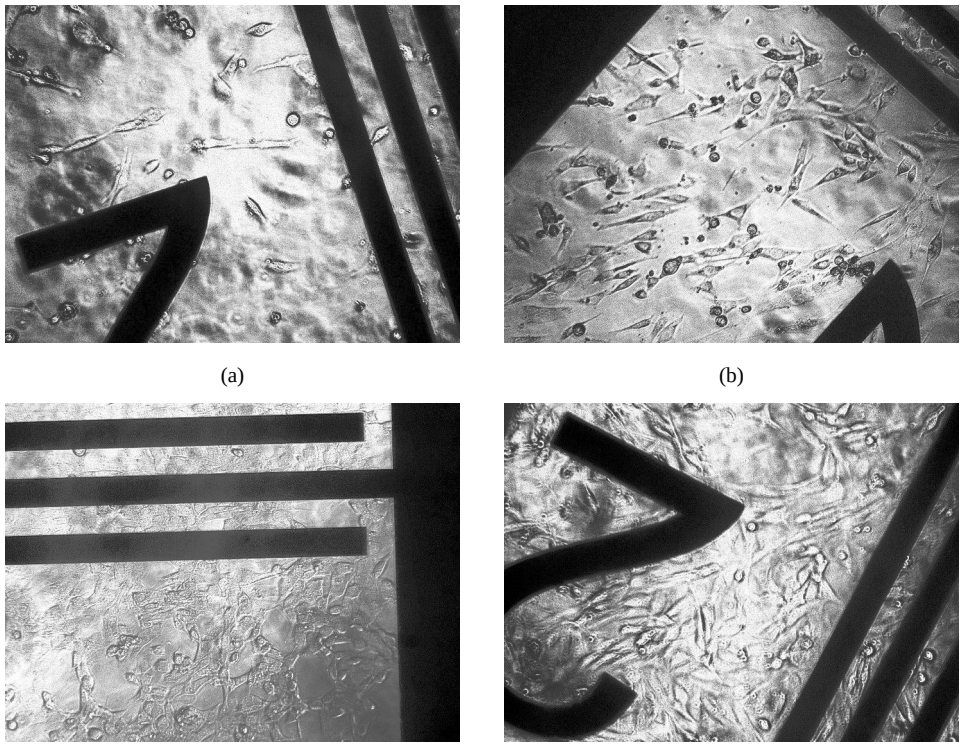

(a) (b)

(c) (d)

FIG 5.4: Phase contrast microscopy of the growth of 3T3 fibroblasts. The opaque metal stripes have a width of 50 µm. **(a)** and **(b)** show a low confluence of 5 to 10 %. **(c)** and **(d)** show examples of confluence >70 %.

Whenever the microtiter plate had to be taken out of the incubator for culture medium exchange or some kind of a treatment of cell samples, a microscopic inspection was done. The measured impedance was an averaged value for the sensing area, e.g. the impedance data did not make a difference in a low confluence and a void in the cell layer. Chapter 6 provides a detailed discussion on that topic.

## 2. Sensor step response

The first experiment gives an answer to the achievable sensor response, i.e. the impedance change due to full cell coverage of the sensor. Furthermore, the herein presented data provides an overview of environmental effects which occur due to cell adherence, spreading and migration, and culture medium loss.

A step response requires the whole growth area to be completely covered with cells. If a cell passage is done for a 5 to 10 % confluent layer at a culture flask of 25 $cm^2$, $10^5$ cells are seeded. Therefore, a 100 % confluence would be achieved with 20,000 cells for a 50 $mm^2$ area at the sensor device. A higher number of 50,000 is selected to guarantee 100 % confluence.

A microtiter plate as previously shown in FIG 5.2 was prepared. One sample was used as a blank, i.e. it did only contain culture medium, while three were supplemented with cells (two sensors fail due to electrical contact problems at the sensors). FIG 5.5 shows the sensor impedance split into real and imaginary part.

The sensor was initially loaded with culture medium for 24 h, cells were then seeded. Within six hours after seeding at $t = 0$ the cells attached and spread. During preparation for the cell seeding the cells were suspended in DMEM where they had an almost spherical shape. When those cells settled on the sensor surface it took a few hours until they spread and became flat (FIG 2.5 shows the change of the shape after seeding in a culture flask).

It is assumed that the electric current path is mainly located in the space between the cells, thus the impedance is higher due to the still spherical shape of the cells. After the attachment process cells are still able to migrate or modify their shape which may be the reason for the slightly different evolution within the first 24 h.

After seeding, a continuous decrease of the ohmic impedance of the blank could be observed which correlated well with the evaporated amount of culture medium. The evaporation of culture medium only affects the watery part but ions still remain in the residual volume. Hence the ohmic resistance dropped. Cell were able to adapt to that new condition whereas that process could take several hours.

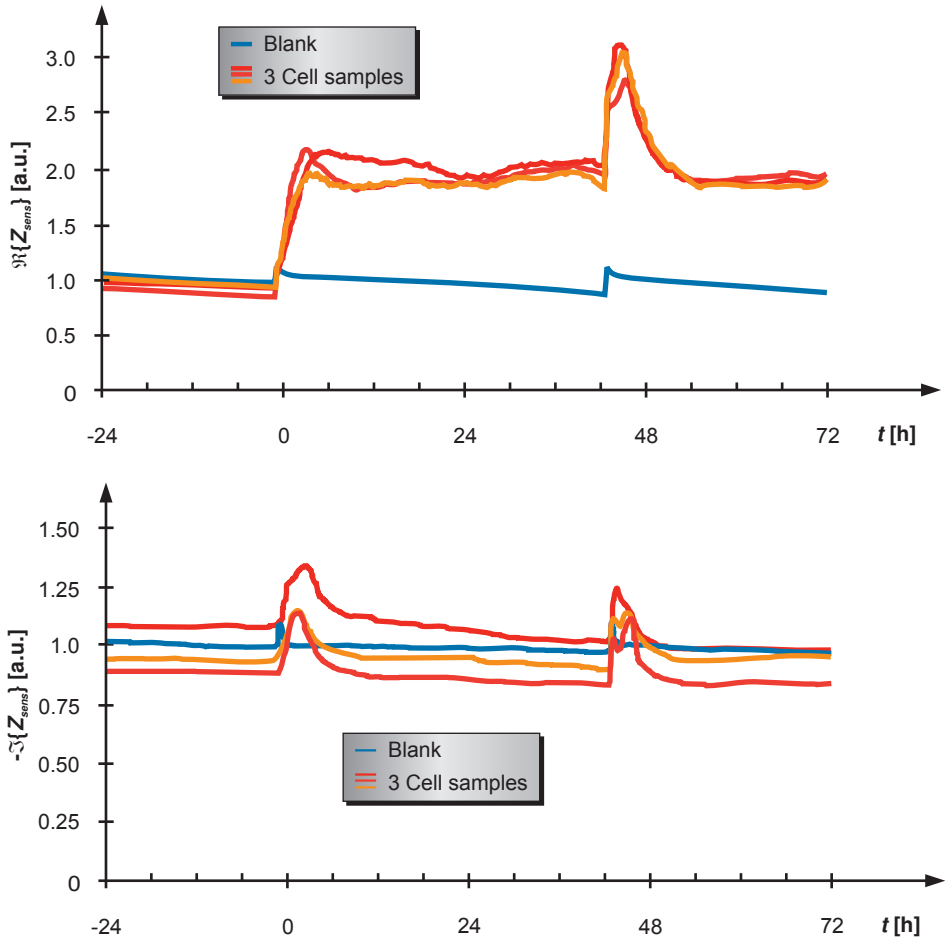


FIG 5.5: Sensor measurement at a frequency of 10 kHz split up into the real part $\Re\{Z_{sens}\}$ and imaginary part $\Im\{Z_{sens}\}$. Values are given in arbitrary units whereas 100 % are 120 Ω for the real part and 200 Ω for the imaginary part. The blank sample shows a decrease of its resistance associated with the evaporation of culture medium.

After 44 hours culture medium was exchanged. The blank regenerated to its initial value while the cell-loaded sensors showed a characteristic behavior due to two effects. First, the real part was mainly influenced by the conductivity of the culture medium which had a lower value after exchange. Thus, the medium exchange had the same effect as for the blank. The other effect is an assumption as a microscopic inspection did not allow a clear distinction: The cytosol was adapted for the higher ion concentration in the medium. Following the medium exchange the ion concentration mismatch let water flow into the cells and let them swell. The residual path for the sensing current narrowed and elongated comparable to the seeding process. An influence of that effect could also be found at the imaginary part. Normally cells are attached to the surface via Cell Adhesion Molecules

(CAM) in a distance of 20 to 100 nm but the osmotic pressure may have led to a contact of the cell membrane (or its surface proteins) to the electrode surface. FIG 5.6 shows the impedance data starting at 72 h following those of FIG 5.5 for the first 72 h.

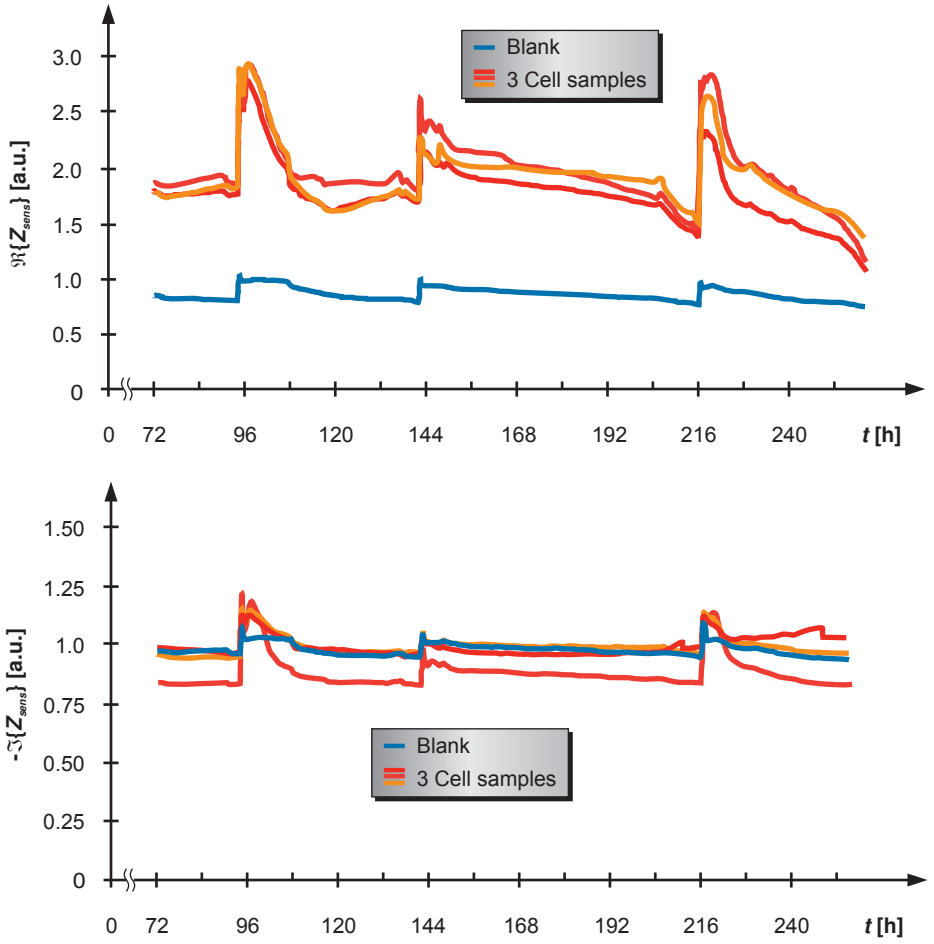


FIG 5.6: Sensor measurement at a frequency of 10 kHz. Values are given in arbitrary units whereas 100 % are 120 Ω for the real part and 200 Ω for the imaginary part.

Culture medium was again exchanged after 94 h. There, the incubator door was not closed properly which caused the temperature drop to about 30 °C and the $CO_2$-level was reduced to about 1 % until 108 h.

A cell culture passage was conducted at the same time as the medium exchange. A microscopic inspection showed that those cells did adhere but did not start doubling.

Temperature is known to be a critical parameter for proliferation [12]. The blank impedance showed that due to the lower temperature the medium evaporation could be ignored. The combination of decreasing temperature and the adaption of the cells to the new culture medium (again due to the osmotic pressure) did not allow a clear distinction of both effects. However, microscopic inspections showed that the cell cultures were alife when after 144 h another medium exchange was done.

Then the cell samples showed an impedance decrease with every medium exchange. Several experiments with a 100 % confluent cell layer showed that a decrease of the ohmic sensor impedance started about 5 to 8 days after the cell culture reached confluence. There are several possibilities for that behavior. First, the used cell cultures had already passed the 90$^{th}$ passage and may had signs of senescence (cell ageing). For comparison, an OECD guideline for testing chemicals recommends the use of 3T3 cultures younger than 100$^{th}$ passage [OECD 2004].

In the field of toxicological testing, 3T3 cell lines are used to analyze the influence of a certain substance on the cell growth behavior, DNA changes, etc. For that purpose, cells are seeded in a concentration of about 10 % and proliferate for a few days. The used serum contains the necessary growth factors, i.e. molecules which initiate the cell doubling. On the other hand side, cell doubling is attenuated by a cell-property called contact inhibition. This means, that cells stop doubling if there is not enough growth area left. This contact inhibition is in opposite to the growth factors in the serum and may cause come kind of a stress which in turn could lead to apoptosis (cell death).

It should be noted that after 264 h (not shown in the graph) another culture medium exchange was done. The same behavior was found., i.e. an initial strong increase of impedance followed by a rapid decrease.

## 3. Continuous cell growth

Several toxicity tests [ICCVAM 2006] rely on the detection of the proliferation performance of certain cell cultures whereas the culture medium is treated with the investigated (toxic) substance. Conventional endpoint-based tests such as cell counting methods after a few days do not allow the monitoring of the time-resolved proliferation kinetics of the cell cultures.

The impedance monitoring of cell growth provides such time-resolved data. Within the following measurements the effect of culture medium evaporation is visible again. A method for the compensation of that effect on the measurement data is presented and applied to the results.

[12] For humans, the core temperature also is about 37 °C but an increase of just 1 to 2 K leads to discomfort. In opposite, a temperature below 33 °C already is hyopthermia.

**Measurement #1**

5000 cells per sensor (about 10 % confluence) were seeded at $t = 0$. Culture medium was exchanged after 26, 54, and 74 h. Data of three samples were averaged, normalized and a compensation of the culture medium loss was carried out. It is assumed that the residual current path along the culture medium dominates the sensor impedance while the current through the cells can be neglected. Thus, the data of the sensor samples were divided by the time-corresponding blank value to compensate the change of the ionic medium conductivity. Then, each sample was normalized to a timestamp where all three samples showed the same confluence. In the present case this time-stamp was at 40 h after the first culture medium exchange.

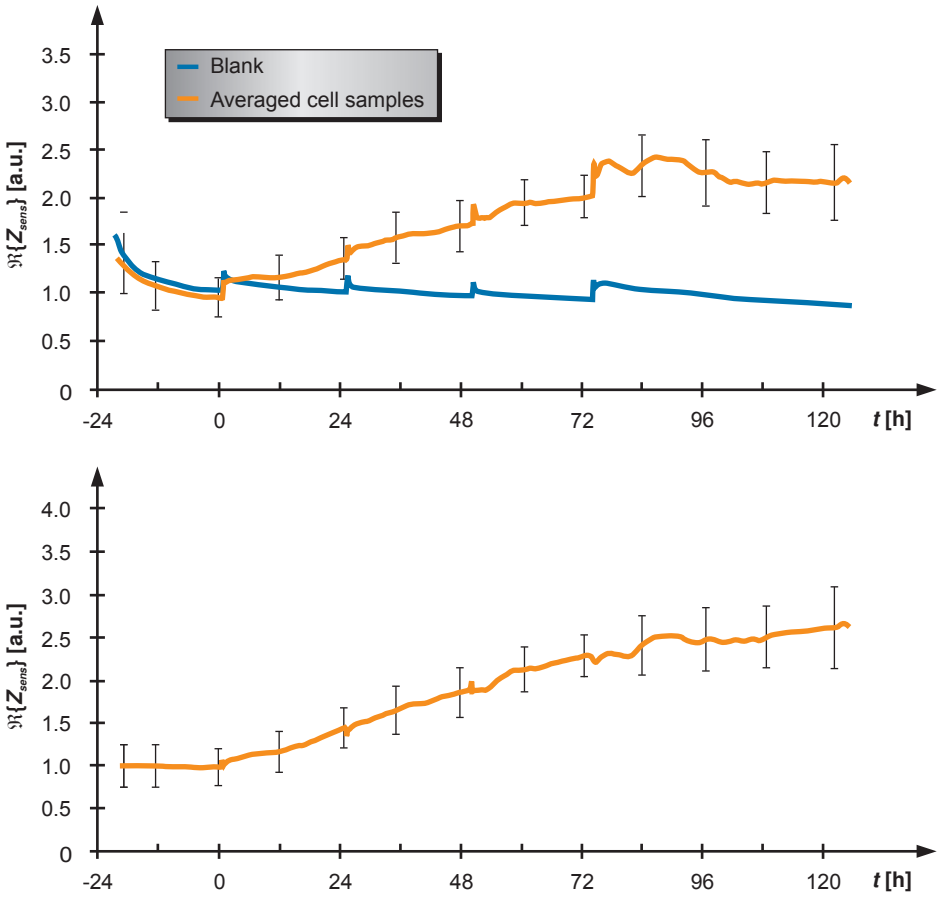


FIG 5.7: Upper graph: raw data, normalized. Lower graph: Each line is referenced to timestamp 40 h and divided by the time-resolved blank value to compensate culture medium loss.

**Measurement #2**

A second measurement with the same starting conditions was carried out. In contrast to the previous measurement, the first medium exchange was done two days after seeding. The following figure shows the real part of the sensor impedance normalized and medium loss-compensated.

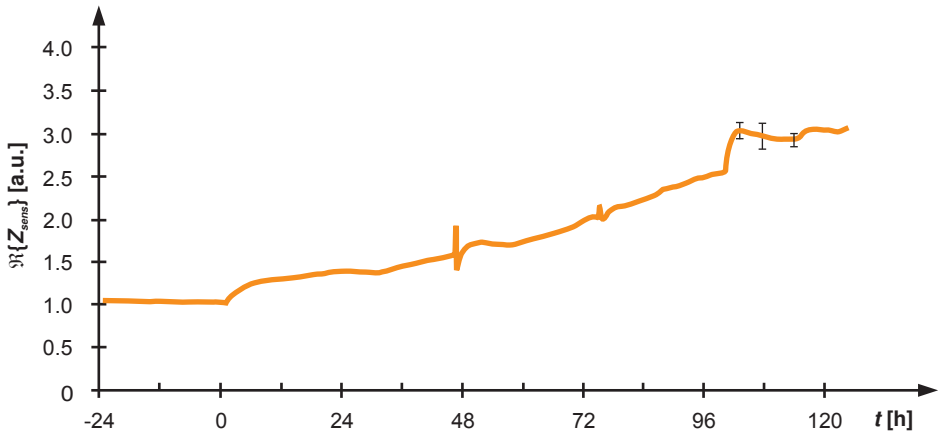


FIG 5.8: 5000 cells per sensor were seeded at $t = 0$. Culture medium exchange was done after 48 and 98 hours. Within the first 4 days the standard deviation was less than 10 %.

This second measurement did not show a significant difference in the growth behavior. Generally, the culture medium exchange had two reasons. First, some components of the medium denatured and needed to be replaced. Second, essential parts of the medium were consumed by the cells for doubling. The initially small number of cells did not require that much nutrients. Hence this second measurement did not show a reduced growth rate.

A significant difference to a fully confluent layer at seeding was the different endpoint of the impedance. The step response showed an impedance increase to 200 to 250 % (including evaporation compensation) while the plateau at cell growth is at 250 to 300 % of the cell-free values in both measurements.

In some cases it was found that during population doubling those cells arranged themselves with an elongated, spindle-like shaping which was not true in the case of initially confluent layers. It is assumed that due to cell growth the intercellular gaps were smaller which in turn led to higher sensor impedances.

## 4. Continuous cell growth with cell termination

500 cells (1 % confluence) were seeded per sensor at three samples. Two blanks were left which did only get culture medium without cells. In most cases an initial confluence of 10 % ore more is selected for an adequate cell expansion. This experiment should show the behavior of the system on a very low cell number and also eliminate concerns about possible negative influences of the glass/metal/PDMS material combination on the cell

growth. FIG 5.9 shows the normalized real part and the evaporation-compensated data. The compensation was done using the average data of both blanks.

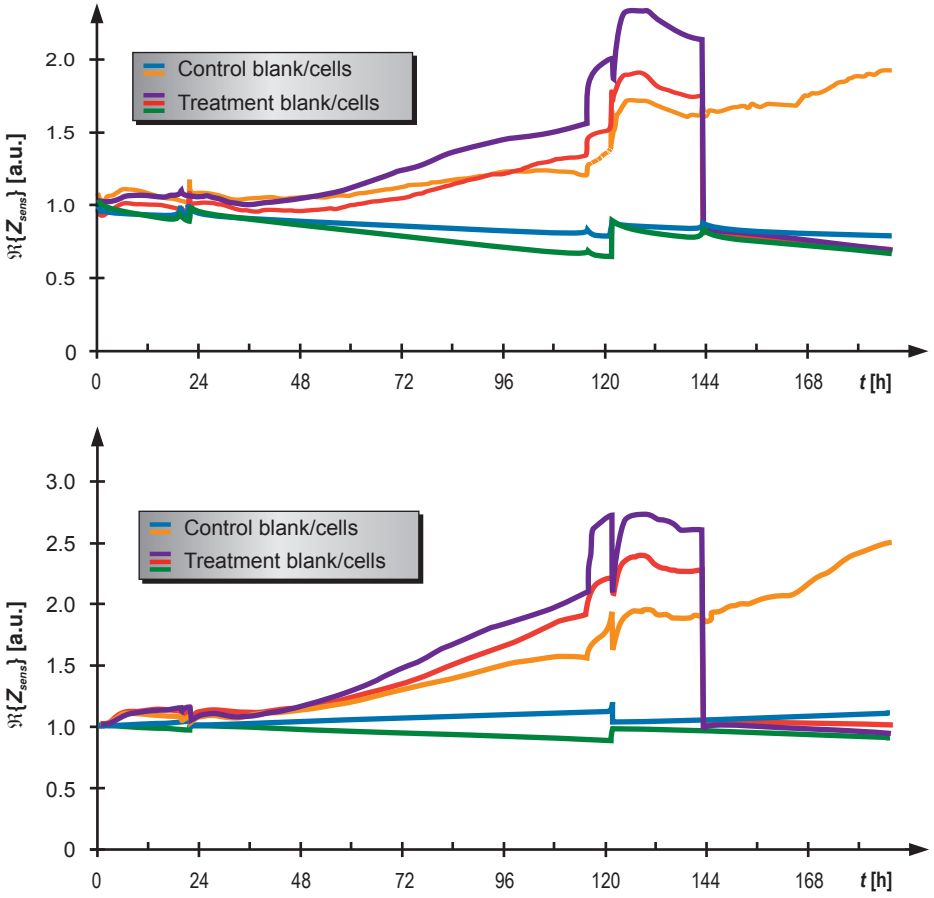


FIG 5.9: 500 cells (1% confluence) seeded at $t = 0$. First visual inspection and culture medium exchange were done 20 h later No further action was done until 116 h with another visual inspection. The bump in the data caused by that cannot be well explained. Culture medium exchange occurred after 121 h. Another medium exchange was done after 141 h where one blank and one cell sample were treated with 0.1 % Triton X-100. Cells died immediately. The second sample was left growing for another two days. Top: Raw data normalized to seeding time. Bottom: Additional compensation of evaporation. The average time-resolved values of both blanks were used for the correction for the evaporation.

24 hours after seeding the culture medium was exchanged. It was found that about 30 µl culture medium per well evaporated during the first day. Due to the shadowing effect of the sensor metallization the confluence could not be determined that time (in theory about 70 to 80 at that time per sensor). After 119 hours a visual inspection was done where about 50 % confluence was found on all three samples. This fits the approximation that cell doubling occurs in an interval of 20 to 24 hours [Todaro and Green 1963]. It was

already shown that during these checks the microtiter plate and the tags inside cooled down to room temperature, so that impedance changes occured [Ehret *et al.* 2007, Ceriotti *et al.* 2007]. The impedance step following the inspection fit the information that temperature-related impedance change is about -1 %/K but it did not explain the following impedance increase. One option is that during microscopic inspection a drop of condense water from the microtiter plate's cover came into the medium and reduced the effective ion concentration. This would in turn have led to a swelling of the cells as previously assumed. Culture medium was then changed at 125 h. Within the adaption to the new culture medium (and the different nutrient and ion concentrations) the cell samples continued population doubling.

One day later culture medium was changed again whereas the medium of two cell-loaded samples and one blank was treated with 0.1 vol% of Triton X-100. Triton X-100 is a non-ionic detergent and dissolves membrane proteins. Cells were immediately killed while the detergent did not influence the electrical properties of the culture medium. A microscopic inspection of the Triton X-100-treated cells showed that the cell membranes were entirely dissolved and the cytosol resolved by the culture medium. Only the nuclei were left. The serial resistance of the cell-loaded sample dropped within minutes to the value range of the blanks. One sample was left proliferating as a control for two further days.

Generally, a small number of cells, i.e. 500 per sensor in that setup, caused a strong deviation of the number of cells which settled down on the sensor area. In the present setup that area was 1.8 $mm^2$ while the seeding area was 50 $mm^2$. Hence the initial average number of cells on the sensor element was about 20 on the metal structures. The preparation of a cell suspension required a trypsinization and centrifugation which generally means stress to cells. If only one or two of them were not be able to proliferate the initial cell numbers varied by almost 10 %. This deviation was reflected by different sensor values during the proliferation. That effect faded away by the time which could be related to contact inhibition, i.e. samples with an initially slightly bigger number of cells showed an earlier reduction of their growth rate.

The treatment with a highly toxic substance showed the importance of the monitoring of the cell proliferation kinetics. Endpoint-based methods (e.g. cell counting 24 h after treatment) would not be able to distinguish between a toxic substance which causes a slow cell death and the immediate cell-membrane-resolving effect of Triton X-100.

## 5.3. Human Mesenchymal Stem Cells

Human mesenchymal stem cells (MSC) are multipotent cells that can differentiate into various cell types of the mesenchyme lineage and form tissues such as bone, fat, cartilage. In bone marrow MSC share a common niche with haematopoietic stem cells (HSC) and support the formation of blood cellular components [Méndez-Ferrer 2010]. In regenerative medicine MSC have been successfully employed in many cell therapeutic

approaches (combined with gene therapy) but also in the generation of tissue samples for subsequent transplantation [Kassem and Abdallah 2008, Lepperdinger et al. 2008]. However, up to now there is not standardized method available to reliably quantify the quality of MSC, i.e. their *stemness*. Biosensors based on impedance sensing may provide a tool for establishing standardize quality protocols and controls.

The following experiments utilized MSC, which were harvested from bone marrow biopsies of healthy individuals. Stem cell isolation and cultivation as well as MSC seeding and differentiation on the biosensor including histological documentation of the experiments were performed in collaboration with the Lepperdinger Group of the Institute for Biomedical Aging Research at the ÖAW.

## 1. Sensor step response

A number of 50,000 cells per sensor was seeded on six sensors and monitored over an interval of 27 h. FIG 5.10 depicts the average value of the real part of the sensor impedances with standard deviation. In comparison to fibroblasts the initial peak after seeding was much more pronounced. That may be related to the longer period which the cells needed to flatten and spread.

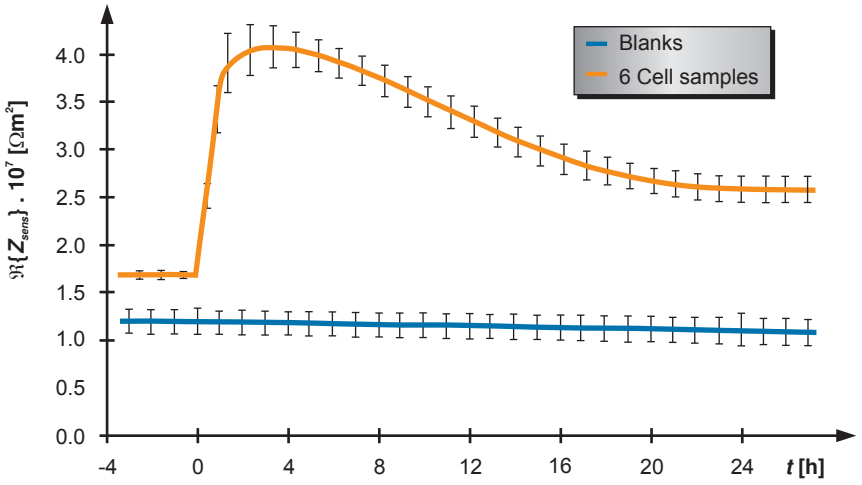


FIG 5.10: Sensor response to a confluent layer of hMSC cells. 50,000 cells per sensor were seeded at 0 h. The continuous line is the mean value of 6 samples. Bars indicate the standard deviation. The values represent the real part of the sensor impedance related to the sensor's electrode area of 0.9 mm$^2$.

FIG 5.11 shows images taken at 0, 1, 3, 6, 12, and 22 hours after seeding. Six hours after seeding almost all cells were adhered which was indicated by the impedance peak. Then cells spread and flattened. 22 hours after seeding a plateau was reached.

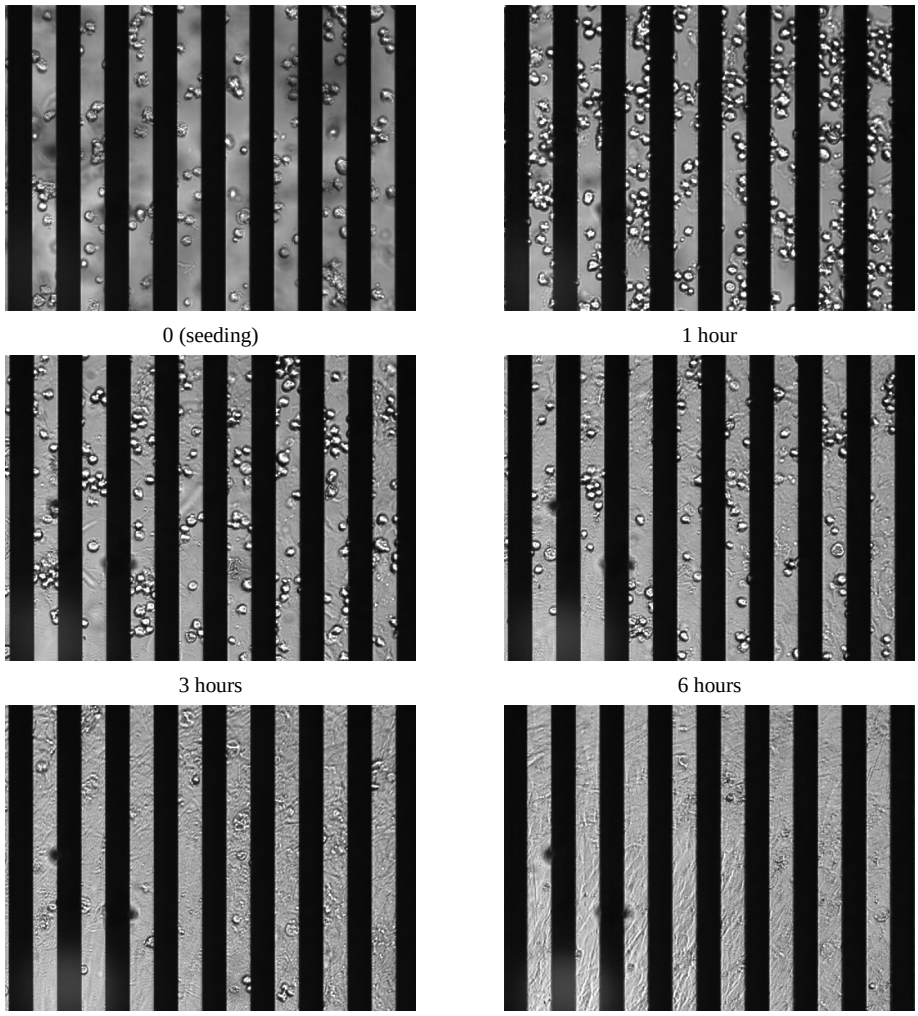


FIG 5.11: Seeding, adherence and growth of hMSC cells with 100 % confluence. Almost all cells adhered within six hours after seeding which was followed by spreading and flattening.

## 2. Cell Viability

The influence of the applied electric field on the cell viability during impedance measurement was tested. The step response measurement was repeated whereas two groups were formed with three samples per group. The impedance monitoring was active for one group while the other group served as control, i.e. no impedance measurement, no electric field or current flow.

The final staining with 7AAD was used to detect apoptosis (cell death) while Hoechst 33342 attached to DNA of living cells. Notably, such a test method is toxic to cell cultures. A significant influence of the electrical current during measurement could not be found. Cell viability for activated and disabled tags was less than 3 % mean value for both activated and disabled tags. Hence, impedance monitoring does not cause a no significant influence on the cell viability. FIG 5.12 shows a picture of such a viability test.

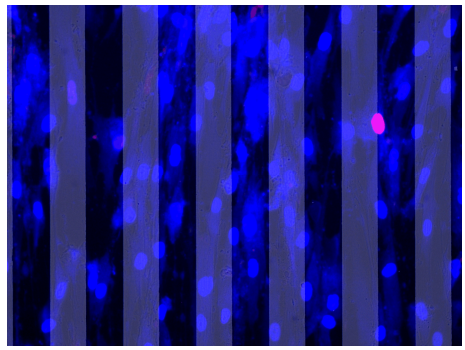

FIG 5.12: Viability test on hMSC using 7-amino-actinomycin staining (7AAD, 10 µg/ml) and Hoechst 33342 (25 µg/ml) as a counter stain in PBS. The grey bars indicate the electrode fingers, viable cells are blue and a single dead cell can be found on the right side of the picture as a purplish dot.

## 3. Adipogenic and osteogenic differentiation

Human MSC were cultivated at 37 °C, 3 % $O_2$ and 5 % $CO_2$-concentration in MEM supplemented with 20 % FCS, 100 units/ml Penicillin, and 100 µg/ml Streptomycin. 50,000 MSC from passage #2 were seeded per sensor and cultivated at 20 % $O_2$. At 48 h medium was exchanged and loosely adhered cells were discarded. The following experiment was done at two times, once for osteogenic and once for adipogenic differentiation.

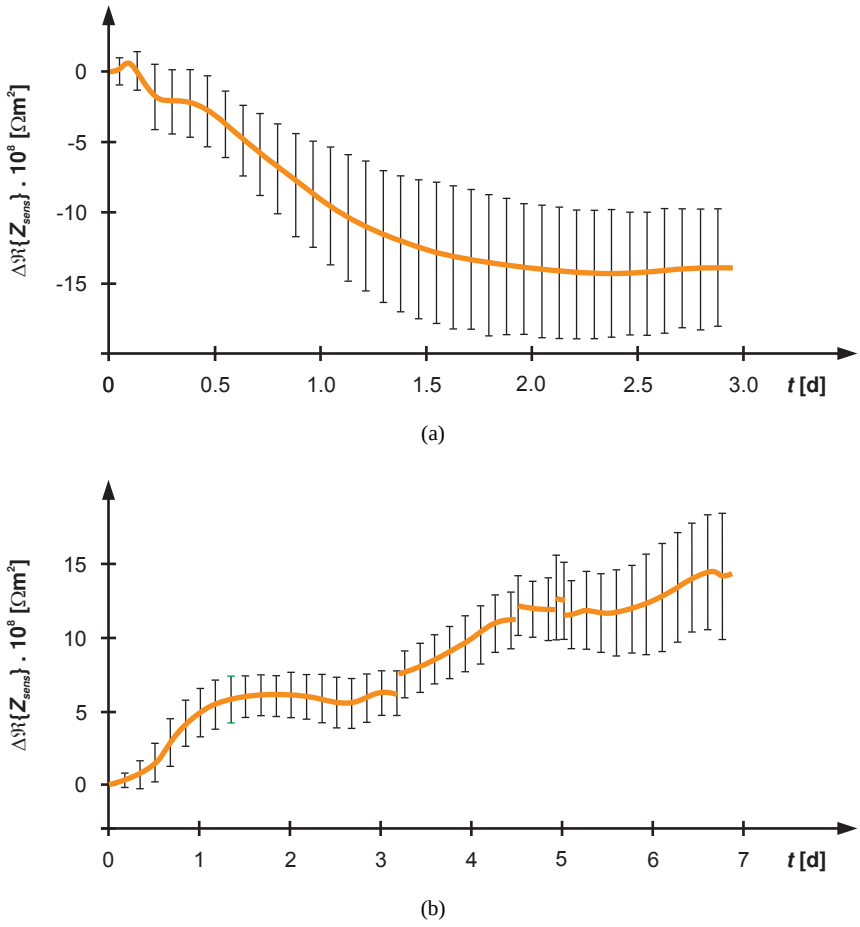


FIG 5.13: Sensor-area related differences of the real parts of the sensor impedance of non-differentiated controls with **(a)** Adipogenic differentiated stem cells and **(b)** Osteogenic differentiated stem. The differentiation was started at a confluent layer at $t = 0$.

After 24 h the samples were split into two groups whereas in one group a differentiation was induced. The second group was for control. Two base stations were operating simultaneously which allowed the assessment of 4 samples per group. Blanks in each microtiter plate were used to monitor the culture medium. For ostegenesis the culture medium MEM was supplemented with 1 mM β-glycerol Phosphate, 100 nM Dexamethasone, and 500 nM ascorbate-2-phosphate and for adipogenesis with 60 µM Indomethacin, 1 µM Dexamethasone, 500 nM Hydrocortisone, 50 µM 3-Isobutyl-1-Methylxanthine. Media were changed 3, 5, and 7 days after the differentiation was intiated. FIG 5.13 shows the time-resolved difference of the real part of the sensor values.

The differentiated cells are made visible by staining. FIG 5.14 pictures the differentiated cells. Fat vacuoles as well as the calcite mineralization are not uniformly distributed which is reflected in the stronger standard deviation of the measured impedances.

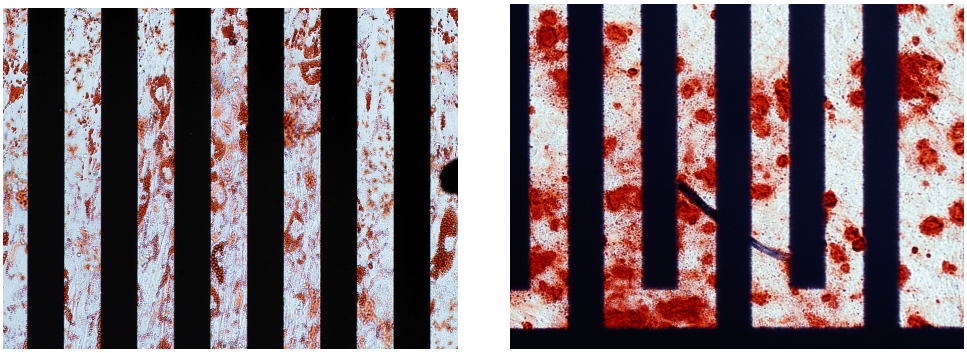

(a) (b)

FIG 5.14: **(a)** Adipogenic differentiated stem cells 12 days after induction. Red areas indicate fat vesicles made visible via Oil Red. **(b)** Osteogenic differentiated stem cells 18 days after induction. Red areas indicate the calcite matrix expressed by the cells made visible with Alizarin red S.

## 4. Long-term measurement with osteogenic differentiation

Previous hMSC monitoring with induced differentiation started with a 100 % confluent cell layer. In contrast, the following experiment starts with 20 % confluence. First, the impedance plateau for 100 % confluence was compared to that of the step response at a 10 kHz probe frequency.

This was followed by an investigation of the impedance change behavior depending on the measurement frequency whereas probe frequencies of 5, 10, 20.8 and 50 kHz were used. The long-term cultivation did also show how long cells could be cultivated with the induced differentiation.

10,000 cells per sensor of type hMSC51 were cultivated in MEM with 10 % FCS. 10 samples were prepared with two base stations performing simultaneous measurements. Seven days after seeding the osteogenic differentiation was induced on five samples. The effect on the measured impedance took place within the first day as shown in the previous chapter. Monitoring went on for another 14 days. This measurement was performed on four frequencies 5, 10, 20.83, and 50 kHz. FIG 5.15 shows the cell growth within the first seven days before differentiation at a single frequency of 10 kHz. FIG 5.16(A-D) depict the impedance behavior for the full measurement period of 19 days for all four measurement frequencies, cell-free blanks were not available in that setup. Each sensor data is normalized to its value at timestamp 168 h, which is the timestamp of induced differentiation. Culture media was exchanged on days 9, 12, 14, 16, 19, and 21.

Normalization was done with the real part and imaginary part 36 hours after seeding when the sensors had confluent layers. The data lines show the averaged values for each sample group whereas the standard deviation was about 10 %.

**Seeding and growth, induced differentiation**

FIG 5.15 shows the sensor impedances at a frequency of 10 kHz. Culture medium was exchanged after 48 h and 120 h. Then, the samples were split up into two groups. After 168 h and at all further culture media exchanges one group had a medium supplemented with differentiation factors. The cells of that group differentiated to bone cells.

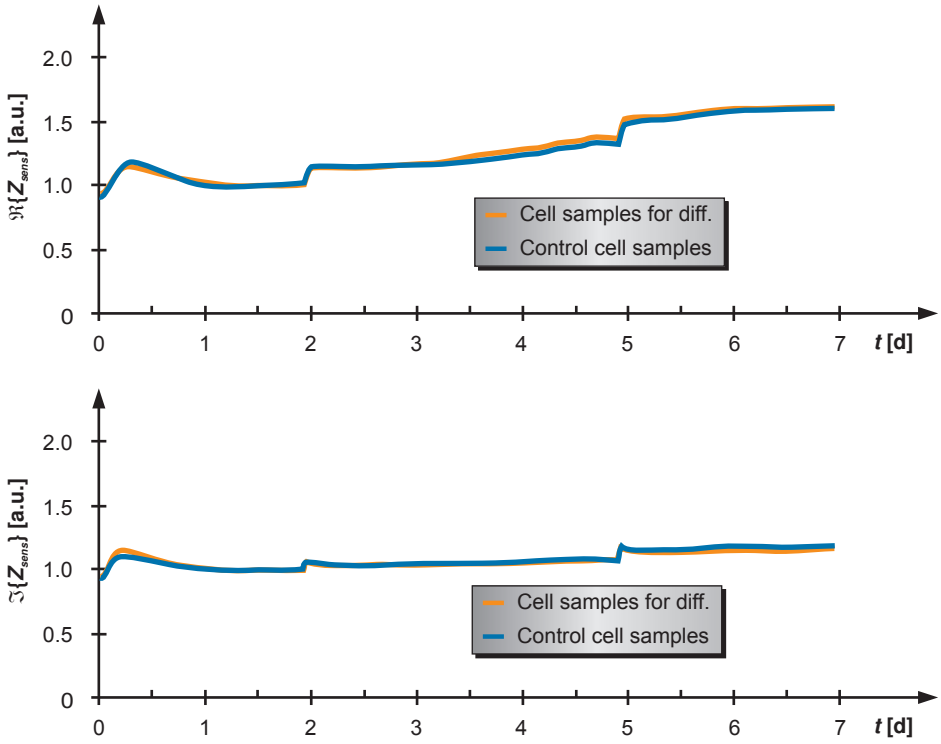


FIG 5.15: Seeding, adherence and cell growth of cell line hMSC51 within the first 7 days. Data shows the normalized sensor impedance at a frequency of 10 kHz. .The reference point for normalization was set to 24 h.

With respect to the initial step response measurement (initial value 1.6 a.u., plateau after 22 h at 2.7 a.u., i.e. 70 % change of the real part) the continuous cell growth shows the same plateau.

**Measurement results at 5 kHz**

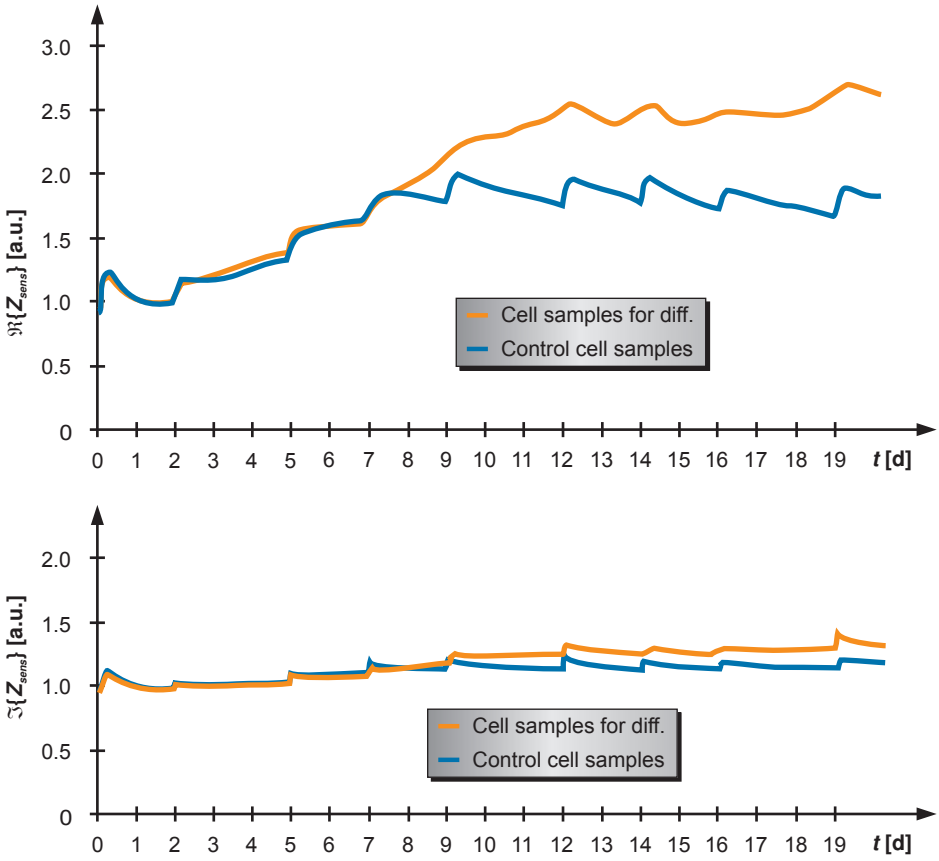


FIG 5.16A: Long-term measurement on hMSC after induced osteogenic differentiation at 168 h. Real and imaginary part of the sensor data for a measurement frequency of 5 kHz is shown.

**Measurement results at 10 kHz**

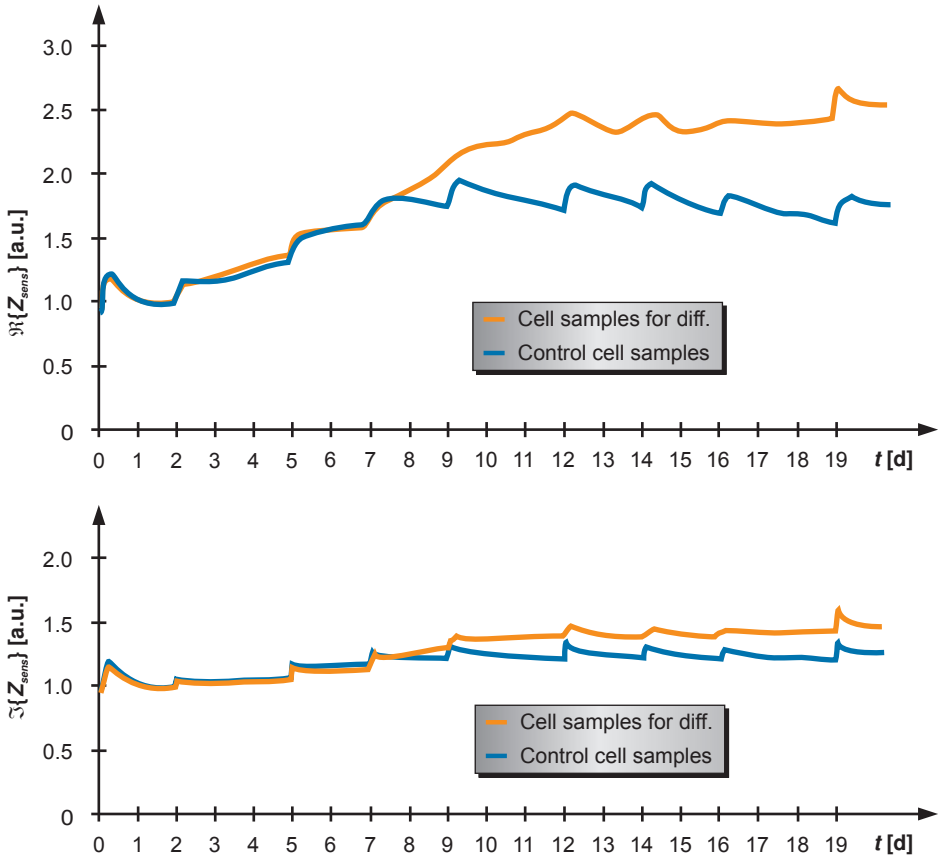


FIG 5.16B: Long-term measurement on hMSC after induced osteogenic differentiation at 168 h. Real and imaginary part of the sensor data for a measurement frequency of 10 kHz is shown.

**Measurement results at 20.8 kHz**

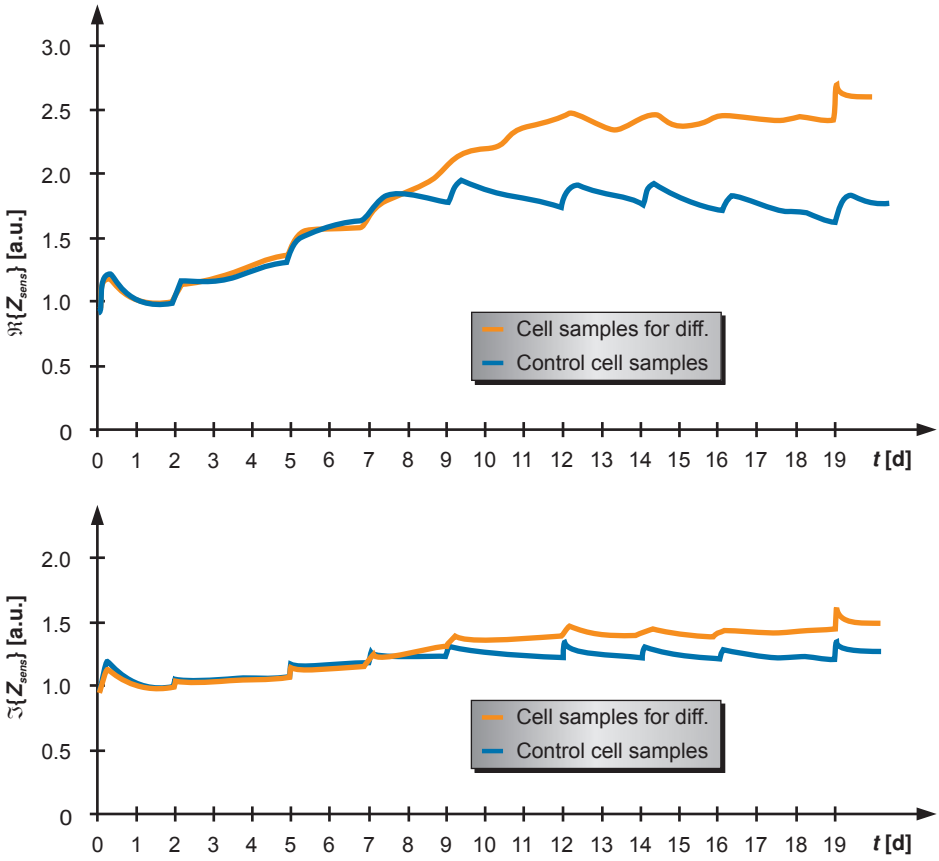


FIG 5.16C: Long-term measurement on hMSC after induced osteogenic differentiation at 168 h. Real and imaginary part of the sensor data for a measurement frequency of 20.83 kHz is shown.

**Measurement results at 50 kHz**

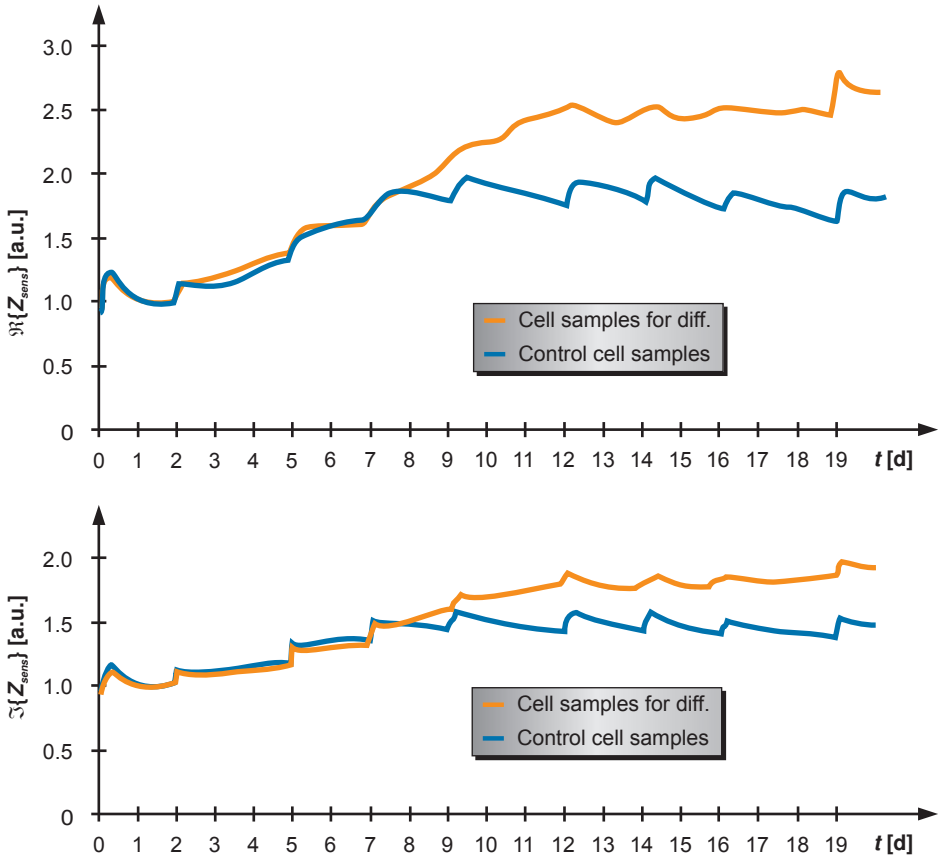


FIG 5.16D: Long-term measurement on hMSC after induced osteogenic differentiation at 168 h. Real and imaginary part of the sensor data for a measurement frequency of 50 kHz is shown.

The normalization of the data shows that the relative difference or the real part of the sensor impedance of induced and control cell lines is almost independent on the measurement frequency. However, the absolute difference becomes smaller as the absolute values decrease with increasing measurement frequency.

The imaginary data is most interesting. There, the relative difference increases with increasing measurement frequency. A possible reason is because the double layer capacity and Warburg impedance decrease with increasing frequency. The influence of the cell membrane and its environment is in turn increased. Previous measurements on 3T3 cells showed a small growth-related influence on the imaginary data. However, the information quantity is limited because of the small difference and the big influence of the cleanliness of the electrode area. Expressed calcite minerals may show the electrical behavior of capacitors lying in series to the cells which may explain the frequency-dependence of the imaginary part.

Especially after the 9th day each culture medium exchange showed a characteristic bump of the impedance data which then relaxed within a few hours. This effect is related to the culture medium evaporation and the temporary swelling of the cells when new medium is added. The characteristic zig-zag-shape of the impedance data related to that effect is also found at the results of other research groups [Bagnaninchi and Drummond 2011]. After 19 days of cultivation the cells showed signs of senescence which is characterized by a continuous decrease of sensor impedance.

## 5.4. Discussion

When cells settle on the electrode the electrode-electrolyte-interface is disturbed reflected by the imaginary part. However, this effect mostly relaxes which makes the imaginary part not suitable for the detection of cell growth. Also, the relative change is much smaller than in the real part.

Another aspect is the strong correlation to the cleaning procedure. During long-term measurements a superficial contamination was found on the electrodes which could almost not be removed. It was initially assumed to be a result of a small DC-offset but it was almost always found even in those cases when a tag was left as a control and no measurements were performed during investigations on cell cultures. It is assumed that some proteins expressed by the cells attach on the gold surface. This effect is primarily found on cell-loaded sensors. However, an influence on the sensor impedance was not found. Within this context it is worth to note that cells seem to prefer the presence of certain metals such as gold or platinum (but not silver).

To the author's knowledge the only available impedance measurements on (human mesenchymal) stem cells were conducted with ECIS systems with the single circular electrode briefly described in chapter 3. Results presented by Bagnaninchi *et al.* also show the effect of an impedance increase after culture medium exchange. The blank line has a behavior as found within the herein presented work and may also be related to the loss of culture medium [Angstmann *et al.* 2011, Bagnaninchi *et al.* 2011].

Even though fat vacuoles of adipocytes can be expected to be bad electrical conductors the impedance becomes smaller. It is assumed that the vacuoles give the cells a more spherical shape. Then the cell membranes partly detach from the sensor surface which in turn leads to an impedance decrease.

In contrast, osteocytes express calcite precipitates. Those calcites narrow the path for the current flow resulting in an impedance increase. The long-term measurement on osteogenic differentiation does not show significant differences in the used measurement frequency. Also, the imaginary data does not provide additional information which may give a hint to a contamination by the calcite precipitates. The microscopic pictures of stained cells show non-uniform distributions of cells with fat vacuoles and calcite minerals, respectively. That explains the comparably large deviations of the calculated sensor data.

The measurement on several frequencies was expected to deliver additional information. Even though it was known that the overall sensor impedance decreases with increasing frequency it was quite surprising that the only additional information may be acquired by the imaginary part. That data was ignored in the previous measurements on 3T3 cells as the real part of the sensor data showed more details. However, it should be mentioned that the significant influence on the imaginary part seems to be a result of the changing properties of stem cells due to differentiation. The results led to a closer view of the first detailed work with the used sensor type conducted by Ehret *et al*. There, the investigated cell lines were *Normal African Green Monkey Kidney Fibroblast Cells* CV-1 and *Human Caucasian Colon Carcinoma Cells* LS 174T. The provided sensor conductance and phase with and without cells was analyzed and it was found that even there the relative change of the ohmic component of the sensor impedance was 2.8 to 3 for a frequency range from 1 kHz to 100 kHz. Therefore, it has to be assumed that an (adherent) cell culture shows an almost isolating behavior with respect to the culture medium. The electrical data of the membrane depicted in chapter 3 (about 6 mF/m² and 0.01 to 10 $\Omega m^2$) leads to a cutoff-frequency-range from to 2 Hz to 2500 Hz, depending on the cell type. A cell-covered electrode-area of 0.9 $mm^2$ then has an impedance of at least 20 kΩ without the cytosol. In contrast, culture medium has a resistance of about 10 Ω if a cell-height of 10 µm is assumed. Hence the real part of the sensor impedance may only change its value by frequency-dependent parts such as the Warburg-Impedance. However, within this context the question is how the culture medium ingredients do really behave in the complex composition. Until now, only one work is known which models the impedance behavior of a single cell on a circular electrode [Huang *et al*. 2004].

A system-inherent limitation within the conducted measurements was the small number of possible samples. That enforced a more detailed investigation on the effects of temperature and medium evaporation. Conventional toxicological test routines state the use of samples only containing culture medium but no cells, known as *blanks*. In the field of impedance measurements those blanks are of great importance for the control of the environmental conditions. Culture medium evaporation directly influences the sensor impedance and leads to measurement artifacts.

Especially in the case of a fully confluent cell layer a culture medium exchange causes a characteristic excess of the impedance data. Even though an optical verification was not possible it is assumed that this effect is directly linked to osmotic pressure. When culture medium evaporates the nutrients and salts remain in the residual volume, i.e. the effective concentration of them continuously increases. Cells are – within limits – able to adapt to that changes. When culture medium is exchanged the nutrient and salt concentrations drop to their set-values. Cells cannot to accommodate that fast and, as a consequence, water passes the cell membranes and let the cells swell. Both, the change of the salt concentration and the swelling cause a characteristic bump at the impedance data. The falling slope of the bump indicates that it takes cells several hours to adapt to that new situation.

Impedance artifacts can partially be compensated by the parallel monitoring of blanks. It was found that the relative loss of culture medium in a well corresponds very well to the relative decrease of the ohmic resistance of such a blank. Therefore, that data can be used to correct the sensor data of cell-loaded samples as the experimental data on *3T3 fibroblasts with final cell termination* showed. The intensity of the impedance-bump is strongly correlated to the intensity of evaporation, i.e. the intensity of the use of the incubator by different operators within a short period. Hence, a separate incubator for investigations utilizing impedance monitoring is highly recommended.

## 5.5. Bibliography

Angstmann M., Brinkmann I., Bieback K., Breitkreutz D., Maercker C.: *Monitoring human mesenchymal stromal cell differentiation by electrochemical impedance sensing*. Cytotherapy 13, pp. 1074-1089 (2011).

Bagnanichi P.O., Drummond N.: *Real-time label-free monitoring of adipose-derived stem cell differentiation with electric cell-substrate impedance sensing*. Proc. Natl. Acad. Sci. USA 108 (16), pp. 6462-6467 (2011).

Ceriotti L., Ponti J., Colpo P., Sabbioni E., Rossi F.: *Assessment of cytotoxicity by impedance spectroscopy*. Biosens. Bioel. 22, pp. 3057-3063 (2007).

Ehret R., Baumann W., Brischwein M., Schwinde A., Stegbauer K., Wolf B.: *Monitoring of cellular behaviour by impedance measurements on interdigitated electrode structures*. Biosens. Bioel. 12, pp. 29-41, 1997.

Huang X., Nguyen D., Greve D.W., Domach M.M.: *Simulation of Microelectrode Impedance Changes Due to Cell Growth*. IEEE Sensors J. 4 (5), pp. 576-583 (2004).

Interagency Coordinating Committee on the Validation of Alternative Methods (ICCVAM): *Test method evaluation report Appendix C*. November 2006.

Kassem M., Abdallah B.: *Human bone-marrow-derived mesenchymal stem cells: Biological characteristics and potential role in therapy of degenerative diseases*. Cell and Tissue Research 331 (1), pp. 157-163 (2008).

Keese C.R., Giaever I.: *A Biosensor that Monitors Cell Morphology with Electrical Fields*. IEEE Eng. Med. Biol. Mag. 13 (3), pp. 402-408 (1994).

Méndez-Ferrer S., Michurina T.V., Ferraro F., Mazloom A.R., Macarthur B.D., Lira S.A., Scadden D.T., Ma'ayan A., Enikolopov G.N., Frenette P.S.: *Mesenchymal and haematopoietic stem cells form a unique bone marrow niche*. Nature 466 (7308), pp. 829-34 (2010).

Organisation for Economic Co-operation and Development (OECD): *OECD guideline for testing chemicals - In Vitro 3T3 NRU phototoxicity test*. Adopted April 13th 2004.

Schmitz S.: *Der Experimentator: Zellkultur*. 1. Auflage, Elsevier GmbH München, ISBN 978-3-8274-1564-6 (2007).

Todaro G.J., Green H.: *Quantitative Studies of the Growth of Mouse Embryo Cells in Culture and their Development into established Lines*. J. Cell Biol. 17, pp. 299-313 (1963).

# Chapter 6

# OUTLOOK

This thesis presented electrical impedance measurement on adherent cell cultures. One conventional method on toxicological research on a certain substance is to mix that substance with culture medium in several concentrations. Cells are seeded with a concentration of about 10 % with that culture medium. The growth behavior and viability is compared to cells with non-treated culture medium [ICCVAM 2006].

In an inverted way a cell layer is grown and the influence of a certain substance is tested [Arndt *et al.* 2004]. An example for such a process was presented by the induced differentiation or the treatment of 3T3 fibroblasts with Triton X-100. Also, a cell-cell-interaction can be investigated. For instance, a cell layer is grown to an adherent layer and the influence of cancer cells or viruses on such a layer can then be observed [Campbell *et al.* 2007, Rahim and Üren 2011].

The incorporated sensor may also be coated with biochemically active components, such as specific proteins. The attachment and proliferation of cell cultures on such treated surfaces allows an investigation of single cell and cell-cell reactions on specific molecules [Wegener *et al.* 2000, Asphahani *et al.* 2008, Yun *et al.* 2009].

## 6.1. Design proposal

The invented wireless approach showed a high reliability and robustness. This makes the RF technique a serious alternative for several wire-bound attempts [Acea Biosiences and Roche Applied Sciences, Applied Biophysics]. A weakness of the actual system is the small number of samples per microtiter plate. This results by the lack of a low power IC for impedance measurement. If such an IC was available the setup depicted in FIG 4.16 would allow a highly modular integration in a 24-well-system.

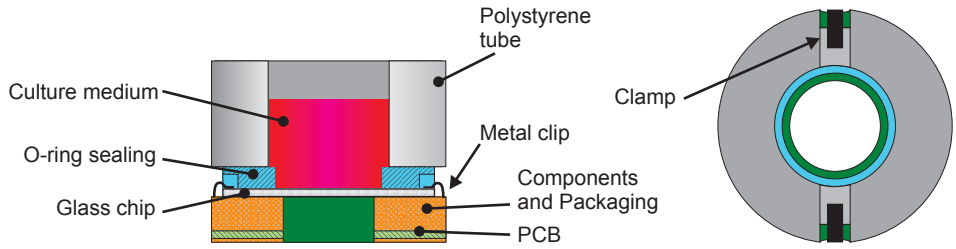


FIG 6.1: Concept for a 24-well-implementation in a 2:1 scale. **Left**: Cross cut section with a PCB carrying the electronics, a glass chip held and connected via metal clips and a polystyrene tube to form a well with an O-ring as sealing. **Right**: Top view with two clamps pressing all parts together.

The suggested PCB has an outer diameter of 15.5 mm, and a hole of 6 mm for microscopic inspections. The bottom has the coil integrated as a lithographic patterned conductor and the top side carries the necessary measurement IC in a flip-chip-technique, a microcontroller, capacitors and resistors, and two metal clips for contacting the sensor chip. The whole PCB needs to be packaged, a round glass chip with the sensor device on it can be positioned on that device, electrically contacted and mechanically held in place via the clips. A properly shaped O-ring sealing followed by a polystyrene tube forms the well. Two clamps from the top of the PS-tube down to the PCB hold the parts together.

Such a setup only requires the glass chip to be replaced while all other parts can be reused. Sensor design requires a defined position of the contact pads only. Even though the already realized system as well as this suggestion is not completely free of electromechanical contacts, the number of those contacts is minimized.

The actual system has the glass chip surface with a distance of about 5 mm from the well's bottom of the microtiter plate. Hence the microscopy can only be done with a zoom factor 4. The suggested layout would reduce the distance to less than 4 mm and could allow a 10-fold zoom.

## 6.2. A Monitoring Technique for the Incubator

The use of blank sensors, i.e. only culture medium or a proper electrolyte such as PBS, was found to reflect the environment of an incubator. Hence, this method may also be a possibility as a general sensing mechanism for the incubator atmosphere. Conventional electronic methods for humidity detection via hygroscopic materials or capacitive properties (e.g. *SHT71* and *SHT75* from *Sensirion*) have limited functionality if the humidity level is close to 100 %, also offsets and linearity errors. Such a sensor would be positioned in the incubator but wouldn't indicate the evaporation process itself. In contrast, the IDES sensor directly reflects the conditions for cell cultures. The time-related change of the ohmic impedance correlates with the evaporation rate and short-term temperature-drops are recognized by impedance peaks (compare blanks of FIG 5.9).

## 6.3. Impedance measurement: A feasible Standard Assessment Technique?

Several cell lines have been investigated since the measurement on adherent cell cultures were pushed in the 1980's. The following table gives a short overview of publications found for different cell lines.

TABLE 6.I: List of Publications with investigated Cell Lines

| Publication | Cell lines |
|---|---|
| Giaever and Keese 1984 | WI-38 (Human embryonic fibroblast, lung-derived) |
| Tiruppathi et al. 1992 | BPMVEC (Bovine pulmonary microvessel endothelian), BPAEC (Bovine pulmonary artery endothelian) |
| Lo et al. 1995 | MDCK (Madin-darby canine kidney) |
| Ehret et al. 1997 | CV-1 (Normal african green monkey kidney fibroblasts), LS 174T (Colon carcinoma) |
| Huang et al. 2004a | 3T3 (Mouse embryonic fibroblasts), HCT-116 (Human colorectal carcinoma) |
| Arndt et al. 2004 | PBCEC (Porcine Brain capillary endothelian) |
| Rissanen et al. 2005 | BACC-EC (Bovine adrenal cortex capillary endothelian) |
| Xiao et al. 2005 | V79 (Chinese hamster fibroblast) |
| Campbell et al. 2007 | CHSE-214 (Chinook salmonid embryonic) |
| Seriburi et al. 2007 | RAW 264.7 (Mouse leukaemic monocyte macrophage) |
| Opp et al. 2009 | HUVEC (Human umbilical vein endothelian) |
| Rümenapp et al. 2009 | L929 (Murine fibroblasts), MDA (Human breast adenocarcinoma) |
| Park et al. 2010 | hMSC (Human mesenchymal stem cells) |

This listing is not complete and the measurement frequencies and sensor types are different. Microbiological laboratories and their operators need to have experience with the cell lines, the used culture media and sera, cell culture plastics, etc. Thus, most authors limit their investigations to a single cell line with a certain sensor construction. In several cases the systems were run by microbiologists. The presented impedance measurement data was not always self-contained, e.g. absolute impedance data was presented without a phase information. Within the following years it will become necessary to get a set of suitable reference data for different cell cultures. Also, the data

needs to be linked to the physical and electrochemical properties of cells, culture media and sensor layouts. Until now the only available simulation deals with a single cell on a circular electrode [Huang *et al.* 2004b].

One utilization of impedance measurement is the general investigation of a cell line and its reaction on certain substances, growth behavior, or wound healing. For that purpose a combination of the impedance measurement with classical microscopic methods including marker substances, will be necessary. Microscopic pictures can provide space-resolved images with a resolution of a few micrometers. Specific marker substances allow a closer look to special structures but at the price of the loss of the sample due to possible influences of the marker substance itself on the cell behavior.

In contrast, impedance measurement, as it was performed within this work, is an averaging method. It allows a continuous monitoring and in certain cases the detection of effects which cannot be explored with conventional optical methods. That may be, for instance, a swelling of cells due to culture medium evaporation (this is still an assumption and needs to be verified). Especially the induced adipogenic differentiation showed an interesting effect. Even though fat vacuoles can be assumed to be bad conductors the sensor impedance decreased which can only be linked with a change of the cell shape. The osteogenic differentiation did not show a change of the imaginary part of the sensor impedance – the expressed calcite minerals are therefore not deposited on the electrode structure. All these described effects occur within the sub-micrometer-range.

As soon as a reference dataset for cells exists, impedance measurement has the potential to become a standardized screening method for certain substances and samples, e.g. doping agents. A more specific result may be achieved with functionalized sensors. That is, the sensor surface is treated with proteins or similar chemicals. Moreover, impedance data can show significant changes within a fraction of the required cell proliferation period for staining methods. To sum up, for research purposes optical methods and impedance measurement complement one another. Screenings may be conducted with just a final optical check.

## 6.4. Bibliography

Acea Biosiences, Roche Applied Science: *RTCA-system*. Datasheet and characterization available online www.aceabio.com or www.roche-applied-science.com.

Applied Biophysics: *ECIS system*. Datasheets available online www.biophysics.com.

Arndt S., Seebach J., Psathaki K., Galla H.-J., Wegener J.: *Bioelectrical impedance assay to monitor changes in cell shape during apoptosis.* Biosens. Bioel. 19, pp. 583-594 (2004).

Asphahani F., Thein M., Veiseh O., Edmondson D., Kosai R., Veiseh M., Xu J., Zhang M.: *Influence of cell adhesion and spreading on impedance characteristics of cell-based sensors*. Biosens. Bioel. 23, pp. 1307-1313 (2008).

Campbell C.E., Motzfeldt Laane M., Haugarvoll E., Giaever I.: *Monitoring viral-induced cell death using electric cell-substrate impedance sensing*. Biosens. Bioel. 23, pp. 536-542 (2007).

Ehret R., Baumann W., Brischwein M., Schwinde A., Stegbauer K., Wolf B.: *Monitoring of cellular behaviour by impedance measurements on interdigitated electrode structures*. Biosens. Bioel. 12, pp. 29-41 (1997).

Giaever I., Keese C.R.: *Monitoring fibroblast behavior in tissue culture with an applied electric field*. Proc. National Academy of Sciences USA 81 (12 I), pp. 3761-3764 (1984).

Huang X., Nausieda I., Greve D.W., Domach M.M., Nguyen D.: *Development of Active Matrix Biosensor Array for Cell Screening*. Proc. IEEE Sensors 1, ISBN 0-7803-8692-2, pp. 72-75 (2004).

Huang X., Nguyen D., Greve D.W., Domach M.M.: *Simulation of Microelectrode Impedance Changes Due to Cell Growth*. IEEE Sensors J. 4 (5), pp. 576-583 (2004).

Interagency Coordinating Committee on the Validation of Alternative Methods (ICCVAM): *Test method evaluation report Appendix C*. November 2006.

Lepperdinger G., Brunauer R., Jamnig A., Laschober G., Kassem M.,: *Controversial issue: is it safe to employ mesenchymal stem cells in cell-based therapies?* Exp. Gerontol. 43 (11), pp. 1018-1023 (2008).

Lo C.-M., Keese C.R., Giaever I.: *Impedance Analysis of MDCK Cells Measured by Electric Cell-Substrate Impedance Sensing*. Biophys. J. 69, pp. 2800-2807 (1995).

Opp D., Wafula B., Lim J., Huang E., Lo J.-C., Lo C.-M.: *Use of electric cell-substrate impedance sensing to assess in vitro cytotoxicity*. Biosens. Bioel. 24, pp. 2625-2629 (2009).

Park H.E., Kim D., Koh H.S., Cho S., Sung J.-S., Kim J.Y.: *Real-Time Monitoring of Neural Differentiation of Human Mesenchymal Stem Cells by Electric Cell-Substrate Impedance Sensing*. J. Biomed. Biotech., Art. No. 485173 (2010).

Rahim S, Üren A.: *A real-time electrical impedance based technique to measure invasion of endothelial cell monolayer by cancer cells*. J Vis Exp. 50 (2011).

Rissanen A.K., Ostrovidov S., Lennon E., Senez V., Kim J., Kim B., Sakai Furukawa K., Ushida T., Sakai Y., Fujii T.: *Monitoring Capillary Endothelian Cell Culture and Capillary Formation in a Microdevice by Impedance Spectroscopy Measurements*. Proc. 3rd Ann. Int. IEEE EMBS Special Topics Conf. Microtechn. Med. Biol., pp. 201-204 (2005).

Rümenapp C., Remm M., Wolf B., Gleich B.: *Improved method for impedance measurements of mammalian cells*. Biosens Bioel. 24, pp. 2915-2919 (2009).

Seriburi P., Shastry A., Ren T., Gales S., Böhringer K.F., Meldrum D.: *Using Electric Cell-Substrate Impedance Sensing to measure Chnges in the Projected Area of Individual Cells*. Transducers & Eurosensors '07, pp. 469-472 (2007).

Tiruppathi C., Malik A.B., Del Vecchio P.J., Keese C.R., Giaever K.: *Electrical method for detection of endothelian cell shape change in real time: Assessment of endothelial barrier function*. Proc. Natl. Acad. Sci. USA 89, pp. 7919-7923 (1992).

Wegener J., Keese C.R., Giaever I.: *Electric Cell–Substrate Impedance Sensing (ECIS) as a Noninvasive Means to Monitor the Kinetics of Cell Spreading to Artificial Surfaces*. Experimental Cell Research 259, pp. 158-166 (2000).

Xiao C., Luong J.H.T.: *Assessment of cytotoxicity by emerging impedance spectroscopy*. Toxicology and Appl. Pharmacology 206, pp. 102-112 (2005).

Yun Y.-H., Bhattacharya A., Watts N.B., Schulz M.J.: *A Label-free Electronic Biosensor for Detection of Bone Turnover Markers*. Sensors 9, pp. 7957-7969 (2009).

# DANKSAGUNG

Zu Beginn möchte ich Prof. Dr. Michael Vellekoop danken, der sich bereiterklärt hat die Betreuung dieser Arbeit zu übernehmen. Vor allem seine pointierten Kommentare bei wissenschaftlichen Publikationen wie auch dieser Arbeit haben diesen den letzten Schliff gegeben. Je kürzer diese Kommentare und Anregungen waren, desto schwerer waren sie meistens einzuarbeiten: Ein einfaches „warum" hat manchmal gereicht damit ich mir wegen des einen oder anderen Graphen oder einer Aussage nochmals eine Nacht um die Ohren schlage. Am Ende dieser Mühen steht nun eine Dissertation, die ich mit Stolz in Händen halte.

Das vorausgegangene CellMonitor-Projekt war eine Kooperation der Abteilungen *Nano-Systemtechnologien* und *Life Science* innerhalb des AIT. Das vielschichtige Thema dieser Arbeit bedurfte der Konsulatation und Mithilfe etlicher Leute aus den Bereichen Mikrobiologie, Materialwissenschaften, Elektronik und Nachrichtentechnik. Ich möchte versuchen mich kurz zu fassen und die wichtigsten zu nennen. Die Projektleitung oblag Rudolf Heer. Ihm verdanke ich es vor allem, daß meine anfangs unstrukturierte Herangehensweise an die Arbeit eine Geradlinigkeit erhalten hat – für das eine oder andere seiner graue Haare zeichne ich sicher auch verantwortlich. Die Produktion der Glaschips wurde durch Thomas Maier und Marcus Milnera sichergestellt, welche damit oftmals tagelang im Reinraum ausgelastet waren. Letizia Farmer und Christine Höpfner haben mit dem neu entworfenen Meßsystem erste Gehversuche in der Impedanzmessung an Zellkulturen unternommen. Ebenso haben sie mich in die praktische Arbeit mit Zellkulturen eingewiesen.

Mit der Einrichtung des mikrobiologischen Labors in Wien konnten viele Versuche vor Ort durchgeführt werden. In weiterer Folge waren mir Verena Charwat und vor allem Lukas Richter wichtige Ansprechpartner, wenn es um Fragen die Zellkulturen betreffend ging. Deren Projektleiter Peter Ertl verdanke ich den Kontakt zu Günter Lepperdinger, dessen Gruppe an der Österreichischen Akademie der Wissenschaften war es, die die Messung an Stammzellen möglich gemacht hat. Letztere wurden vornehmlich von Werner Kapferer und Stefan Reitinger ausgeführt. Die damit verbundenen Besuche in Innsbruck waren dabei für mich mit ein Grund meine Arbeit bei Med-El und auch meinen neuen Lebensmittelpunkt in Tirol zu finden.

Ich habe nun einer ganze Reihe von Personen meine Anerkennung ausprechen können, weil es zwei besondere Menschen gibt, die den Grundstein für meinen bisherigen Lebensweg und akademischen Werdegang gelegt haben – meinen Vater und meine Mutter. Die Schlußworte und mein größter Dank gilt euch beiden.

# ACKNOWLEDGEMENTS

First of all, I'd like to thank Prof. Dr. Michael Vellekoop who agreed to supervise my work. Especially his incisive comments on the drafts of my publications as well as on this work gave them their final touch. The shorter those comments were the harder they were to implement: A simple "why" on a graph or a statement was enough to burn the midnight oil. I think at the end of all that work, there is a thesis which can proudly be presented.

The CellMonitor project was a cooperation of the departments *Nano-Systemtechnologies* and *Life Science* inside AIT. The complex topic of this work required the consulting and help by a lot of people from the areas of microbiology, material sciences, electronics and communications engineering. I'd like to make it short and appoint the most important ones. The leader of the CellMonitor project was Rudolf Heer. Thanks to him my confuse approach became a straight forward one – I guess I am responsible for a few of his grey hairs. The production of the glass chips was done by Thomas Maier and Marcus Milnera who spent several days in the clean room for that work. Letizia Farmer and Christine Höpfner were the first microbiologists using the newly designed measurement system on cell cultures. The did also gave me an introduction to the practical work with cell cultures.

The installation of a microbiological laboratory in Vienna allowed to do several investigations on site. During the following months Verena Charwat and especially Lukas Richter were important contact persons for microbiological questions. Thanks to their project leader Peter Ertl I came in contact with Günter Lepperdinger whose group at the Austrian Academy of Sciences in Innsbruck conducted the impedance measurements on stem cells. The laboratory work was done by Werner Kapferer and Stefan Reitinger. The visits in Innsbruck gave the impulse finding my new work at Med-El and my new home in Tyrol.

I was now able to give several persons my acknowledgements because of two special people who cleared my path of life and academic career – my father and my mother. These final words and my biggest gratitude belong to you.

# LIST OF PUBLICATIONS

**Journal Publications**

Wissenwasser J., Vellekoop M., Heer R.: *Highly sensitive passive RFID based sensor systems*. Rev Sci Instrum 81, pp. 025106, doi 10.1063/1.3316804 (2010).

Wissenwasser J., Vellekoop M., Heer R.: *Signal Generator for Wireless Impedance Monitoring of Microbiological Systems*. IEEE T Instrum Meas 60 (6), pp. 2039-2046, doi 10.1109/TIM.2011.2113127 (2011).

Wissenwasser J., Vellekoop M., Kapferer W., Lepperdinger G., Heer R.: *Multifrequency Impedance Measurement Technique for Wireless Characterization of Microbiological Cell Cultures*. Rev Sci Instrum 82, pp. 1151110, doi 10.1063/1.3664614 (2011). [13]

Reitinger S., Wissenwasser J., Kapferer W., Heer R., Lepperdinger G.: *Electric impedance sensing in cell-substrates for rapid and selectivemultipotential differentiation capacity monitoring of human mesenchymal stem cells*. Biosens Bioel 34, pp. 63-69, doi 10.1016/j.bios.2012.01.013 (2012).

**International conferences**

Wissenwasser J., Nicolics J., Vellekoop M.: *Silicone-based encapsulation of a cell culture measurement device under physiological conditions*. 32nd Int. Spring Seminar on Electronics Technology, Brno (CZ) 2009, ISBN 978-1-4244-4260-7, doi 10.1109/ISSE.2009.5207052 (2009). [14]

Wissenwasser J., Milnera M., Farmer L., Höpfner C., Vellekoop M., Heer R.: *Monitoring adherent cell cultures in microtiter-plates by a wireless sensory system*. World Congress on Medical Physics and Biomedical Engineering, IFMBE Proceedings 25/VIII, ISBN 978−3−642−03897−6 (vol. I-XIII), pp. 261-264, doi 10.1007/978-3-642-03887-7_76 (2009).

Heer R., Wissenwasser J., Milnera M., Farmer L., Höpfner C., Vellekoop M.: *Wireless powered electronic sensors for biological applications.* Conf on Eng Med Biol, Buenos Aires (RA), ISBN 978-1-4244-4124-2, pp. 700-703, doi 10.1109/IEMBS.2010.5626184 (2010).

[13] Selected article for the Virtual Journal of Biological Physical Research 22 (11) (2011).
[14] Excellent Poster Award for Young Scientists.

**Patents**

Heer R., Wissenwasser J., Brückl H., Kroath H.: *Verfahren zur Datenübertragung*. Austrian Patent AT 505632 B1 (2009).

Heer R., Brueckl H., Kroath H., J. Wissenwasser J.: *Method for Wireless Data Transmission between a Measurement Module and a Transmission Unit*. WO 2009/137858 A1, priority date May 14th 2008, published November 19th 2009.

**Other**

Wissenwasser J., Maier T., Milnera M., Farmer L., Höpfner C., Heer R., Vellekoop M.: *Online-Monitoring von Zellkulturen für High Throughput-Systeme auf der Basis von RFID-Technologie*. ME-Tagung 2008, Tagungsband zur Informationstagung Mikroelektronik 08, ISBN 978−3−85133−049−6, OVE Österreichischer Verband für Elektrotechnik (2008).

Wissenwasser J., Maier T., Milnera M., Farmer L., Höpfner C., Heer R., Vellekoop M.: *A RFID-based high volume biosensor system*. ARGE Sensorik, PhD Summit, ISBN 978−3−9502856−0−4 (Online-Publication) (2009).

Wissenwasser J., Heer R.: *Zellmonitor - Berührungsloses Monitoring von Zellkulturen*. Fachzeitschrift Elektronik 20/2010, pp. 38-43 (2010).

Heer R., Wissenwasser J., Milnera M., Vellekoop M.: *Wireless monitoring of adherent biological cell cultures*. ME Tagung 2012, Tagungsband zur Informationstagung Mikroelektronik 12, ISBN: 978−3−85133−071−7, OVE Österreichischer Verband für Elektrotechnik, pp. 85-89 (2012).

# Über den Autor

Jürgen Wissenwasser wurde 1979 in Wien, Österreich, geboren. Von 1994 to 1999 besuchte er die *Höhere Technische Bundeslehr- und Versuchsanstalt St. Pölten, Abteilung Elektrotechnik* und absolvierte die Matura mit Ausgezeichnetem Erfolg.

Nach dem Militärdienst als Panzerfahrer und Milizionär begann er im Jahr 2000 das Diplomstudium der Elektrotechnik an der *Technischen Universität Wien* und beendete es 2006 mit Ausgezeichnetem Erfolg Die Diplomarbeit wurde bei *Infineon Technologies* am Standort Villach ausgeführt und behandelte Degradationsprozesse und die Zuverlässigkeit von Leistungshalbleiterbauelementen.

Von 2006 bis 2010 war Jürgen Wissenwasser am *Austrian Institute of Technology* in der Abteilung Nano-Systemtechnologien. Diese Dissertation basiert auf dem CellMonitor-Projekt, das dort bearbeitet wurde.

Seit 2011 ist er als Emerging Applications-Ingenieur beim Cochleaimplantat-Hersteller *MED-EL* in Innsbruck, Österreich, beschäftigt, wo er neue Technologien für aktive medizinische Implantate entwickelt.

# ABOUT THE AUTHOR

Jürgen Wissenwasser was born in Vienna, Austria, 1979. From 1994 to 1999 he attended the *Höhere Technische Bundeslehr- und Versuchsanstalt St. Pölten, Abteilung Elektrotechnik* (Secondary Technical School, Dept. of Electrotechnical Engineering) and passed the final exam with honors.

After the Military Service as tank driver and militiaman he started his studies on Electrotechnical Engineering at the *Vienna University of Technology* in 2000 and graduated with honors in 2006. The diploma thesis was conducted at *Infineon Technologies* in Villach, Austria, and discussed degradation processes and the reliability of silicon power devices.

From 2006 to 2010 Jürgen Wissenwasser was with the *Austrian Institute of Technology* in the Nano-Systemtechnologies department . This Doctor Thesis is based on the CellMonitor project he was working on there.

Since 2011 he is Emerging Applications Engineer at the Cochlear Implant Company *MED-EL*, located in Innsbruck, where he is developing new technologies for active medical implants.

# Appendix A

# MICROBIOLOGY

This appendix provides an overview of the ingredients of culture medium DMEM, the composition of PBS and the procedure for cell passages. Also the recommended method for toxicity test using 3T3 mouse embryonic fibroblasts is described.

## A.1 Dulbecco's Modified Eagle's Medium

TABLE A.I: List of ingredients of DMEM.

| Substance | Concentration [mg/l] | Substance | Concentration [mg/l] |
|---|---|---|---|
| NaCl | 6400 | L-Methionin | 30 |
| KCl | 400 | L-Phenylalanin | 68 |
| $CaCl_2$ | 200 | L-Threonin | 95 |
| $MgSO_4 \cdot 7H_2O$ | 200 | L-Tryptophan | 16 |
| D-Glucose | 1000 | L-Tyrosin | 72 |
| $Fe(NO_3)_3 \cdot 9H_2O$ | 0.1 | L-Valin | 94 |
| Na-Pyruvate | 110 | Glycin | 30 |
| Phenolred | 15 | L-Serin | 42 |
| $NaH_2PO_4$ | 124 | Cholin chloride | 4 |
| L-Arginin-HCl | 84 | Folic acid | 4 |
| L-Cystine | 48 | Myo-inositol | 7.2 |
| L-Glutamine | 580 | Nicotinamide | 4 |
| L-Histidine · HCl · $H_2O$ | 42 | D-Ca-Pantothenat | 4 |
| L-Isoleucine | 105 | Pyridoxine · HCl | 4 |
| L-Leucine | 106 | Riboflavin | 0.4 |
| L-Lysine · HCl | 146 | Thiamin · HCl | 4 |

Dulbecco's Modified Eagle's Medium (DMEM) is a standardized nutrient solution for cell cultures with a broad application field for different kinds of animal cell cultures. This mixture is standardized and is also available with different add-ons, depending on the exact application. Phenol red is used as a pH-indicator. Below $pH \approx 6.8$ the culture

medium color is yellow, above 8 it is violet. Within that range it changes to red and red-violet. A slight violet fog can be found for culture medium which is stored for a long period, e.g. in a fridge. When it is in use the $CO_2$ of the incubator atmosphere dissociates as a carbon acid and stabilizes the pH value.

The upper listing is a basic mixture. 1000 mg/l or 4500 mg/l Glucose is added, depending on the metabolism of the cultivated cells. Also, 3.7 mg/l $NaHCO_3$ is mostly supplemented to adjust the pH level within a range of 7.2 to 7.4.

## A.2 Phosphate Buffered Saline Solution

TABLE A.II: List of ingredients for PBS.

| Substance | Concentration [mg/l] |
|---|---|
| NaCl | 8000 |
| KCl | 200 |
| $KH_2PO_4$ | 200 |
| $CaCl_2$ | 100 |

The listed ingredients of the most common PBS – Dulbecco's PBS (DPBS). Earle's salts (EPBS) and Hanks' salts (HPBS) are slightly different or have additional supplements. In contrast to DMEM the concentration of NaCl is significantly higher (8000 vs. 6400 mg/l). Therefore, the electrical conductivity of PBS is higher by about 25 %.

## A.3 Procedure for Cell Passage

The following procedure is a possible method for passaging adherent cells. Some investigations do not allow the use of enzymes for the detachment process. For instance, research on cell membrane proteins may prohibit the use of Trypsin. The values within the following description refer to a flask with a growth area of 25 $cm^2$.

(a) The culture medium is decanted from the flask and the residual cell layer rinsed twice with a 5 ml phosphate buffered solution (PBS). PBS is then also discarded.
(b) 1 ml of a proper PBS-solution with a defined enzyme concentration for the detachment of the cell layer is applied and the flask incubated for several minutes depending on the recommendations by the enzyme producer. This enzyme may be Trypsin, Accutase (II) or others.
(c) When the cells are detached from the surface they float in the PBS/enzyme solution. This solution is sucked out of the flask and put into an Eppendorf-flask.
(d) The flask is centrifuged with a specific g-force (about 200 g) for several minutes causing the sedimentation of the cells.

(e) The residual solution is sucked out and the flask with the cells on its bottom is again filled with a defined volume of a fresh culture medium. Repeated suction and injection dispenses the cells in the solution .

(f) A defined volume is extracted and the cell density measured utilizing cytometry. Also, new flasks are prepared and filled with culture medium.

(g) For a new seeding the necessary volume is calculated, extracted from the Eppendorf-flask and injected into the new flask(s). For instance, a reasonable growth performance can be achieved if the confluence is about 10 %. For a 25 $cm^2$ flask this means about $10^5$ cells.

## A.4 96-well plate configuration for positive control and test substances

This procedure is a brief sum-up of the ICCVAM recommendations for in-vitro toxicity test methods. The schematic shows the setup for a test with a 96-well microtiter plate. VC1 and VC2 are vehicle controls, C1 to C8 have the test substances or positive control (PC, Sodium Lauryl Sulfate) at eight concentrations ($C_1$ = highest, $C_8$ = lowest), Cxb are blanks (test substance or PC, but contain no cells) while VCb are VC blanks (contain no cells).

| | 1 | 2 | 3 | 4 | 5 | 6 | 7 | 8 | 9 | 10 | 11 | 12 |
|---|---|---|---|---|---|---|---|---|---|---|---|---|
| A | VCb | VCb | C1b | C2b | C3b | C4b | C5b | C6b | C7b | C8b | VCb | VCb |
| B | VCb | VC1 | C1 | C2 | C3 | C4 | C5 | C6 | C7 | C8 | VC2 | VCb |
| C | VCb | VC1 | C1 | C2 | C3 | C4 | C5 | C6 | C7 | C8 | VC2 | VCb |
| D | VCb | VC1 | C1 | C2 | C3 | C4 | C5 | C6 | C7 | C8 | VC2 | VCb |
| E | VCb | VC1 | C1 | C2 | C3 | C4 | C5 | C6 | C7 | C8 | VC2 | VCb |
| F | VCb | VC1 | C1 | C2 | C3 | C4 | C5 | C6 | C7 | C8 | VC2 | VCb |
| G | VCb | VC1 | C1 | C2 | C3 | C4 | C5 | C6 | C7 | C8 | VC2 | VCb |
| H | VCb | VCb | C1b | C2b | C3b | C4b | C5b | C6b | C7b | C8b | VCb | VCb |

- Incubate cells for 24 hours ±2 hours ($37^{\pm 1}$ °C, $90^{\pm 10}$ % humidity, $5.0^{\pm 1.0}$ % $CO_2$/air) so that cells form a less than half (<50 %) confluent monolayer. This incubation period assures cell recovery and adherence and progression to exponential growth phase. Note the seeding density to ensure that the cells in the control wells are not overgrown after three days (i.e., 24 hour incubation and 48 hour exposure to test substances). Prepare one plate per substance to be tested.
- Examine each plate under a phase contrast microscope to assure that cell growth is relatively even across the microtiter plate. This check is performed to identify experimental and systemic cell seeding errors.

## A.5 Bibliography

Biochrom AG: *Dulbecco's MEM*. Datasheet downloaded from http://www.biochrom.de/fileadmin/user_upload/service/produktinformation/deutsch/BC_Katalog_42_43_DMEM.pdf in January 2012.

Cell Signaling Technology: *Phosphate Buffered Saline (PBS-20X)*, datasheet downloaded from http://www.cellsignal.com/pdf/9808.pdf in January 2012.

Interagency Coordinating Committee on the Validation of Alternative Methods (ICCVAM): *Test method evaluation report Appendix C*. November 2006.

# Appendix B

# BASE STATION

The base station uses the RF-chip *MLX90121* from *Melexis Inc*. This IC is designed for its use in RFID-applications with a base frequency of 13.56 MHz. Nevertheless, its receiver section does also allow the detection of non-ISO-conform data transmission. The circuitry is an adaption of Melexis' evaluation board *EVB90121*. The following schematics do only describe the RF-generator and receiver section. Residual circuitry of the base station is trivial. The base station consists of a box holding the PCB with its circuitry and a top plate carrying six antenna coils as depicted in FIG B.1.

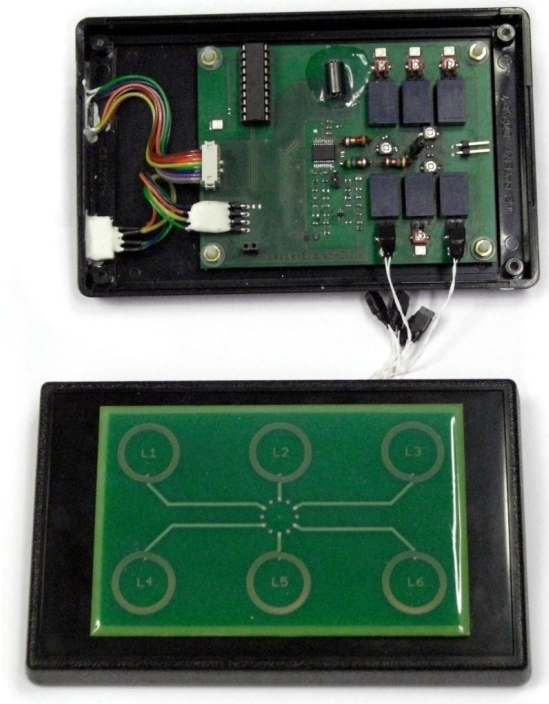


FIG B.1: Base station. **Top**: PCB inside the station carrying electronics. Connectors to power supply and data communication as well as a display are located on the left side. The multiplexer relais are arranged on the right side of the PCB. The RF-generator, impedance matching and detector circuitry have a T-shaped arrangement. **Bottom**: Cover of the base station with the antenna plate mounted on it. The plate has an additional epoxy resin coating to protect the coils. Connectors to the multiplexer with twisted pair lines are visible

## B.1 RF-Generator

The RF-generator shown in FIG B.2 is a switched circuit whereas switch *S* is a MOSFET within the MLX90121. $C_4$ is fine-tuned for matching a 50 Ω antenna. The quality factors of inductors $L_2$ to $L_4$ have a strong influence on the output power. Their values provided in TABLE B.I should not be under-run.

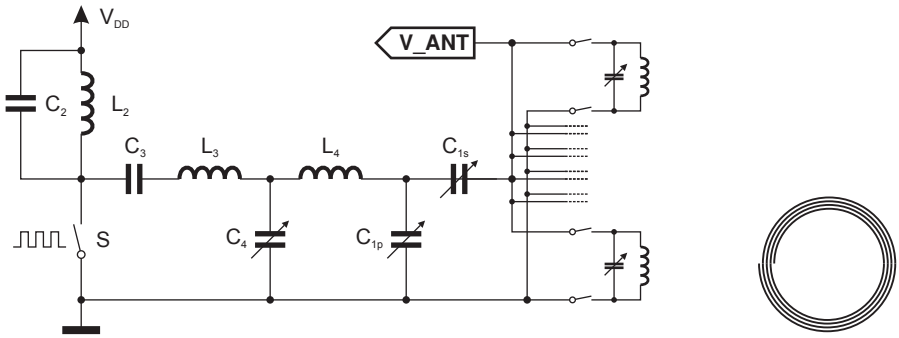


(a) (b)

FIG B.2: **(a)** RF-generator for a 50 Ω-antenna based on the evaluation board EVB90121 from Melexis Inc. The impedance matching capacitors are followed by a multiplexer for the selection of a certain antenna. Each of them has a 20 pF trimming capacitor for fine-tuning of each antenna connection. **(b)** Base station coil $L_1$ 2-fold enlarged.

The multiplexer for the selection of a certain antenna of the base station is formed by relays. The conductors to a common antenna plate are within a bundle which could influence the impedance matching by parasitic capacities. Hence, all poles of each antenna are disconnected by relays.

## B.2 Receiver section

The receiver input hat a sensitivity of at least -35 dBm at 100 kΩ small signal input impedance, i.e. about 180 mV rms. The effective antenna voltage $V_{\mathrm{Ant}}$ varies due to position mismatches, device ageing and production-related differences of the tags' LC-circuits. Hence the signal for the detection of load modulation needs to be pre-processed. The detection and signal recovery circuit shown in FIG B.3 consists of three parts. The envelope detector is followed by a DC-correction to 2.5 V and signal buffer and amplifier $OA_1$. This OA is built up as a non-inverting amplifier with an amplification of 2 for small input signals. The small Gain-Bandwidth-Product of 5 MHz suppresses residual ripple of the original antenna signal. An AC-voltage limiter is built up with resistor $R_4$ and diodes $D_2$ and $D_3$. AC-peaks above 0.3 V are limited. Capacitor $C_8$ defines the DC-level and in the case of small signals capacitor $C_7$ and $R_4$ form an additional low pass filter.

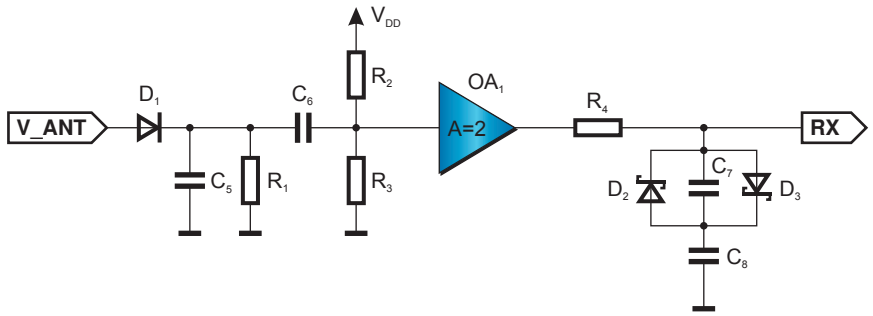


FIG B.3: Incoherent detector and signal recovery. The signal recovery consists of an enevelope detector, DC-level shifter and signal buffer and an AC-peak-limiter.

The recovered signal has a DC-level of 2.5 V and a maximum amplitude of 0.3 V. This signal can be directly fed into the receiver section of the MLX90121.

TABLE B.I: List of Electronic Devices of the RF-Generator and Detector Circuitry.

| Device | Model / Producer |
|---|---|
| | **Generator** |
| $L_2$ | 1.2 uH, $Q \geq 55$ at 8 MHz |
| $C_2$ | 47 pF, C0G dielectric |
| $L_3$ | 5.6 uH, $Q \geq 60$ at 8 MHz |
| $C_3$ | 100 nF |
| $L_4$ | 4.7 uH, $Q \geq 50$ at 8 MHz |
| $C_4$ | 7.5 to 50 pF |
| | **Antenna** |
| $C_{1s}$ | 145 pF (nominal) |
| $C_{1p}$ | 730 pF (nominal |
| $L_1$ | 6x450 µH by PCB-layout |
| | **Detector and Signal recovery** |
| $OA_1$ | AD8515 / Analog Devices |
| $D_1$ | BAS316 |
| $D_2$, $D_3$ | RB520S |
| $C_5$ | 100 pF |
| $C_6$, $C_8$ | 100 nF |
| $C_7$ | 68 pF |
| $R_1$ | 22 kΩ |
| $R_2$, $R_3$ | 10 kΩ |
| $R_4$ | 2.2 kΩ |

## B.3 Bit detection at RF-communication

Data is transmitted via load modulation on the RF-interface. A logic High, i.e. a bit '1', is represented by a subcarrier-frequency $f_{sc} = 250\,\text{kHz}$ for a nominal period of $68\,\mu\text{s}$. A subcarrier-frequency causes a logic High at the RX_IN input pin of the microcontroller and lasts as long as the subcarrier frequency is detected. In every other case the input should be Low but the incoherent detection as well as noise on the power supply lines cause spikes.

The whole communication incorporating the detection of 24 bits needs to take place within a known time frame of 100 ms. If this time frame is exceeded an interrupt occurs which reconfigures the RX_IN pin as an output and sets this output to High. Furthermore, an error-flag is set. Those two mechanisms eliminate the possibility of an infinite loop and allow a detection of erroneous or missing communication. The detection mechanism utilizes the Capture-Compare-unit of the PIC16F690 for a suitable time-resolved analysis of the RX_IN signal.

Whenever the input RX_IN, i.e. the digital output of the RF receiver section, has a falling edge the Capture-Compare- (CCP) flag is set. The left part of the flowchart in Fig B.4 shows the algorithm for the start bit detection. Spikes shorter than $1.5\,\mu\text{s}$ can only be distinguished by the CCP-module. A valid start bit is given if logic 1 is detected for $63\,\mu\text{s}$. This shorter period takes care on the possibility of oscillator timing mismatches of the base station and tag microcontroller. The difference may be up to 4 %. This algorithm would cause an infinite loop in the case of a missing communication which is prevented by the previously described interrupt routine.

When the algorithm reaches the right branch a period of $63\,\mu\text{s}$ is awaited. If the 100 ms-period is exceeded and the error-flag set, then the timing period is also discontinued. Finally, the RX_IN pin is reconfigured as an input (if the interrupt occurred). During the detection time span the CCP-flag will only be set if RX_in changes to 0 after the detected start bit. This does not happen if the receiver output sends a continuous High. Thus, the CCP-flag can be used to define the detected bit.

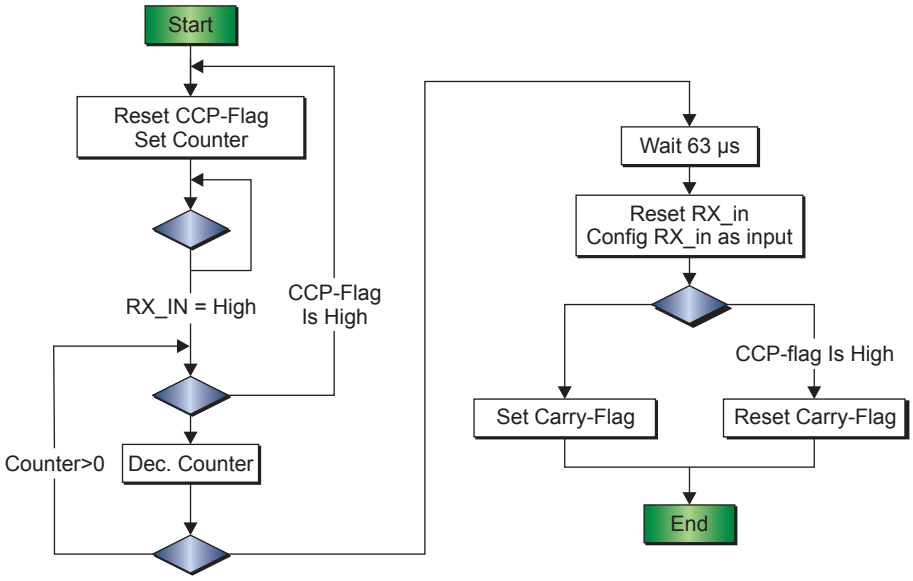


FIG B.4: Flow chart for the detection of a single bit. The given Counter-values incorporate the instruction cycle timings.

# Appendix C

# TAG CIRCUITRY

## C.1 Measurement circuit device list

The used devices listed in TABLE C.I relate to the presented measurement system in chapter *4.2 Measurement Electronics* and lead to a current consumption of only 2.5 mA at a single voltage supply of 3.3 V.

TABLE C.I: List of Electronic Devices of the Measurement Electronics.

| Device | Model / Producer |
|---|---|
| **General devices** | |
| Microcontroller | PIC16F688 / Microchip |
| $OA_1$,$OA_2$ | AD8515 / Analog Devices |
| $OA_3$ | AD8606 / Analog Devices |
| $S_1$, $S_2$ | ADG736 / Analog Devices |
| $S_3$, $S_4$ | ADG711 / Analog Devices |
| **Signal generator** | |
| Capacitors (filter stage #1) | 2.7 nF |
| Resistors (filter stage #1) | 22 kΩ |
| Capacitors (filter stage #2) | 680 pF |
| Switchable capacitor | 5.6 nF |
| Resistors (filter stage #2) | 15 kΩ |
| **I/V converter** | |
| $Z_{ref}$ | 220 Ω (only ohmic) |
| $C_3$ | 100 nF |
| $C_4$ | 10 pF |
| $R_3$, $R_4$ | 12 kΩ |
| $R_5$ | 6.8 kΩ |
| **Sample-Hold element** | |
| $C_5$, $C_6$ | 100 pF |
| $R_6$ | 2.2 kΩ |

The resistors had tolerance values of 1 % or less and the capacitors had dielectrics of type X7R or higher quality. The system then worked properly in a temperature range from 0 to 40 °C. An extended temperature range can be utilized if X8R or C0G dielectrics are used to avoid problems with temperature-related variations of the capacities. In addition to $R_5$ another resistor with 2.2 kΩ can be connected in parallel by an additional switch. The effective feedback impedances are then 12, 4.34, 1.86, and 1.46 kΩ covering a sensor impedance range from 40 Ω to 7 kΩ.

## C.2 Probe signal bit pattern

FIG C.1 depicts the circuitry for the generation of a certain probe signal $x(t)$.

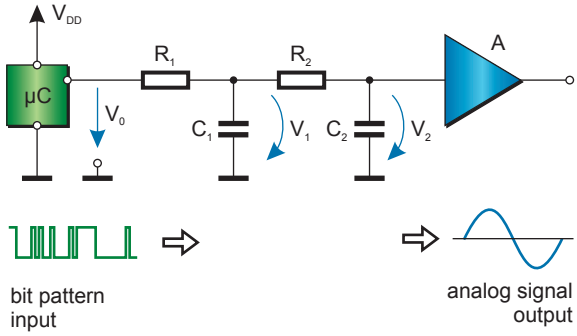


FIG C.1: Basic schematic of the signal generation. Voltage $V_0$ is a digital output of the microcontroller with voltage levels 0 and $V_{DD}$. The RC-network is followed by a voltage buffer $A$.

Equations (6.1) and (6.2) describe the signals $V_1(t_2)$ and $V_2(t_2)$ with respect to a voltage $V_0$ being constant within time span ($t_2$-$t_1$). and initial voltage $V_1(t_1)$ and $V_2(t_1)$. Handling is simplified by setting $R_1 = R_2 = R$ and $C_1 = C_2 = C$ with a time constant $\tau = R\,C$.

$$\begin{pmatrix} V_1(t_2) \\ V_2(t_2) \end{pmatrix} = \begin{pmatrix} V_1(t_1) \\ V_2(t_1) \end{pmatrix} + \alpha \cdot \begin{pmatrix} 2 \\ m \end{pmatrix} \cdot [1 - \exp(\lambda_1 (t_2 - t_1))] + \beta \cdot \begin{pmatrix} 2 \\ n \end{pmatrix} \cdot [1 - \exp(\lambda_2 (t_2 - t_1))] \tag{6.1}$$

with parameters

$$\begin{pmatrix} \alpha \\ \beta \end{pmatrix} = \frac{1}{4\sqrt{5}} \begin{pmatrix} -m & -n & 2 \\ n & m & -2 \end{pmatrix} \cdot \begin{pmatrix} V_0 \\ V_1(t_1) \\ V_2(t_1) \end{pmatrix} \tag{6.2a,b}$$

$$m = \left(1 + \sqrt{5}\right),\ n = \left(1 - \sqrt{5}\right),\ \lambda_1 = -\frac{3 + \sqrt{5}}{2\tau},\ \lambda_2 = -\frac{3 - \sqrt{5}}{2\tau},\ \text{and} \tag{6.3a,b,c,d}$$

FIG C.2 shows the flowchart for the generation of a bit pattern of length $N = T_X/T_C$ whereas $T_X = 1/f_X$ is the period of the probe signal $x(t)$ and $T_C$ the instruction period of the tag-µC.

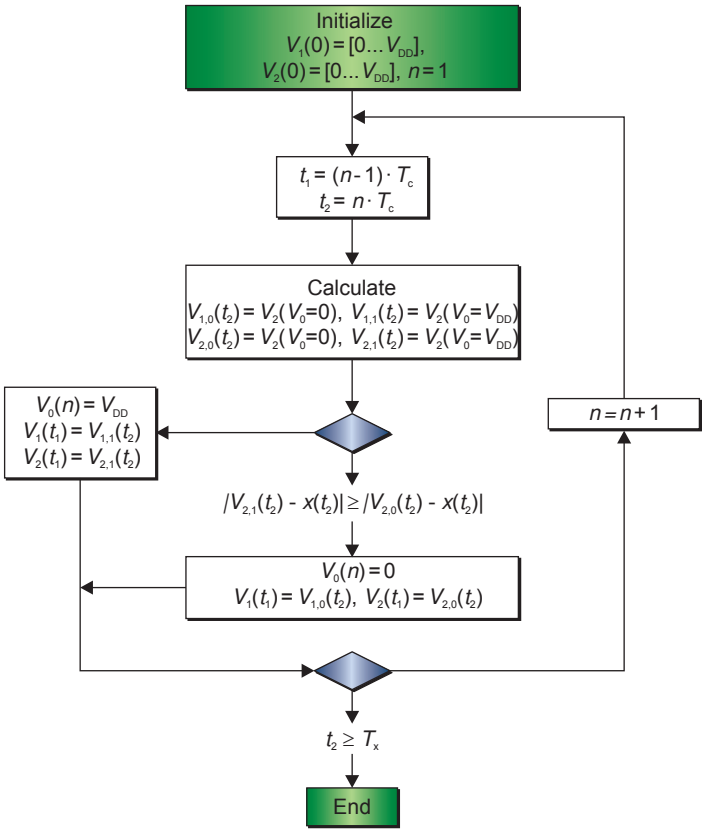


FIG C.2: Flow chart for bit pattern generation. $T_C$ is the instruction cycle duration of the tag microcontroller. Index n refers to the position within the bit pattern. The number of bits is $T_X/T_C$.

The following bit patterns are true for the 5 and 10 kHz-signal for a low pass filter time constant $\tau = 22\,\mathrm{k\Omega} \cdot 2.2\,\mathrm{nF} = 48.4\,\mu\mathrm{s}$, i.e. a cutoff-frequency $f_{co} = 3.3\,\mathrm{kHz}$. 'c' marks an unchanged state within the pattern.

**5kHz bit pattern**

```
0cc1cc0c1c01c0c1c0101c0c1cc0c1c01c0c1c0101c0c1cc0c
1ccc01c0c1cc0c1c010101c0c1cc0c101cc0cc1cc010c1cc0c
10cccc1c0101010101c0c101c0c1c0c1c010c1c0c1c0c1c0c1
01c0c101010c1c010c101c0cc1c0c1c0c1010c1c0c1010c1c0
c1ccc0cc101010c1010c1c0c10c1c0cc1c010cc1c0c1c0cc10
1ccccc010ccc101c0cc1c0c1c0cc1c0c101010c1c0c101010c
1cccc0ccc1cc0cc1c0c1c0c1c0c101c0c101c0c101010cc1c0
c1c0c1cc0cc1cc0c1010c10c1cc0c1c0c1cc0cc1ccc0cc1ccc
```

**10kHz bit pattern**

```
1c0101cc0c1c01c0c1cc0cc1ccc0ccc1cc0cc1c0c1c0cc1010
c1010cc1c0ccc1010c10c10cc1010ccc1c0ccc1c0ccc1010c1
0c1010cc1c0c10c1c0c1010c1c010c1c010101c0c1cc0c1c01
c0101cc0101c01c01cc0c1cccc0c1cc01c01cc0c1ccc0101c0
```

# Appendix D

# CREATIVE COMMONS ATTRIBUTION SHARE-ALIKE 3.0 UNPORTED

CREATIVE COMMONS CORPORATION IS NOT A LAW FIRM AND DOES NOT PROVIDE LEGAL SERVICES. DISTRIBUTION OF THIS LICENSE DOES NOT CREATE AN ATTORNEY-CLIENT RELATIONSHIP. CREATIVE COMMONS PROVIDES THIS INFORMATION ON AN "AS-IS" BASIS. CREATIVE COMMONS MAKES NO WARRANTIES REGARDING THE INFORMATION PROVIDED, AND DISCLAIMS LIABILITY FOR DAMAGES RESULTING FROM ITS USE.

## License

THE WORK (AS DEFINED BELOW) IS PROVIDED UNDER THE TERMS OF THIS CREATIVE COMMONS PUBLIC LICENSE ("CCPL" OR "LICENSE"). THE WORK IS PROTECTED BY COPYRIGHT AND/OR OTHER APPLICABLE LAW. ANY USE OF THE WORK OTHER THAN AS AUTHORIZED UNDER THIS LICENSE OR COPYRIGHT LAW IS PROHIBITED.
BY EXERCISING ANY RIGHTS TO THE WORK PROVIDED HERE, YOU ACCEPT AND AGREE TO BE BOUND BY THE TERMS OF THIS LICENSE. TO THE EXTENT THIS LICENSE MAY BE CONSIDERED TO BE A CONTRACT, THE LICENSOR GRANTS YOU THE RIGHTS CONTAINED HERE IN CONSIDERATION OF YOUR ACCEPTANCE OF SUCH TERMS AND CONDITIONS.

## 1. Definitions

(a) **"Adaptation"** means a work based upon the Work, or upon the Work and other pre-existing works, such as a translation, adaptation, derivative work, arrangement of music or other alterations of a literary or artistic work, or phonogram or performance and includes cinematographic adaptations or any other form in which the Work may be recast, transformed, or adapted including in any form recognizably derived from the original, except that a work that constitutes a Collection will not be considered an Adaptation for the purpose of this License. For the avoidance of doubt, where the Work is a musical work, performance or phonogram, the synchronization of the Work in timed-relation with a moving image ("synching") will be considered an Adaptation for the purpose of this License.
(b) **"Collection"** means a collection of literary or artistic works, such as encyclopedias and anthologies, or performances, phonograms or broadcasts, or other works or subject matter other than works listed in Section 1(f) below, which, by reason of the selection and arrangement of their contents, constitute intellectual creations, in which the Work is included in its entirety in unmodified form along with one or more other contributions, each constituting separate and independent works in themselves, which together are assembled into a collective whole. A work that constitutes a Collection will not be considered an Adaptation (as defined below) for the purposes of this License.
(c) **"Creative Commons Compatible License"** means a license that is listed at http://creativecommons.org/compatiblelicenses that has been approved by Creative Commons as being essentially equivalent to this License, including, at a minimum, because that license: (i) contains terms that have the same purpose, meaning and effect as the License Elements of this License; and, (ii) explicitly permits the relicensing of adaptations of works made available under that license under this License or a Creative Commons jurisdiction license with the same License Elements as this License.
(d) **"Distribute"** means to make available to the public the original and copies of the Work or Adaptation, as appropriate, through sale or other transfer of ownership.

(e) **"License Elements"** means the following high-level license attributes as selected by Licensor and indicated in the title of this License: Attribution, ShareAlike.
(f) **"Licensor"** means the individual, individuals, entity or entities that offer(s) the Work under the terms of this License.
(g) **"Original Author"** means, in the case of a literary or artistic work, the individual, individuals, entity or entities who created the Work or if no individual or entity can be identified, the publisher; and in addition (i) in the case of a performance the actors, singers, musicians, dancers, and other persons who act, sing, deliver, declaim, play in, interpret or otherwise perform literary or artistic works or expressions of folklore; (ii) in the case of a phonogram the producer being the person or legal entity who first fixes the sounds of a performance or other sounds; and, (iii) in the case of broadcasts, the organization that transmits the broadcast.
(h) **"Work"** means the literary and/or artistic work offered under the terms of this License including without limitation any production in the literary, scientific and artistic domain, whatever may be the mode or form of its expression including digital form, such as a book, pamphlet and other writing; a lecture, address, sermon or other work of the same nature; a dramatic or dramatico-musical work; a choreographic work or entertainment in dumb show; a musical composition with or without words; a cinematographic work to which are assimilated works expressed by a process analogous to cinematography; a work of drawing, painting, architecture, sculpture, engraving or lithography; a photographic work to which are assimilated works expressed by a process analogous to photography; a work of applied art; an illustration, map, plan, sketch or three-dimensional work relative to geography, topography, architecture or science; a performance; a broadcast; a phonogram; a compilation of data to the extent it is protected as a copyrightable work; or a work performed by a variety or circus performer to the extent it is not otherwise considered a literary or artistic work.
(i) **"You"** means an individual or entity exercising rights under this License who has not previously violated the terms of this License with respect to the Work, or who has received express permission from the Licensor to exercise rights under this License despite a previous violation.
(j) **"Publicly Perform"** means to perform public recitations of the Work and to communicate to the public those public recitations, by any means or process, including by wire or wireless means or public digital performances; to make available to the public Works in such a way that members of the public may access these Works from a place and at a place individually chosen by them; to perform the Work to the public by any means or process and the communication to the public of the performances of the Work, including by public digital performance; to broadcast and rebroadcast the Work by any means including signs, sounds or images.
(k) **"Reproduce"** means to make copies of the Work by any means including without limitation by sound or visual recordings and the right of fixation and reproducing fixations of the Work, including storage of a protected performance or phonogram in digital form or other electronic medium.

**2. Fair Dealing Rights.** Nothing in this License is intended to reduce, limit, or restrict any uses free from copyright or rights arising from limitations or exceptions that are provided for in connection with the copyright protection under copyright law or other applicable laws.
**3. License Grant.** Subject to the terms and conditions of this License, Licensor hereby grants You a worldwide, royalty-free, non-exclusive, perpetual (for the duration of the applicable copyright) license to exercise the rights in the Work as stated below:
(a) to Reproduce the Work, to incorporate the Work into one or more Collections, and to Reproduce the Work as incorporated in the Collections;
(b) to create and Reproduce Adaptations provided that any such Adaptation, including any translation in any medium, takes reasonable steps to clearly label, demarcate or otherwise identify that changes were made to the original Work. For example, a translation could be marked "The original work was translated from English to Spanish," or a modification could indicate "The original work has been modified.";
(c) to Distribute and Publicly Perform the Work including as incorporated in Collections; and,
(d) to Distribute and Publicly Perform Adaptations.
(e) For the avoidance of doubt:

I. **Non-waivable Compulsory License Schemes**. In those jurisdictions in which the right to collect royalties through any statutory or compulsory licensing scheme cannot be waived, the Licensor reserves the exclusive right to collect such royalties for any exercise by You of the rights granted under this License;
II. **Waivable Compulsory License Schemes**. In those jurisdictions in which the right to collect royalties through any statutory or compulsory licensing scheme can be waived, the Licensor waives

the exclusive right to collect such royalties for any exercise by You of the rights granted under this License; and,

III. **Voluntary License Schemes**. The Licensor waives the right to collect royalties, whether individually or, in the event that the Licensor is a member of a collecting society that administers voluntary licensing schemes, via that society, from any exercise by You of the rights granted under this License.

The above rights may be exercised in all media and formats whether now known or hereafter devised. The above rights include the right to make such modifications as are technically necessary to exercise the rights in other media and formats. Subject to Section 8(f), all rights not expressly granted by Licensor are hereby reserved.

**4. Restrictions.** The license granted in Section 3 above is expressly made subject to and limited by the following restrictions:

(a) You may Distribute or Publicly Perform the Work only under the terms of this License. You must include a copy of, or the Uniform Resource Identifier (URI) for, this License with every copy of the Work You Distribute or Publicly Perform. You may not offer or impose any terms on the Work that restrict the terms of this License or the ability of the recipient of the Work to exercise the rights granted to that recipient under the terms of the License. You may not sublicense the Work. You must keep intact all notices that refer to this License and to the disclaimer of warranties with every copy of the Work You Distribute or Publicly Perform. When You Distribute or Publicly Perform the Work, You may not impose any effective technological measures on the Work that restrict the ability of a recipient of the Work from You to exercise the rights granted to that recipient under the terms of the License. This Section 4(a) applies to the Work as incorporated in a Collection, but this does not require the Collection apart from the Work itself to be made subject to the terms of this License. If You create a Collection, upon notice from any Licensor You must, to the extent practicable, remove from the Collection any credit as required by Section 4(c), as requested. If You create an Adaptation, upon notice from any Licensor You must, to the extent practicable, remove from the Adaptation any credit as required by Section 4(c), as requested.

(b) You may Distribute or Publicly Perform an Adaptation only under the terms of: (i) this License; (ii) a later version of this License with the same License Elements as this License; (iii) a Creative Commons jurisdiction license (either this or a later license version) that contains the same License Elements as this License (e.g., Attribution-ShareAlike 3.0 US)); (iv) a Creative Commons Compatible License. If you license the Adaptation under one of the licenses mentioned in (iv), you must comply with the terms of that license. If you license the Adaptation under the terms of any of the licenses mentioned in (i), (ii) or (iii) (the "Applicable License"), you must comply with the terms of the Applicable License generally and the following provisions: (I) You must include a copy of, or the URI for, the Applicable License with every copy of each Adaptation You Distribute or Publicly Perform; (II) You may not offer or impose any terms on the Adaptation that restrict the terms of the Applicable License or the ability of the recipient of the Adaptation to exercise the rights granted to that recipient under the terms of the Applicable License; (III) You must keep intact all notices that refer to the Applicable License and to the disclaimer of warranties with every copy of the Work as included in the Adaptation You Distribute or Publicly Perform; (IV) when You Distribute or Publicly Perform the Adaptation, You may not impose any effective technological measures on the Adaptation that restrict the ability of a recipient of the Adaptation from You to exercise the rights granted to that recipient under the terms of the Applicable License. This Section 4(b) applies to the Adaptation as incorporated in a Collection, but this does not require the Collection apart from the Adaptation itself to be made subject to the terms of the Applicable License.

(c) If You Distribute, or Publicly Perform the Work or any Adaptations or Collections, You must, unless a request has been made pursuant to Section 4(a), keep intact all copyright notices for the Work and provide, reasonable to the medium or means You are utilizing: (i) the name of the Original Author (or pseudonym, if applicable) if supplied, and/or if the Original Author and/or Licensor designate another party or parties (e.g., a sponsor institute, publishing entity, journal) for attribution ("Attribution Parties") in Licensor's copyright notice, terms of service or by other reasonable means, the name of such party or parties; (ii) the title of the Work if supplied; (iii) to the extent reasonably practicable, the URI, if any, that Licensor specifies to be associated with the Work, unless such URI does not refer to the copyright notice or licensing information for the Work; and (iv) , consistent with Section 3(b), in the case of an Adaptation, a credit identifying the use of the Work in the Adaptation (e.g., "French translation of the Work by Original Author," or "Screenplay based on original Work by Original Author"). The credit required by this Section 4(c) may be implemented in any

reasonable manner; provided, however, that in the case of a Adaptation or Collection, at a minimum such credit will appear, if a credit for all contributing authors of the Adaptation or Collection appears, then as part of these credits and in a manner at least as prominent as the credits for the other contributing authors. For the avoidance of doubt, You may only use the credit required by this Section for the purpose of attribution in the manner set out above and, by exercising Your rights under this License, You may not implicitly or explicitly assert or imply any connection with, sponsorship or endorsement by the Original Author, Licensor and/or Attribution Parties, as appropriate, of You or Your use of the Work, without the separate, express prior written permission of the Original Author, Licensor and/or Attribution Parties.

(d) Except as otherwise agreed in writing by the Licensor or as may be otherwise permitted by applicable law, if You Reproduce, Distribute or Publicly Perform the Work either by itself or as part of any Adaptations or Collections, You must not distort, mutilate, modify or take other derogatory action in relation to the Work which would be prejudicial to the Original Author's honor or reputation. Licensor agrees that in those jurisdictions (e.g. Japan), in which any exercise of the right granted in Section 3(b) of this License (the right to make Adaptations) would be deemed to be a distortion, mutilation, modification or other derogatory action prejudicial to the Original Author's honor and reputation, the Licensor will waive or not assert, as appropriate, this Section, to the fullest extent permitted by the applicable national law, to enable You to reasonably exercise Your right under Section 3(b) of this License (right to make Adaptations) but not otherwise.

## 5. Representations, Warranties and Disclaimer

UNLESS OTHERWISE MUTUALLY AGREED TO BY THE PARTIES IN WRITING, LICENSOR OFFERS THE WORK AS-IS AND MAKES NO REPRESENTATIONS OR WARRANTIES OF ANY KIND CONCERNING THE WORK, EXPRESS, IMPLIED, STATUTORY OR OTHERWISE, INCLUDING, WITHOUT LIMITATION, WARRANTIES OF TITLE, MERCHANTIBILITY, FITNESS FOR A PARTICULAR PURPOSE, NONINFRINGEMENT, OR THE ABSENCE OF LATENT OR OTHER DEFECTS, ACCURACY, OR THE PRESENCE OF ABSENCE OF ERRORS, WHETHER OR NOT DISCOVERABLE. SOME JURISDICTIONS DO NOT ALLOW THE EXCLUSION OF IMPLIED WARRANTIES, SO SUCH EXCLUSION MAY NOT APPLY TO YOU.

**6. Limitation on Liability.** EXCEPT TO THE EXTENT REQUIRED BY APPLICABLE LAW, IN NO EVENT WILL LICENSOR BE LIABLE TO YOU ON ANY LEGAL THEORY FOR ANY SPECIAL, INCIDENTAL, CONSEQUENTIAL, PUNITIVE OR EXEMPLARY DAMAGES ARISING OUT OF THIS LICENSE OR THE USE OF THE WORK, EVEN IF LICENSOR HAS BEEN ADVISED OF THE POSSIBILITY OF SUCH DAMAGES.

## 7. Termination

(a) This License and the rights granted hereunder will terminate automatically upon any breach by You of the terms of this License. Individuals or entities who have received Adaptations or Collections from You under this License, however, will not have their licenses terminated provided such individuals or entities remain in full compliance with those licenses. Sections 1, 2, 5, 6, 7, and 8 will survive any termination of this License.

(b) Subject to the above terms and conditions, the license granted here is perpetual (for the duration of the applicable copyright in the Work). Notwithstanding the above, Licensor reserves the right to release the Work under different license terms or to stop distributing the Work at any time; provided, however that any such election will not serve to withdraw this License (or any other license that has been, or is required to be, granted under the terms of this License), and this License will continue in full force and effect unless terminated as stated above.

## 8. Miscellaneous

(a) Each time You Distribute or Publicly Perform the Work or a Collection, the Licensor offers to the recipient a license to the Work on the same terms and conditions as the license granted to You under this License.

(b) Each time You Distribute or Publicly Perform an Adaptation, Licensor offers to the recipient a license to the original Work on the same terms and conditions as the license granted to You under this License.

(c) If any provision of this License is invalid or unenforceable under applicable law, it shall not affect the validity or enforceability of the remainder of the terms of this License, and without further action by the parties to this agreement, such provision shall be reformed to the minimum extent necessary to make such provision valid and enforceable.
(d) No term or provision of this License shall be deemed waived and no breach consented to unless such waiver or consent shall be in writing and signed by the party to be charged with such waiver or consent.
(e) This License constitutes the entire agreement between the parties with respect to the Work licensed here. There are no understandings, agreements or representations with respect to the Work not specified here. Licensor shall not be bound by any additional provisions that may appear in any communication from You. This License may not be modified without the mutual written agreement of the Licensor and You.
(f) The rights granted under, and the subject matter referenced, in this License were drafted utilizing the terminology of the Berne Convention for the Protection of Literary and Artistic Works (as amended on September 28, 1979), the Rome Convention of 1961, the WIPO Copyright Treaty of 1996, the WIPO Performances and Phonograms Treaty of 1996 and the Universal Copyright Convention (as revised on July 24, 1971). These rights and subject matter take effect in the relevant jurisdiction in which the License terms are sought to be enforced according to the corresponding provisions of the implementation of those treaty provisions in the applicable national law. If the standard suite of rights granted under applicable copyright law includes additional rights not granted under this License, such additional rights are deemed to be included in the License; this License is not intended to restrict the license of any rights under applicable law.

## Creative Commons Notice

Creative Commons is not a party to this License, and makes no warranty whatsoever in connection with the Work. Creative Commons will not be liable to You or any party on any legal theory for any damages whatsoever, including without limitation any general, special, incidental or consequential damages arising in connection to this license. Notwithstanding the foregoing two (2) sentences, if Creative Commons has expressly identified itself as the Licensor hereunder, it shall have all rights and obligations of Licensor.
Except for the limited purpose of indicating to the public that the Work is licensed under the CCPL, Creative Commons does not authorize the use by either party of the trademark “Creative Commons” or any related trademark or logo of Creative Commons without the prior written consent of Creative Commons. Any permitted use will be in compliance with Creative Commons’ then-current trademark usage guidelines, as may be published on its website or otherwise made available upon request from time to time. For the avoidance of doubt, this trademark restriction does not form part of the License.
Creative Commons may be contacted at http://creativecommons.org/.